

SINTERING OF SILICON CARBIDE

by

RICARDO I. FUENTES

B.S. Instituto Tecnológico y de Estudios Superiores de Monterrey, Mexico, (1979)
M.S. Massachusetts Institute of Technology, (1983)

Submitted to the Department of
Materials Science and Engineering
in Partial Fulfillment of the
Requirements of the
Degree of

DOCTOR OF PHILOSOPHY

at the

MASSACHUSETTS INSTITUTE OF TECHNOLOGY

September 1986

© Ricardo I. Fuentes 1986

The author hereby grants to M.I.T. permission to reproduce and
to distribute copies of this thesis document in whole or in part.

Signature of Author _____

Department of ~~Materials Science~~ and Engineering
August 8, 1986

Certified by _____

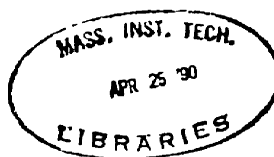
Robert L. Coble
Thesis Supervisor

Accepted by _____

Bernhardt J. Wuensch
Chairman, Departmental Committee on Graduate Students

ARCHIVES

1



SINTERING OF SILICON CARBIDE

by

RICARDO I. FUENTES

Submitted to the Department of
Materials Science and Engineering
on August 8, 1986 in partial
fulfillment of the requirements for the
Degree of Doctor of Philosophy.

2. Abstract

Sintering studies were carried out on boron and carbon doped silicon carbide (SiC) of both alpha and beta forms, and in Al₂O₃ doped alpha SiC. The effect of CaO addition on Al₂O₃ doped SiC is investigated.

Sintering is found to proceed by a liquid phase sintering mechanism in the systems SiC-Al₂O₃ and SiC-Al₂O₃-CaO. The liquid forms in the Al₂O₃-Al₄O₄C binary at temperatures greater than 1840 °C. CaO was found to enhance the sintering rate of Al₂O₃ doped SiC by promoting the formation and transport of aluminum rich vapor species. Void free specimens were obtained in the SiC-Al₂O₃-CaO system with the addition of 7.7 W% Al₂O₃ and 0.3 W% CaO to alpha SiC powders fired at temperatures higher than 1835 ± 20 °C for one hour. Boron's principal role in the sintering of SiC appears to be the inhibition of early coarsening. The role of carbon is the removal of oxygen and free silicon.

Thesis Supervisor: Robert L. Coble

Title: Professor of Ceramics

3. Table of Contents

1. Title Page.....	1
2. Abstract.....	2
3. Table of Contents.....	3
4. Acknowledgments.....	6
5. Introduction.....	7
6. Literature Review.....	9
6.1. Sintering Models.....	9
6.1.1. Solid State Sintering.....	9
6.1.2. Liquid Phase Sintering.....	16
6.2. Dopants.....	19
6.2.1. Boron, Aluminum and Carbon.....	19
6.2.2. Metal Oxides.....	23
6.3. Boundary Phases.....	25
6.3.1. Boron, Aluminum and Carbon Doped SiC.....	25
6.3.2. Al ₂ O ₃ Doped SiC.....	26
6.4. Phase Relations.....	28
6.4.1. SiC-Al ₂ O ₃ -C-CaO System.....	28
6.4.1.1. Al ₂ O ₃ -C.....	29
6.4.1.2. Al ₂ O ₃ -Al ₄ C ₃	30
6.4.1.3. SiC-Al ₄ C ₃	32
6.4.1.4. Al ₄ C ₃ -Al ₂ O ₃ vs. Al ₄ C ₃ -SiC.....	35
6.4.1.5. Al ₂ O ₃ -CaO.....	37
6.4.1.6. CaO as a Catalyst.....	37
6.4.2. SiC-B-C System.....	39
6.5. Mechanical Properties.....	41
7. Experimental Procedures.....	43
7.1. System SiC-B-C.....	43
7.1.1. SiC Powders.....	43
7.1.1.1. Alpha Powders.....	43
7.1.1.2. Beta Powders.....	44
7.1.2. Powder preparation and Processing.....	45
7.1.2.1. Doping.....	45
7.1.2.2. Cold Pressing.....	47
7.1.2.3. Firing.....	47
7.2. System SiC-Al ₂ O ₃ -CaO.....	49
7.2.1. SiC Powders.....	49
7.2.2. Additives.....	50
7.2.2.1. CaO.....	50
7.2.2.2. Al ₂ O ₃	51
7.2.3. Powder Preparation and Processing.....	51
7.2.3.1. Cold Pressing.....	52
7.2.3.2. Furnace.....	52
7.2.3.3. Firing Atmosphere.....	53

7.2.3.4.	Heating Rate.....	53
7.2.3.5.	Sample Arrangement.....	53
7.2.3.6.	Packing Powders.....	54
7.2.3.7.	Temperature Measurement.....	54
7.2.4.	Density Measurement.....	55
7.2.4.1.	Geometric Determination.....	55
7.2.4.2.	Pore Count.....	56
7.2.4.3.	Pycnometry.....	57
7.2.5.	SEM and STEM.....	57
7.2.5.1.	SEM: Sample preparation.....	57
7.2.5.2.	STEM: Sample Preparation.....	58
7.2.5.3.	X-Ray Elemental Analysis.....	59
8.	Results.....	60
8.1.	System SiC-B-C.....	60
8.1.1.	Alpha vs. Beta SiC powders.....	60
8.1.2.	Effect of Boron and Carbon Additions.....	60
8.1.2.1.	On final density.....	61
8.1.2.2.	On linear shrinkage.....	61
8.1.2.3.	On weight loss.....	61
8.1.2.4.	Form of addition.....	62
8.1.3.	Effect of gas flow.....	62
8.1.4.	Effect of heating rate.....	63
8.2.	System SiC-Al ₂ O ₃ -CaO.....	63
8.2.1.	Final Density vs. CaO content.....	63
8.2.2.	Final Density vs. Packing Powder.....	64
8.2.3.	Final Density vs. time.....	65
8.2.4.	Final Density vs. Temperature.....	66
8.2.5.	Linear Shrinkage and Weight Change.....	67
8.2.6.	SEM: Microstructure.....	69
8.2.6.1.	Porosity.....	70
8.2.6.2.	Grain Size.....	70
8.2.6.3.	Fracture surfaces.....	71
8.2.6.4.	Voids.....	71
8.2.6.5.	Grain Boundaries.....	72
8.2.6.6.	General Features.....	72
8.2.7.	SEM: Energy Dispersive X-Ray Analysis.....	72
8.2.8.	STEM: Microstructure.....	73
8.2.8.1.	Grain Size.....	74
8.2.8.2.	Grain Shapes.....	74
8.2.8.3.	Grain Boundary Phase.....	74
8.2.9.	STEM: Microdiffraction.....	75
8.2.10.	STEM: X-Ray Elemental Analysis.....	76
8.2.10.1.	Sample "h6".....	76
8.2.10.2.	Sample "T11".....	77
9.	Discussion.....	82
9.1.	System SiC-B-C.....	82
9.1.1.	Gas transport.....	82
9.1.2.	Temperature effect.....	83
9.1.3.	Microstructure.....	84
9.1.4.	Form of addition.....	85

9.1.5.	Powder Size Distribution.....	85
9.1.6.	Weight loss.....	86
9.2.	System SiC-Al ₂ O ₃ -CaO.....	87
9.2.1.	SiC-Al ₂ O ₃ -CaO.....	87
9.2.2.	SiC-Al ₂ O ₃	88
9.2.3.	Composition of the boundary phase.....	89
9.2.4.	Boundary Phase Stoichiometry.....	90
9.2.5.	Mechanism of Liquid formation.....	92
9.2.5.1.	Al ₂ O ₃ -C.....	93
9.2.5.2.	The Role of CaO.....	96
9.2.6.	Sintering Mechanism.....	98
9.2.7.	Boundary Phase Decomposition and Weight Loss	101
9.2.8.	Summary.....	112
10.	Conclusions.....	114
11.	Suggestions for Future Work.....	118
12.	Figures.....	119
13.	References.....	152
14.	Appendix 1: Carburization and VLS Growth.....	160
15.	Biographical Note.....	163

4. Acknowledgments

I wish to thank Professor Robert L. Coble for his patience, guidance and valuable criticisms along the course of this work. It was a privilege working with him.

I also would like to thank Professor Bernhardt J. Wuensch for all his helpful advice and support.

I thank Professors W. David Kingery, Yet Ming Chiang and Erik Spjut for his suggestions and comments.

I am grateful to Pat Kearney for the many times he helped me to make things possible around the lab.

My work was always made easier and more pleasant thanks to John Centorino, Art Gregor, Leonard Sudenfield and Joe DiMaria, to them I express my gratitude.

I am grateful to Chen Wei Li for his help with the STEM work on my samples and our discussions. I am also indebted to Jose M. Delgado for his help with the powder X-ray diffraction data.

I acknowledge and thank Dumbar Birnie III and Alexana Rhosko for the helpful discussions and comments.

I also thank Diana and Eduardo Barzana for the many great moments we spent together. I am also grateful to Chris S. Wee and Cecilia Chin Ley for their friendship.

Thanks to Aurora and Carlos Valdes for their trust and encouragement over the last few years.

My deepest gratitude to my parents, Indalecio and Siria, for all their love and support over the years.

Finally, a person who makes my work, and everything else, a enjoyable experience; my wife Irma. It is to her that I dedicate this thesis.

5. Introduction

The present work deals with the study of the sintering behavior of silicon carbide (SiC). The aim was at understanding the processes that take place during heat treatment of a powders compact. Two sets of sintering additives were separately investigated: 1.-) boron and carbon, and 2.-) Al_2O_3 -CaO. Both systems are separately dealt with along the course of the text, since several differences exist amongst them, this is deemed appropriate. In the remaining of this section, a brief overview of the state of the affairs is given, followed in the next section by a thorough literature review.

Silicon Carbide, as with most materials in which the atomic bonding is predominantly covalent, is considered to be unsinterable in the absence of additives [1,2] in the range of particle sizes and chemical compositions investigated so far. Pressed compacts undergo significant coarsening without any shrinkage or densification.

Additives such as boron, aluminum and carbon are commonly used in amounts typically of a few tenths of a percent of B and Al and a few percent of C [3,4,5]. B and C seem to promote sintering via a solid state process [5,6,7,8]. Metal oxides have been successfully used as sintering additives [9,10] although their presence is presumed to promote the formation of a

liquid during sintering. Aluminum and carbon doping do not yield final densities as high as do boron and carbon doped specimens [11,12]. Furthermore, Al does not inhibit normal coarsening as effectively as does B [13]. The role of aluminum is not well understood so far, though it seems to participate in the formation of a liquid phase, perhaps transient in nature [13,4] when co-doped with boron.

Sintering atmospheres have a marked effect on the densification of SiC [15]. Leaching of some of the additives, reaction with them, or promotion of early coarsening via vapor or surface transport are several alternate effects. Inert atmospheres (Ar, He or vacuum) are commonly used with success. Typical sintering temperatures range from 1900 to 2150 °C [16] for intervals of 20 minutes to one hour in the case of B, Al and C and yield densities greater than 96% of theoretical with "clean" powder appropriately fabricated. For some oxide additives, sintering times up to 10 hs have been used to achieve densities greater than 96 %th. [9].

Average strengths in sintered SiC are in the vicinity of 350 Mpa. [12] for B and C additions. Strengths up to 930 Mpa. have been obtained in some cases with oxide additives [9].

6. Literature Review

6.1. Sintering Models

6.1.1. Solid State Sintering

For densification to take place matter has to be transported along certain paths (through the lattice or grain boundary) as opposed to others (surface or vapor). This situation usually implies the competition of multiple mechanisms for the transport of the material down the chemical potential gradients. Depending on the relative contribution of each of the mechanisms, the body will densify and/or coarsen to different extents.

During densification, the pores present in the compact will shrink and change shape and grain growth generally occurs during the process. Coble [14] identifies three different stages that the compact undergoes sequentially during sintering¹: 1.-) The initial stage, characterized by interparticle neck growth and center to center approach (shrinkage) of several percent [17, 18]. With densification mechanisms

1. The terms "Sintering" and "Densification" will be used indistinctly in the text to describe a process by means of which particle bonding and center to center approach occurs.

dominant, no grain growth takes place during this stage and the point at which it first occurs is considered the end of the initial stage. 2.-) The intermediate stage. In this stage, as the interparticle contacts grow, the pore surfaces intersected by grain boundaries configure themselves as to satisfy the force balance in the triple surface intercepts defining a unique angle (dihedral angle) which will depend on the solid-vapor:solid-solid surface energy ratio [19,20]. The pore phase is continuous throughout the body running along triple surface intersections (i.e. three grain junctions). During this stage the pore phase shrinks until eventually it becomes discontinuous marking the end of the intermediate stage. c.-) From the point in which the porosity becomes isolated the final stage is begun. Closed, nearly spherical pores are thermodynamically favored to locate in four grain corners. Pores in this configuration can shrink to closure if gas entrapment and discontinuous grain growth do not prevent them from doing so. Discontinuous grain growth may inhibit pore closure by moving the grain boundaries away from the pores and hence increase the diffusion distance.

Coble points out [14] that a sintering model consists essentially of a diffusion equation written for a small segment of the total structure, which is taken to represent the geometric changes of the total structure.

Initial stage sintering models for the individual mechanisms are considered satisfactory for first order estimates [21]

since they are solutions to well posed mathematical problems [22]. Differences among the models for a given mechanism usually arise from approximations made because of the complexity of geometry. Coblenz et.al. [22] critically reviewed the numerous published initial stage sintering models for surface diffusion, lattice diffusion, evaporation condensation and grain boundary diffusion. They conclude that models for boundary diffusion, surface diffusion and evaporation condensation appear adequate. Proper accounting for undercutting on the neck geometry is an issue in surface diffusion models and the cause for major differences between the proposed models. Lattice diffusion models are less satisfactory in the sense that important issues such as the form of the flux equation for transport from the surface to the neck and the neck geometry (i.e. undercutting) have not been treated properly. The problem still remains of properly treating the effects of multiple transport paths. The neck growth rate can be approximated to an additive function of the rates of the participant mechanisms [21]. Nevertheless, the problem of describing the proper neck geometry remains because the degree of undercutting and the amount of mass transported from the boundary both depend on the relative magnitudes of transport on the various paths [22].

A precise relationship between the neck size and the specific surface area has been developed by German et.al. [23,24]. This analysis provides an additional parameter to aid

in the identification of the controlling mechanism and the treatment of simultaneous multiple transport paths.

Initial stage sintering modeling of angular particles predicts a different time exponent² for neck growth than for spherical particles, because of the different neck geometry [21]. However, the size effects are identical as predicted by Herring's scaling laws [25].

Given the complexity of the resulting expressions for neck growth when multiple mechanisms are taken into account, numerical simulation has been useful to study the sintering behavior [26]. Nichols and Mullins [27], Easterling and Tholen [28], German and Lathrop [29] and Bross and Exner [30] among others have considered different combinations of transport mechanisms. Of particular interest are the papers of Bross and Exner [30], who combined boundary and surface diffusion, and that by Johnson et.al [31-34]. They included surface and grain boundary diffusion along with lattice diffusion from sources in the boundary and particle surface. The computer simulations have shown that boundary lines dividing the predominance regions of different mechanisms in sintering diagrams (Ashby, [35]) also depend upon particle size and heating rate [26]. Non isothermal simulations have confirmed the hypothesis of Harmer [36], that surface diffusion is minimized by rapid heating. Hwang

2. The neck growth can be described as the change of the ratio of the particle to neck radius as a function of $t^{1/n}$. "1/n" is the time exponent.

and German [37] have simulated by computer the sintering of a row of spherical particles using a method that eliminates the geometric approximations. This is achieved by incrementing the geometrical change in very small steps and calculating the neck growth for each case separately. Their results show that significant errors could result if geometrical approximations are involved. It is also shown that the rate law exponent depends on the heating rate, sintering temperature and atmosphere.

Once the initial stage is over, the geometry of the particle arrangement becomes far more complicated. Kuczynski [38,39] developed a statistical approach to the problem and hence circumvented some of the restrictions of conventional diffusion modeling. He assumes that the intermediate stage can be modeled as a solid perforated by a cylindrical pore of varying radius of total length per unit volume " L_v ", located along the grain intersections. Similarly when the pore phase becomes discrete, the final stage consists of " N_v " spherical particles per unit volume. In this case the pore may or may not reside at the grain boundary.

Diffusional modeling of the intermediate and final stages is represented by Coble's [14] treatment of the problem. He deals with densification proceeding by lattice and grain boundary diffusion separately. The first step in the formulation of the model is the choosing of a suitable grain shape, in this case a tetrakaidecahedron is selected with the continuous pores running along the triple grain junctions. The pore phase is ap-

proximated to a circular cross section. The next step is the selection of a diffusion-flux equation.

The same grain shape is retained for modeling purposes when the porosity is closed and assumed to be located at four grain junctions. Coble shows that if the pore is small enough as compared to the diffusion distance, then the pore radius is the geometric feature which is rate controlling. This assumption allows for the selection of an analytical solution to the diffusion problem. These models predict that the rate of density change is constant if the diffusion coefficient and the grain size are constant. The decrease in densification rate with discontinuous grain growth is predicted in terms of pore spacing and grain size.

Cranmer et.al. [10,41] utilized a final stage sintering model to analyze the effects of particle size, green density and controlling transport mechanisms (coarsening vs. densifying) on the final density of SiC powder compacts. They used the same model to approximate the behavior from the onset of the intermediate stage.

For the surface diffusion-grain boundary diffusion pair the final density will depend lightly on the green density but will be rather insensitive to initial grain size; depending on the ratio of surface to grain boundary diffusivities the body will reach theoretical density or approach it asymptotically. A similar case applies for the pair: vapor diffusion-lattice diffusion. Evaporation/condensation-grain boundary diffusion,

evaporation/condensation-lattice diffusion and vapor diffusion-grain boundary diffusion, all behave similarly in that there is a grain size below which coarsening is small and sizes beyond which full densification is approached only asymptotically. Another combination, surface diffusion-lattice diffusion, behaves rather differently; full density can always be approached and the larger the starting grain size the less coarsening there will be. With this pair the final grain size and sintering time to full density are rather independent of starting grain size.

Greskovich and Lay [43] studied grain growth in porous Al_2O_3 compacts and proposed that it can be viewed as the growth of necks between particles followed by rapid migration of the boundary into the smaller one. They used Nichols and Mullins [27] model for neck growth by surface diffusion and arrived at the conclusion that surface diffusion controlled grain growth should be approximately dependent on $t^{1/4}$, as observed in their experiments. SiC powder compacts seem to have an asymptotic approach to some final density close to theoretical [16,42]. Green density does have an effect on final density though it is small [43] because a lower green density is almost offset by increase in shrinkage, fig.1, and the final density does not seem to be strongly linked to the starting grain size [44]. Furthermore, undoped powders increase in grain size as a function of $t^{1/4}$ [1], which is predicted to be the time exponent for a surface controlled coarsening system [45,27], while B and

C doped SiC powders show a $t^{1/3}$ time dependence of grain growth [8].

Coarsening does not seem to be a strong function of initial grain size [44], SiC powders with starting diameters of 0.49 and 0.18 microns ended up with average grain sizes of about 20 and 8 microns and had fractional size increments of 40% and 44% respectively. Discontinuous grain growth does seem to be influenced by the size distribution in the initial powder [44].

6.1.2. Liquid Phase Sintering

Liquid phase sintering can be considered to be a particular case of reactive sintering [46] in which a liquid forms out of the solid phases at the sintering temperature. A simple case is represented by a system of two components just above a eutectic temperature and away from the eutectic composition which forms a solid solution in equilibrium with a liquid. Real systems are frequently more complex and a variety of reaction products can occur and among them a liquid may be formed. Liquid phase sintering is characterized by rapid densification beyond a certain temperature and is usually faster than its solid state counterpart. Phenomenological descriptions of the process [47-49] include three sequential steps: 1.-) a rearrangement stage, 2.-) a solution precipitation process and 3.-) a coalescence stage. Later, Kingery [50] derived a kinetic treatment for the process predicting different densification

rates for the different stages. During the rearrangement process a sharp density increase occurs due mostly to a increase in the packing efficiency. A liquid is formed and the solid particles flow under the influence of capillary forces. Depending on the liquid volume fraction a certain maximum amount of densification will result directly out of this stage, at approximately 35 vol% of liquid all the void space will be occupied by it after rearrangement. The amount of densification decreases linearly down to no rearrangement at no liquid content. It is concluded [50] that the linear shrinkage during this stage will depend on t^{1+y} where y is a small fraction, so $(1+y)$ is close to unity. During the solution-precipitation stage the shrinkage is predicted to be a function of the one-third power of time and of the minus four-thirds power of the initial particle radius if the rate limiting step is the diffusion of matter out of the contact area. During this stage densification is achieved by transport of material away from the contact area so center to center approach takes place. The driving force is the increase in chemical potential of matter in the contact area due to enhanced solubility caused by the contact point pressure exerted by the capillary forces and surface tension of the liquid. The coalescence stage is considered to be the end of the (liquid phase) sintering process. Further densification is likely to proceed by a solid state sintering process, if at all. It has been pointed out [51] that the termination of the solution-precipitation process in

practical systems may be due to other factors such as gas entrapment, gross imperfections and fabrication flaws, etc., as opposed to simple intergrowth of favorably oriented grains and the formation of a skeleton. The different stages of liquid phase sintering are not sharply separated from each other [52] and considerable interaction between the different processes may take place. Necks may form during heat-up and some dissolution process has to occur before accommodation can take place, or perhaps, before melt penetration between particle grain boundaries causes or permits secondary rearrangement [53]. It has been proposed [53] that in the presence of a particle size distribution Ostwald ripening with shape accommodation may account for the observed densification during the solution-precipitation stage as opposed to contact flattening. For this to be the case, growing particles would have to be continuously rearranged so space can be efficiently filled to allow densification to take place. There are three conditions that a liquid formed at the sintering temperature would have to meet in order to considerably enhance the sintering rate. 1.-) Some solubility for the solid phase so it can serve as a transport medium, 2.-) viscosity low enough so dissolution takes place at a substantial rate and 3.-) the liquid must wet the boundaries in order to allow enhanced transport between the solid phase "facets". Solid:solid contacts have to be avoided since matter transport in these places will proceed at rates typical of the solid state process. The amount of liquid

necessary in order to promote densification was formerly thought to be in the range of 10 to 30 vol%, but densification has been shown to proceed with as little as approximately 1 vol% liquid [54] in some metal systems.

6.2. Dopants

SiC does not densify in the absence of dopants [55]. B, Al and C are the most commonly used, although oxide additives have been successful in promoting densification in SiC powders [10,40]. Both groups will be discussed, but separately.

6.2.1. Boron, Aluminum and Carbon

Carbon added without boron does not lead to densification and the compact usually undergoes a considerable amount of coarsening [55,1,40,41], shrinkage is generally negligible; some samples even show expansion. Surface area reduction kinetics indicate that coarsening takes place via a surface controlled mechanism [1]. In the absence of boron, the loss of surface area and consequently the driving force for densification, begins to occur at approximately 250 °C lower (1250 °C vs. 1500 °C) and at a faster rate (at constant heating rate) than if the compacts have had both B and C added [15,1], fig.2. Coblenz [56] performed grain boundary grooving experiments on Si under conditions where surface boron segregation was ob-

served by Auger spectroscopy and found boron to reduce the diffusivity in the surface of B-doped silicon by a factor greater than 10^3 . Hence boron's primary role seems to be the inhibition of surface transport, so as to prevent coarsening in the early stages of sintering.

SiC powders doped with B and C have been found to shrink, in the early stages, following a $t^{1/3}$ time dependence³ when fired in He at temperatures ranging from 1700 to 1900 °C [8], suggesting that densification is taking place via grain boundary diffusion.

On the other hand, boron addition in absence of carbon results in a fine microstructure which has undergone small shrinkage (less than 5%) [3,55,1], the minimal loss of surface area is evident, however the compact did not densify. SiO₂ is an excellent diffusion barrier on SiC and is greatly responsible for SiC's outstanding oxidation resistance [12,57,58]. During firing SiO₂ could be incorporated into the boundaries and act as an impediment to matter transport along them and thus hinder densification. At constant boron content the grain sizes are usually larger in the C poor compositions than in the C rich ones, this could be due to the elimination of Si from the powders which is suspected to promote coarsening [15] by vapor transport or to grain boundary pinning by the carbon particles. So it is presumed that the role of carbon is to rid

3. Shrinkage can be described as the fractional change in a linear dimension as a function of $t^{1/n}$.

the powders of the oxide layer and to react with any excess silicon present or formed during sintering [3] and in consequence permit densification to take place. Excess carbon is undesirable because it will coalesce and form porous inclusions, lowering the final density.

The oxygen content of the powder has been acknowledged to be of concern and low oxygen contents are regarded as requisite for high densities to be achieved [59,7,55,6,60], fig.3. The contamination is in the form of a SiO_2 film coating the powder particles, frequently originating from the manufacturing of the powders. Empirical limits on oxygen content have been proposed and range from <0.1% to <1% [61,62]. Several methods for removal of this oxide have been devised and range from acid baths and solvent rinses [55,3] to heterogeneous gas-solid reactions [60]. Nevertheless, a few tenths of a percent are usually left after treatment. The presence of oxygen in the starting SiC powders has proven to be detrimental when sintering with the aid of boron and carbon is intended [7]. It has been found that the ratio of the difference of the content of free carbon available minus oxygen content divided by the free silicon content of the powders has to be close to unity for densification to proceed, fig.3.

The form that boron takes once added (either as elemental B or B_4C) is not well established. It has been proposed that it enters solid solution in the SiC particles since its segregation on the boundaries or surfaces has not been found by high

resolution Auger spectroscopy studies in B and C doped samples [63,64] or by autoradiography techniques [65]. Boron solubility in SiC is reported to be about 0.1 W% at 2500 °C [66-70]. On the other hand, lattice parameter measurements suggest that boron is not significantly soluble in SiC at least up to 1950 °C [71] so it is expected to be part of some (extremely thin) intergranular phase (<1 nm), perhaps B₄C (see page 27).

Al added in the presence of carbon does not promote densification as effectively as do B and C [13,12,11]. Al is known to segregate to grain boundaries in SiC [72] and Al is more soluble in SiC than B, 0.26 w% at 1800 °C and 0.5 w% at 2000 °C. Furthermore, Al is thought to substitute for Si in the SiC lattice [73] while for B, Electron Spin Resonance (ESR) studies indicate it substitutes for C [74] and lattice parameter measurements suggest that it enters SiC into the Si site [75,68,69]. Strain and bond stability considerations indicate B may substitute for either Si or C. If the vacancy population of either Si or C is being depleted by the presence of an additive [76,77], this may explain the discrepancies in the literature.

Even though Al and B both act as acceptors in SiC [70-82], the defect complexes they generate may be different, giving different effects in the transport properties of SiC. By segregating to the boundary Al may impede matter transport along the boundary. Finally, Al seems to promote the beta to alpha transformation, stabilize the 4H polytype, fig.4, and to

enhance basal growth. By this means it appears to promote the evolution of a more homogeneous microstructure than that of SiC materials sintered with only B and C [8,3,4].

On the other hand, if Al is used in conjunction with B and C additions its effect seems to be favorable: it suppresses the exaggerated grain growth of the alpha SiC platelets [5]; lowers the sintering temperature [13]; and increases the final density over that obtained with either additive alone (B and C or Al and C). In this case the Al addition seems to promote the formation of a liquid, identified by X-ray analysis as $Al_8B_4C_7$ by Shinozaki et.al. [4].

Liquid was reported to exist around the $Al_8B_4C_7$ composition over 1800 °C [8,4]. The absence of grain boundary phases in Al doped SiC [13] could be explained by transient liquid phase sintering (Al absorbed) when the additions are in very small amounts. Given the known solubilities of B and Al in SiC this seems to be feasible. At greater amounts of Al [4] the boundary phase persists in the sintered compact.

6.2.2. Metal Oxides

Oxide additives have been successfully used for SiC pressureless sintering. Yttrium and Aluminum oxides obtained from the reactions of $Al(OH)_3$ with HCl and $Y(OH)_3$ with HCOOH respectively, were used as additives [10] to densify beta SiC powders: densities of up to 96.8 %th were obtained with equal

weight mixtures of both additives (5 w% each). Yttrium oxide alone does not enhance densification, while aluminum oxide does, although the mixture gives better results than either one alone. The sintered pieces show a considerable amount of Y_2O_3 left in the compact by X-ray diffraction. In contrast no Al_2O_3 was found. Aluminum remaining in the fired compacts did not correlate with the amount of the addition, so it is suspected to be sublimating, while the yttrium content did correlate well with the amounts added. In a different study [9] Al_2O_3 added to submicron beta SiC powder gave densification to about 98 %th density. The sintering time at 1950 °C is greater than 20 hs to achieve final density and the final microstructure consists almost completely of 4H SiC in an interlocked structure with no exaggerated grain growth. The oxide was added as high purity Alumina in amounts of 2 w% and 15 w%. The fracture strength is over twice as high (930 Mpa) as other current sintered alpha SiC bodies (350 Mpa). This increased strength is attributed to the slightly elongated grains present and thus to the tortuous path the crack propagation front is forced to follow during fracture. The fracture in the denser compacts occurred by a mixture of intergranular and transgranular fracture paths. The addition of Al_2O_3 to hot pressed SiC is reported to result in increased fracture strength over pressureless sintered SiC [85], though in this case the increase in strength is attributed to a crack deflection process which involves the reduced fracture resistance of the intergranular phase. The

sintering mechanism is proposed to proceed via liquid phase even though no intergranular phase was detected. Aluminum content in the compact decreases with sintering time corresponding to the total weight losses.

6.3. Boundary Phases

6.3.1. Boron, Aluminum and Carbon Doped SiC

The existence of a grain boundary phase in sintered SiC has been proposed by several investigators, in Al, B and C doped bodies [4,13] an intergranular phase identified by energy dispersive X-ray analysis, Electron Energy Loss Spectroscopy (EELS) and Selected Area Diffraction Patterns (SAD) patterns has been reported. In B and C doped sintered SiC powder compacts the existence of a intergranular phase is proposed to exist and control densification [8,71] and lattice fringe electron micrographs suggest a possible thickness of less than 0.8 nm [71]. In most cases, though, no intergranular phase is found [64,63,55] and its existence may be closely related to the amounts of additives used.

Calculations show that if an addition of 0.6 w% of boron plus excess carbon were to react and form a boron rich compound (e.g. B_4C) with 100% efficiency and there were no losses, a coating of about 8 nm would result on grains grown to a size of 5 microns, assuming of course that no B was dissolved into the

grains, this case could have been easily detected. This suggests that either B is dissolving into the grains (B solubility is approximately 0.1W% at 2500 °C [66-70], see page 23) or it is been lost to the gas phase. Since the measured solubility of boron in SiC can not account for the removal of the boron phase from the boundaries its loss through the gas phase seems a definite possibility. Weight losses for a typical composition (0.6 w% B plus 0.8 w% C) amount to a few tenths of a percent (<1%) for beta powders and a few percent for alpha powders (<3%). Oxygen has not been detected in samples sintered under normal conditions (B+C and Al+C inert gas or vacuum atmosphere) [63].

Further evidence from the mechanical behavior of B and C doped SiC sintered compacts at elevated temperatures suggests that no boundary phase is present that affects the macroscopic mechanical behavior of the body. Strength in SiC sintered bodies is maintained up to temperatures of 1400 °C without degradation [57, 12].

6.3.2. Al₂O₃ Doped SiC

Al₂O₃ has been used as sintering [11,9] or hot pressing [86,87] aid for SiC in several investigations. A boundary phase was clearly present in hot pressed samples of SiC with additions of Al₂O₃ [87]. Since the powders contained a considerable amount of impurities and electron microprobe analysis

showed aluminum and oxygen to be present in the boundary phase, it was proposed to be an alumino-impurity-silicate that formed the liquid. The SiC powder used contained a minimum of 1.2 wt% free carbon. The geometry of the interfaces between the SiC grains and the boundary phase indicated clearly that it was liquid during hot pressing and wetted and partly dissolved the SiC grains. In another work [86] no explicit mention is made of a boundary phase, although the toughness of the finished, hot-pressed product was reported to be increased when Al₂O₃ was used as hot pressing aid, presumably by a crack deflection mechanism affected by a boundary phase.

Al₂O₃ has been used as an additive for sintering of SiC with varying degrees of success. Al₂O₃ plus carbon were found to produce excessive weight losses and low final densities [11]. It was concluded that this was not a suitable form of Al addition to SiC for sintering purposes. A different result was obtained with Al₂O₃ addition to SiC as a sintering aid when Suzuki et. al. [9] reached final densities over 98 %th after firing 20 hrs at 1950 °C. Their powders were quoted as being over 98% SiC, so free carbon was most likely present. A liquid phase sintering mechanism is concluded to be responsible for densification and although a boundary phase is acknowledged to exist during sintering, it is claimed that none remains in the final product. No attempt to characterize the boundary phase was made. This is unlike Y₂O₃ and MgO aided liquid sintering of Si₃N₄ which always has a grain boundary film mostly of amor-

phous phase [57] remaining in the final product and in contrast to the notion that liquid phase sintering will, for practical sintering intervals, leave a film on the grain boundaries [88,89]. Nevertheless, the possibility remains of a disappearing boundary phase which after the long sintering periods, may diffuse away, volatilize, and/or be partly absorbed into the solid.

6.4. Phase Relations

In the following sections the literature will be reviewed concerning information on the most important systems involved in the present work. These include the $\text{Al}_2\text{O}_3\text{-C}$, $\text{Al}_2\text{O}_3\text{-Al}_4\text{C}_3$, $\text{SiC-Al}_4\text{C}_3$ and $\text{Al}_2\text{O}_3\text{-CaO}$ systems. Furthermore, the system Si-B-C is reviewed.

6.4.1. $\text{SiC-Al}_2\text{O}_3\text{-C-CaO}$ System

With no CaO present, it is of interest to know the sequence of events that will take place in a mixture of SiC , Al_2O_3 and C .

It has been reported [90] that the reduction of Al_2O_3 with carbon in presence of SiC will proceed initially as in the reduction with carbon alone. Thus the study of the $\text{Al}_2\text{O}_3\text{-C}$ system is relevant. Furthermore, Al_2O_3 reacts with carbon to form Al_4C_3 [91,92] up to a point when the equilibrium between

Al_2O_3 and Al_4C_3 becomes predominant [93], thus the equilibrium between Al_2O_3 and Al_4C_3 is relevant.

Al_4C_3 is known to react with SiC to form Al_4SiC_4 [94] so there is the question of whether it will preferably react with Al_2O_3 or SiC. So the binary SiC- Al_4C_3 is relevant. Furthermore, in this binary exist the only ternary compounds in the system Al-C-Si [90,95-97].

With the addition of CaO to a SiC- Al_2O_3 -C mix, it is important to know at which temperature a given composition will form a liquid in the system Al_2O_3 -CaO, so this binary is relevant.

6.4.1.1. Al_2O_3 -C

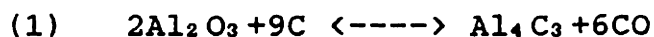
Al_2O_3 is known to react with carbon and readily form Al_4C_3 [91-93]. It is in the Al_2O_3 - Al_4C_3 system that, subsequently, the aluminum oxycarbides are formed.

When Al_2O_3 is heated together with carbon under one atmosphere of argon a vigorous reaction occurs near the Al_2O_3 melting point [93] ($T_{\text{mp}}=2040^\circ\text{C}$) with the evolution of large amounts of CO. If the Al_2O_3 content is greater than about 80 W% a fluid liquid forms at about 100°C below the alumina melting point. When the mix is held briefly at approximately 2000°C , the initially strong CO evolution greatly diminishes and virtually stops after a few minutes, even though carbon was still available to the melt. Either equilibrium was not being achieved or carbon was not a primary participant. The latter

was found to be the case when additions of Al_4C_3 were used along with carbon. When enough Al_4C_3 was used there was no attack on the graphite crucible containing the mix and there was no CO evolution. It was apparent that the relevant system was $\text{Al}_2\text{O}_3\text{-Al}_4\text{C}_3$, and it is assumed that the cessation of CO evolution (with carbon still present) is related to the decrease in oxygen activity in the ternary liquid.

6.4.1.2. $\text{Al}_2\text{O}_3\text{-Al}_4\text{C}_3$

Al_4C_3 was synthesized from aluminum and carbon by Moissan [98] and later by other researchers from Al_2O_3 and carbon [91,99,100]. Equilibrium pressure measurements on the latter system ($\text{Al}_2\text{O}_3\text{-C}$) [91] were in agreement with a reaction such as:



When low melting was observed in the system $\text{Al}_2\text{O}_3\text{-Al}_4\text{C}_3$ at around 13 mol% of the carbide [101] at approximately 2000 °C, an oxycarbide of unknown composition was thought to exist, based in the absence of the yellow aluminum carbide. A condensate in one of the experiments [99] appeared to be aluminum carbonyl ($\text{Al}_4\text{C}_3\text{O}_3$) from the results on weight gain on ignition and total acid soluble aluminum.

Foster et.al. [93] in their work with the system $\text{Al}_2\text{O}_3\text{-Al}_4\text{C}_3$

proposed a phase diagram for the binary, depicted in fig. 5. In this diagram two oxycarbides, $\text{Al}_4\text{O}_4\text{C}$ and Al_2OC are found at 20 and 50 mol% Al_4C_3 respectively. The only eutectic found in the system is between the Al_2O_3 and the $\text{Al}_4\text{O}_4\text{C}$ phase at approximately equal molar contributions from each compound.

Al_2O_3 melts at about 2040 °C and the Al_4C_3 decomposes before reaching its melting point. The melting point of Al_4C_3 has been estimated to be approximately 2700 °C under the saturation pressure of its elements [93]. On the other hand it has been reported to completely decompose at about 2200 °C under one atmosphere of inert gas [102].

$\text{Al}_4\text{O}_4\text{C}$ was readily synthesized from mixes containing up to 35 W% of Al_4C_3 and identified as the white glasslike matrix of the solidified melts. Foster et.al [93] reported the X-ray powder data for this compound. Single crystal x-ray data shows that the structure is orthorhombic, with unit cell dimensions of $a = 9.23$ a.u., $b = 8.64$ a.u., $c = 5.77$ a.u. and $\text{vol.} = 460$ a.u.³, containing two molecules of $\text{Al}_4\text{O}_4\text{C}$. The calculated density is 2.65 gr/cm³. $\text{Al}_4\text{O}_4\text{C}$ seems to melt incongruently at about 1890 °C into Al_2OC +liquid.

Al_2OC was difficult to prepare from equimolar mixtures of Al_2O_3 and Al_4C_3 ; only small amounts of Al_2OC formed up to temperatures just below the Al_2O_3 melting point. However, when a mixture of one part $\text{Al}_4\text{O}_4\text{C}$ to three parts Al_4C_3 was held at 1800 °C for 10 hs the reaction was complete to form Al_2OC . X-ray data for the compound is reported by Foster et.al [93].

The structure is hexagonal, with $a = 3.19$ a.u. and $c = 5.09$ a.u. and contains one Al_2OC molecule per unit cell. The calculated density is 3.00 gr/cm^3 .

6.4.1.3. $\text{SiC-Al}_4\text{C}_3$

SiC and Al_4C_3 are the only compounds in the binary systems Si-C and Al-C , respectively [101-106]. In the join between these two compounds lie the only ternary phases in the system Al-Si-C . The existence of Al_4SiC_4 was first reported by Barczak [108] and it is well documented [107]. On the other hand, $\text{Al}_4\text{Si}_2\text{C}_5$ has been reported and X-ray data provided by Inowe et.al [97] but its existence was not confirmed in the work of Kidwell et.al [95]. A new ternary compound (Al_8SiC_7) was recently reported by Kidwell et.al [95].

Al_4SiC_4 was first described by Barczak [95], who synthesized the compound from equimolar mixtures of Al_4C_3 and SiC fired in a sealed carbon container at 1870°C for 10 min. The phase thus obtained was termed beta Al_4SiC_4 . Alpha Al_4SiC_4 was successfully synthesized from a 4:1 mol mixture of aluminum and silicon in the presence of excess carbon. The formation of Al_4SiC_4 from aluminum-silicon melts with carbon is best described in the work by Dorner [109] and Viala et. al. [96]. Barczak provided X-ray powder diffraction data on both aluminum-silicon carbides. Alpha Al_4SiC_4 was described [95] to be yellow in color, with a hexagonal unit cell ($c = 10.80$ a.u.,

axial ratio 1.65) which contains three molecules and has a calculated density of 3.028 gr/cm³. Inoue et. al. [97] synthesized Al₄SiC₄ from 1:1 mol Al₄C₃-SiC mixtures heated in a graphite die to 2000 °C under argon for a few minutes. They report different cell parameters for the compound (a =3.2772 Å, c =21.676 Å). Behrens and Rinehart [110] synthesized Al₄SiC₄ from stoichiometric mixtures of Al, Si and C at 1800 °C during 2.5 hs. They found that Al₄SiC₄ vaporizes incongruently into Al(g), SiC(s) and graphite. Using Knudsen effusion mass spectrometry they investigated the vaporization thermodynamics of Al₄SiC₄. The enthalpy change for the reaction Al₄SiC₄ <--> 4Al(g)+SiC(s)+3C(s) at 298 °K was calculated to be 1455 ± 79 kJ/mol. The standard enthalpy of formation of Al₄SiC₄(s) from the elements calculated from the vaporization enthalpy and the enthalpies of formation of Al(g) and SiC, at 298 °K, is -221 ±85 kJ/mol. The standard enthalpy of formation of Al₄SiC₄ from its constituent carbides (Al₄C₃ and SiC) is calculated to be 38 ± 92 kJ/mol, (298 °K). Schoennahl et.al. found in their study of the ternary Al-Si-C that Al₄SiC₄ readily decomposes according to the reaction Al₄SiC₄ <--> 4Al(g)+Si(g)+4C(s) above approximately 1700 °C, under one atmosphere of argon.

Al₄Si₂C₅ was synthesized by Inoue et.al. [97] using stoichiometric amounts of SiC and Al₄C₃ packed into a graphite die and heated up to 1970 °C in an argon atmosphere. The specimen was maintained at that temperature for a few minutes and then cooled rapidly. If slow cooling took place Al₄Si₂C₅

would not form, but Al_4SiC_4 and SiC would be formed instead. X-ray crystallographic data is provided by Inoue et.al [97] along with the hexagonal cell parameters, ($a = 3.2512 \text{ \AA}$ and $c = 40.1078 \text{ \AA}$). The existence of $\text{Al}_4\text{Si}_2\text{C}_3$ was not confirmed in the study by Kidwell et.al [95], but nevertheless $\text{Al}_4\text{Si}_2\text{C}_3$ did appear in the investigation of Viala et.al. [96] of the Al-SiC system. Viala et.al could not synthesize $\text{Al}_4\text{Si}_2\text{C}_3$ below $2200 \text{ }^\circ\text{K}$. Below that temperature they obtained Al_4SiC_4 and SiC as reaction products between Al_4C_3 and SiC . They report that the reaction between aluminum and SiC to form Al_4C_3 is a very fast one, since they detect the product after only five minutes of the process in vacuum at only $1150 \text{ }^\circ\text{K}$. Their calculated value for the Gibbs free energy for the formation of Al_4SiC_4 from its constituent elements is $-30,678.5 + 5.403T \text{ J/mole}$.

Al_8SiC_7 is a newly found compound in the system Al-Si-C. Kidwell et.al synthesized the compound from the high purity elements by repeated firing and grinding, twice at $1870 \text{ }^\circ\text{K}$ (2 hs each time) and finally 2 hours at $2270 \text{ }^\circ\text{K}$ under one atmosphere of argon. The compound is stable between room temperature and $2270 \text{ }^\circ\text{K}$, but decomposes between 2270 and $2370 \text{ }^\circ\text{K}$. The crystal symmetry is hexagonal, with $a = 3.3127 \text{ \AA}$, $c = 19.242 \text{ \AA}$ and $V = 182.9 \text{ \AA}^3$. Al_8SiC_7 is proposed to decompose according to the peritectic reaction $\text{Al}_8\text{SiC}_7 \leftrightarrow \text{Al}_4\text{C}_3 + \text{C} + \text{L}$, where the liquid phase is a graphite saturated Al-Si alloy. The dissolved carbon in the liquid alloy at $2270 \text{ }^\circ\text{K}$ precipitated as Al_8SiC_7 and Al_4SiC_4 upon cooling and the remaining liquid alloy

solidified as the Al-Si eutectic at 850 °K.

6.4.1.4. Al_4C_3 - Al_2O_3 vs. Al_4C_3 -SiC

It seems clear from the review above that in the presence of carbon, Al_2O_3 will react with it to form Al_4C_3 irrespective of the presence of SiC. The formation of Al_4C_3 from Al_2O_3 and carbon is a fast reaction, with vigorous CO evolution. No reaction of those characteristics has been described for Al_4C_3 with SiC. Thus it is presumed that in a mixture of SiC, Al_2O_3 and carbon, the predominant reaction will be between Al_2O_3 and carbon to form Al_4C_3 . Subsequently, aluminum oxycarbides ($\text{Al}_4\text{O}_4\text{C}$) will be formed in the system Al_2O_3 - Al_4C_3 , assuming of course that the correct proportions of Al_2O_3 and C are observed.

Yokokawa et.al. [90] studied the reduction of Al_2O_3 in the presence of silicon compounds in a argon atmosphere at 2070 and 2170 °K with powder X-ray diffractometry. They observed that in an Al_2O_3 , SiC and carbon mixture ($\text{Al}_2\text{O}_3+\text{C}+2\text{SiC}$) the Al_2O_3 was reduced by the carbon in the same manner as if SiC were not present. Although the existence of SiC in the mixture was observed to promote the formation of Al_4SiC_4 only after a few hours at 2070 °K. The simultaneous addition of SiO_2 ($2\text{Al}_2\text{O}_3+3\text{SiO}_2+12\text{C}$) enhanced the formation of $\text{Al}_4\text{O}_4\text{C}$.

They found the $\text{Al}_4\text{O}_4\text{C}$ to have a induction period of about one hour, which they attribute to a competition between CO

evolving reactions and the gas phase saturation of a aluminum rich vapor species so nucleation of Al_4O_4C is possible. Kikuchi et.al. [111] found no formation of Al_4O_4C in the reduction of Al_2O_3 with carbon under a CO atmosphere.

Once past the incubation period, Al_4O_4C formation is very fast [90] and quickly becomes the primary component second only to SiC in a starting mixture such as $Al_2O_3 + C + 2SiC$. Al_2O_3 and carbon concentrations decrease sharply and the Al_4SiC_4 concentration is always slowly increasing but much smaller than that of the oxycarbides.

Weight losses were initially fast and attributed to the reaction of Al_2O_3 with carbon (all carbon was practically gone after one hour). A second weight loss stage was very slow and attributed mostly to the volatilization of the oxycarbides and its reaction with SiC.

Al_2OC appears to have a shorter induction period than Al_4O_4C . Thus in addition to the nucleation from the gas phase of Al_4O_4C , the solid-solid reaction of Al_2OC with Al_2O_3 is proposed to be a possible path for the formation of the Al_4O_4C . Actually, Al_2OC was found to disappear simultaneously with the substantial formation of Al_4O_4C while Al_2OC remained where Al_4O_4C was not detected.

The volatilization of the oxycarbides corresponds to a slow weight loss process. It appears [90] that Al_4O_4C evaporates incongruently by developing Al_2O_3 or undergoes disproportionation into Al_2OC and Al_2O_3 . Al_4O_4C will volatilize by reaction

with SiC. Al_2O_3 evaporates incongruently by developing Al_4C_3 which forms, along with SiC, the less volatile Al_4SiC_4 . After the volatilization of the oxygen components in alumina and the oxycarbides, SiC and Al_4SiC_4 remain.

6.4.1.5. Al_2O_3 -CaO

In the Al_2O_3 rich side of the Al_2O_3 -CaO phase diagram, (fig.5b) at less than 8.38 W% CaO, liquid is formed at 1860 °C. In the same composition range under 1860 °C, a solid solution of Al_2O_3 and $\text{CaO} \cdot 6\text{Al}_2\text{O}_3$ [112,113] is in equilibrium. Between 8.38 and 21.54 W% CaO, liquid forms at 1770 °C and under this temperature $\text{CaO} \cdot 2\text{Al}_2\text{O}_3$ is in equilibrium with $\text{CaO} \cdot 6\text{Al}_2\text{O}_3$. Discrepancy exists about the first compound formed in the binary. Auriol et.al. [114] report that at 9.33 W% CaO, $3\text{CaO} \cdot 16\text{Al}_2\text{O}_3$ is formed and is in equilibrium with Al_2O_3 .

6.4.1.6. CaO as a Catalyst

The addition of CaO to SiO_2 during the carbothermic reduction of SiO_2 at temperatures between 1600 and 1800 °C has been reported by Mizin et.al.[135] to result in increased volatilization of silicon. The increase in volatilization rate is greater than a factor of 10. They show that Si is lost as SiO. CaF_2 , MgO and BaO also enhanced the loss of silicon in a similar fashion (10-15 fold increase in volatilization rate).

The loss of Si is increased as the amount of the additions is increased, up to 9W%. The silicon loss became rapid at approximately 1800 °C in the presence of the above mentioned additions. No mechanistic explanation as to how the CaO promotes the formation of the Si suboxide is given.

CaO is an effective catalyst for gasification reactions⁴ of carbon in presence of oxygen and CO₂ [136]. The work of Floess [136] shows that only when the Ca is atomically distributed and forming a cation-carbon bond are the gasification reactions catalyzed. One atomic percent Ca increases the oxygen reaction rate by almost two orders of magnitude and the CO₂ rate by almost three orders of magnitude. The catalyst tends to depress the activation energies by approximately 15%.

The two most widely accepted explanations for a chemical mechanism by which the catalysts enhance the reaction rates are: 1) the electron transfer, and 2) the oxygen transfer mechanisms. In the electron transfer model it is proposed that a bonding "Pi" electron is withdrawn by the catalyst, thus weakening an existing bond and inducing the formation of a new one (i.e. with oxygen or CO₂). The oxygen transfer mechanism proposes that the catalyst undergoes oxidation-reduction cycles, transferring the oxygen onto the substrate.

4. Gasification reactions of carbon in the presence of O₂ or CO₂ involve the reaction of the carbon with them giving the formation of CO₂ and 2CO respectively.

The chemical mechanism by which Ca increases carbon reactivity was not determined by Floess.

6.4.2. SiC-B-C System

The Si-C binary phase diagram was first reported by Nowothony et.al. [115]. The only compound in the binary is SiC and it forms by a peritectic reaction such as: $C+L \leftrightarrow SiC$. The reported peritectic temperature scatters from 2540 ± 40 °C (Dolloff, [103]) to 2830 ± 40 (Scace et.al., [105]). Intermediate values such as 2700 °C by Nowothony [115] and 2760 °C by Kiefer [116] have been reported. Kieffer's value of 2760 °C is commonly accepted under one atmosphere of inert gas.

The first B-C binary phase diagram was reported by Ridgway [117]. Subsequently, a number of different compounds have been reported to exist in the binary. Samsonov et.al. [118] concluded from his study that three compounds existed in the B-C binary, $B_{13}C_2$, B_4C and $B_{33}C_{67}$. On the other hand, Dolloff [121] and Elliott [119] claimed that only B_4C existed and had a wide solution range. The melting point of B_4C is 2450 °C. The eutectic temperatures in the system are: 2375 °C in the C- B_4C side and 2075 °C in the B_4C -B side.

The SiC- B_4C section of the ternary Si-B-C is one of the most frequently studied since it involves two compounds (SiC and B_4C) of considerable industrial importance. One of the early studies on it was done by Tone [120]. Secríst [70] reported a

eutectic at 70 W% B₄C at a temperature of 2300 ± 20 °C. The existing SiC phase in equilibrium below the eutectic was found to be alpha SiC at less than 50 W% B₄C and beta SiC at greater concentrations. The mutual solubility of the carbides was estimated to be less than 2 W% from the microscopic examination of the solidified melts. Earlier, Kalinina et.al found the SiC-B₄C to be a quasi-binary and reported a eutectic at 65 W% of the B₄C which formed a liquid at 2070 °C. Two regions of solubility were established at this temperature; one was an alpha SiC solid solution containing about 4 W% B₄C the other a B₄C solid solution with approximately 15 W% beta SiC. Later, Shaffer [67] confirmed the eutectic composition but found it to melt at 2245 °C and claimed that the solubility of boron in SiC was not to exceed 0.2 W%. Although not quantified the solubility of Si into B₄C was reported as extensive. Boron saturated alpha SiC and a solid phase having the general formula of B₁₂(Si_xC_{3-x}) are stable in contact with a liquid above the eutectic temperature.

Dolloff [121] reported that the high carbon section of the Si-C-B system (C-B₄C-SiC) had a ternary eutectic of composition 15 at% Si, 30 at% C and 55 at% B at a temperature of 2250 °C. Furthermore, Portoni et.al. [122] and Samsonov et.al. [123] reported the existence of two ternary compounds: B₃Si₂C₂ and B₅SiC₂.

Osamura et.al. [124] concludes from their analysis of the Si-C-B system that the eutectic reaction in the ternary men-

tioned previously is correctly described as peritecto-eutectic and that the B_4C -SiC and SiC-B sections of the ternary are not able to be treated as exact quasi-binaries since any tie line protrudes from them.

The conflicting data above would seem to confirm that the system SiC- B_4C cannot be treated as a quasi-binary; perhaps there is also an impurity (or impurities) as an additional component that confuses the issues.

6.5. Mechanical Properties

Silicon carbide has some outstanding intrinsic properties that make it a strong candidate for high temperature structural applications. Among others, it has an excellent oxidation resistance and high strength. SiC polycrystalline fibers reach strengths of 4×10^5 psi (2.7 Gpa) [125] while single crystal whisker SiC has shown strengths up to 4×10^6 psi (27.6 Gpa) [126]. SiC sintered bodies (with additions of B and C) exhibit lower strength (average 5.2×10^4 psi (0.36 Gpa) at room temperature) and 4.7×10^4 psi (0.32 Gpa) at 1370 °C [12]. The addition of Al_2O_3 to SiC powders was reported with strengths up to 1.08×10^5 psi (0.75 Gpa) at room temperature and 5.07×10^4 psi (0.35 Gpa) at 1400 °C. The calculated theoretical strength of SiC is of 6.7×10^6 psi (46.3 Gpa) [127].

In every instance the strength achieved has been controlled by the size, concentration and type of flaws present in the

finished body [126,9,12]. The most typical and detrimental flaws are large pores and inclusions which frequently can be traced back to the processing stages (agglomerates, large voids etc.) and/or the form and distribution of additives (C rich clusters, B rich clusters, glassy boundary phase). Powder fabrication techniques have been developed, powders of fairly uniform size distribution, fine size and high purity [128] are available. These could prevent the kind of inhomogeneities just mentioned, if the proper fabrication procedures are followed.

7. Experimental Procedures

7.1. System SiC-B-C

7.1.1. SiC Powders

In this section all the SiC powders used in the study of the system SiC-B-C are characterized and identified (SiC powders used in the system SiC-Al₂O₃-CaO are described separately, see page 50), in the following sections they are referred to by these ID names. Five different powders, two beta-SiC and three alpha-SiC, were used. The beta powders were GE3 and GE5, alpha powders were ALFA #2, ALFA #14 and ALFA #1, refer to table 1.

7.1.1.1. Alpha Powders

There were two starting alpha powders made by the Acheson process. All the "ALFA" series of powders derive from commercial grade 1500 grit SiC from Carborundum Co., while powder N24 was from Norton 600 grit. With the exception of ALFA #4 all powders were ground and leached. Most powders were milled with steel balls using a vibromill. Different solvents and additives were added to improve dispersion which are listed in table 1. Removal of impurities and residues from the milling

process was accomplished by leaching the powders with HF, HNO₃ and HCl, then the powders were rinsed with water and methanol and finally dried. This initial powder processing was reported elsewhere [129]. Specific surface area measurements were made on the powders using the single point BET method, see table 1.

Powder ID	Surface area	Milled	Solvent	Additive
ALFA #1	6.0 m ² /g	Y	Hexane	Glycerol trioleate
ALFA #2	5.4 "	Y	N-amyl alcohol	Glycerol trioleate
ALFA #4	3.5 "	N	----	----
ALFA #11	5.4 "	Y	Kerosene	Fish oil
ALFA #14	5.5 "	Y	Ethanol	Sodium Oleate
ALFA #16	4.5 "	Y	N-amyl alcohol	Glycerol trioleate
N24	4.9 "	Y	Water	Nitrocellulose

Table 1
Starting alpha SiC powders used in the system SiC-B-C.

The alpha powders used for this study had a wide size distribution with irregular morphology and sharp edges.

7.1.1.2. Beta Powders

The beta powders, listed in table 2, were made by the gas phase reaction of SiCl₄ and CH₄ in an arc by General Electric Co. Some excess carbon is presumed to be present from the decomposition process (SiCl₄+CH₄ <--> SiC+4HCl).

The beta powder GE3 was supplied with 0.6 W% boron and 0.8

W% carbon. Presumably, the boron was added as fine amorphous powder. The carbon may have been residual from preparation. The GE5 powder had approximately 0.8 W% carbon as supplied, see table 2. No detail was available as to the form of the carbon addition. These powders were freeze-dried with benzene after the additions were made.

Powder ID	Surface area (m ² /gr)	Boron (W%)	Carbon (W%)
GE3	8	0.6	0.8
GE5	12	-	0.8

Table 2
As-received beta SiC powders used in the system SiC-B-C

The morphologies, average sizes and size distributions of the alpha and beta powders are quite different. Alpha powders are milled during fabrication and so they have sharp edged, irregular particles and a wide size distribution. Beta SiC powders are finer in the average than alpha SiC powders and have a narrower size distribution.

7.1.2. Powder preparation and Processing

7.1.2.1. Doping

Additional doping was done on beta powder GE5 by dispersing 0.6 W% B as B₄C, (surface area approximately 7 m²/gr). The al-

pha powders were doped with boron either in the form of B₄C or fine amorphous boron (surface area 22 m²/gr) totaling in any case 0.6 W% boron. Carbon was added to the alpha powder as lamp black carbon (surface area approx. 18 m²/gr) totaling 0.8 W% C. When B₄C was used as the source of boron 0.77 W% was introduced with carbon and boron yields of 0.17 W% and 0.6 W% respectively, see table 3.

With the exception of sample series "J", (powder Alfa-5, see table 8), all the other powders used in the system SiC-B-C had 0.5 W% oleic acid added as a pressing and forming aid.

ID	Ground starting powder	B ₄ C W%	Boron W%	Carbon W%	Pellets series
Alfa-1	ALFA #2	-	-	0.8	H
Alfa-2	"	0.77	(0.6)	(0.17)	D
Alfa-3	"	-	0.6	0.8	E
Alfa-4	"	0.77	(0.6)	0.63(0.8)	I
Alfa-5	ALFA #14	-	0.6	-	J
Alfa-6	ALFA #1	-	0.6	0.8	K
Alfa-7	"	0.77	(0.6)	0.63(0.8)	L

NOTE: The number in parenthesis is the total content of the element added to the powder.

Table 3
Prepared alpha SiC powders used in the system SiC-B-C.

The additions were made by dispersing all the powders and the oleic acid in alcohol and then freeze drying to obtain uniform compositions.

For the alpha powders dispersion was achieved by use of an ultrasonic cell disruptor (Heat systems, 200 W max. output) for

3 min.. in a 90% T-butyl and 10% T-amyl alcohols mixture. For the beta powders the mix was dispersed in T-amyl alcohol and vibromilled for 30 min. with approximately 30% volume solids using tungsten carbide balls. The slurries were sprayed into liquid nitrogen and the solvents evaporated in a vacuum dryer. The pure T-amyl alcohol dispersion vacuum drying time was about 3 times as long as the 90% T-butyl-10% T-amyl mixture. It took about 12 hs for the 90%-10% mixture to get the powders ready to press.

7.1.2.2. Cold Pressing

Samples were pressed from alpha and beta silicon carbide powders in a hardened steel, 5/16" diameter die at approximately 26 kpsi; oleic acid was used to lubricate the die walls.

7.1.2.3. Firing

Firing took place in a carbon tube furnace at 1900, 2000, 2100 and 2200 °C for one hour, with the exception of samples A3, A4, E6, I6, K7 and L7 which were fired for 6 hs and sample K10 fired 48 hs (see table 8). The sintering atmosphere was argon flowing at 0.1 scfh. A 2.0 scfh flow was used to investigate the influence of gas flow rate on final density, shrinkage and weight loss in samples J1, J2, J7 and J8. The

temperature was measured by an optical pyrometer through the upstream quartz window of the furnace to avoid clouding of the window affecting the readings, and controlled with an accuracy of about ± 10 degrees.

The samples were placed in the center of the hot zone of the furnace in a covered graphite crucible and usually buried in the same powder from which the samples were made. The crucible laid horizontally and had two small holes, one in each end. Separate crucibles were used for samples with and without boron.

In most cases two samples were fired at the same time (labeled TOP and BOT, for upstream and downstream locations in the crucible, respectively, when only one sample was fired it is labeled TOP-UN).

The samples were heated to 400 to 500 °C, held 30 to 60 minutes and then rapidly heated to temperature. The gas flow rate during initial heat-up was approximately 2 scfh. The maximum heating rate was approximately 133 °C/min. so reaching final sintering temperature in about 15 min. where the sintering period starts. A lower heating rate of about 80 °C/min. was used to investigate the influence of heating rate on properties, (samples B3 and B4, see table 8).

7.2. System SiC-Al₂O₃-CaO

7.2.1. SiC Powders

The silicon carbide powder used in the investigation of the system SiC-Al₂O₃-CaO was manufactured by LONZA and denominated as Carbogran UF 15. It is an alpha powder, mostly of the 6H polytype. The specific BET surface area of these powders is approximately 15 m²/gr.

The chemical analysis of the powder provided by the manufacturer follows:

Impurity	%
Free Carbon	0.39
Free Silicon	0.12
Total Oxygen	0.81
Total Aluminum	0.05
Total Iron	0.04
Total Titanium	0.01
Total Sodium	0.007
Total Tungsten	<0.01
Total Cobalt	<0.01
Total Magnesium	0.006
Total Calcium	0.006
Total Nitrogen	0.009

Table 4
Impurity content in
LONZA Carbogran UF 15
SiC powder.

Among the main impurities, carbon and oxygen stand out because of their role in the sintering process as will be described later and because its almost linear increase with specific surface area. Fig. 6 depicts the situation (impurity increase vs. surface area) for some LONZA Carbogran alpha SiC powders. The size distribution of the powder is graphically illustrated in fig.7.

7.2.2. Additives

7.2.2.1. CaO

CaO was added in a fine powder form. The powders used were manufactured by Mallinckrodt. The lot chemical analysis for the CaO powder is presented in the following table:

Impurity	%	Impurity	%
Ammonium Hydroxide	0.020	Barium	0.005
Calcium	0.05	Chloride	0.010
Iron	0.01	SiO ₂	0.04
Sodium	0.5		

Table 5
Main impurities in the CaO powders.

7.2.2.2. Al₂O₃

The ultrapure Al₂O₃ powders were supplied by the Reynolds Co. and are denominated by the manufacturer as HP DBM Al₂O₃ without MgO.

7.2.3. Powder Preparation and Processing

After weighting the powders in the selected proportions for given samples, they were ultrasonically dispersed with a ultrasonic cell disruptor (Heat Systems, 200 watt maximum output) set at 60 to 70% of its total output power for a period of 6 minutes. A sapphire tip was used in all the dispersions. Water cooling of the beaker was required to dissipate the heat generated during the process.

The solvent was a mixture of nine parts t-butyl alcohol plus one part t-amyl alcohol. In a previous study [130] this system proved to be an effective dispersion and freeze drying medium for SiC powders. The powders had no lubricants or binders added to them. Immediately after the powders were dispersed they were sprayed over a liquid nitrogen reservoir using an art spraying gun kit. Subsequently the frozen powders were set to vacuum dry into a Virtys vacuum dryer under less than 100 micron of pressure. It took approximately 12 hours to completely drive all the solvent out of the powders. After drying

the powders are ready to be pressed.

7.2.3.1. Cold Pressing

The samples were pressed in a hardened steel die 5/16 ths of an inch in diameter with an applied load of 2000 to 3000 lb., depending of the powders' fabrication characteristics. As no binders were used in any of the powders (used to study the SiC-Al₂O₃-CaO system) some compositions were more difficult to fabricate than others. The pellets so formed were marked on the top with a carbide-tipped scribe and weighed immediately. Typically, the resulting density of the samples was about 55% of theoretical (55 %th). Given the finess of the powders and the lack of a lubricant/binder, end-capping and general fabrication flaws were difficult to eliminate.

7.2.3.2. Furnace

For firing purposes a horizontal carbon tube furnace was used. Samples were fired at temperatures ranging from 1760 to 2210 ± 20 °C during periods of 5 minutes to 15 hours. The temperature of the hot zone was controlled within approximately 10 °C of the nominal temperature.

7.2.3.3. Firing Atmosphere

The firing atmosphere always consisted of a flowing inert gas, either argon or helium. Both gases were ultrapurified and analyzed to contain less than 1 ppm oxygen. Helium was used in runs where high densities were expected in order to minimize pore gas entrapment effects. Gas flow rate was always kept at 0.1 scfh in the carbon tube with a internal diameter of 1.25 inches.

7.2.3.4. Heating Rate

Given the fact that the powders did not contain a binder or any organic additives no burnout period was observed during heat up. A typical heating rate was approximately 35 °C/min. until the desired final temperature was reached. The firing time reported is the time the sample was held at the firing temperature; no adjustments were made to compensate for heat-up effects.

7.2.3.5. Sample Arrangement

The samples were always placed inside a graphite crucible. The crucibles were always pre-fired empty at 2210 °C for one hour to rid them of most of the impurities and contaminants

before they were used . The dimensions of the crucibles are of approximately $3/4$ of an inch long by $9/16$ ths of an inch outside diameter. The lid and bottom of some of the crucibles had a $1/16$ th of an inch hole, these are called "open" crucibles. When only the lid was drilled they are called "semi-open", and, with no holes, they are called "closed" crucibles.

7.2.3.6. Packing Powders

Packing powders were used in most runs to affect the weight changes in the sample due to evaporation. The packing falls into either one of three categories: 1.- No packing, 2.- "regular packing", the pellet is packed on the same powder out of which it is made and 3.- "Enriched packing" of which two types were used. Packing powder denominated 10-7 contained 10 parts of SiC powder and seven parts of Al_2O_3 . Packing powder 10-7-0.7 contained, in addition, 0.7 parts of CaO.

7.2.3.7. Temperature Measurement

The temperature was measured with a Leads and Northrup optical pyrometer. The pyrometer calibration was verified against the reading from a type S platinum-rhodium thermocouple up to $1700\text{ }^\circ\text{C}$: no appreciable difference between the readings was observed. Correction for the quartz window losses were made by measuring the temperature of a cavity with the optical

pyrometer with and without a window up to 1700 °C. The correction needed to account for the losses averaged approximately +10 °C. This correction is applied to all the temperatures reported in this work.

7.2.4. Density Measurement

The density of individual samples was measured by one or more of the following methods.

7.2.4.1. Geometric Determination

By this means the density of the samples was routinely determined before and after firing and referred to as green and fired or final density respectively. The only cases in which this method was not used involved excessive deformation of the pellet. Fabrication flaws resulted in some cases in hour glass shaped samples and/or concave ends or the sample was simply damaged or broken, all cases in which a cylindrical approximation for the sample shape would not be appropriate. The volume of the sample was calculated assuming cylindrical shape using the average of several measurements made of each dimension (diameter and height) using a digital readout micrometer with resolution of 0.001 inch. The weight of the samples was measured by using a microbalance with resolution of 0.0001 grams, each sample was weighed at least twice and the average

of those weights used. The density was then determined by dividing the weight by the volume. Typical uncertainties in the linear dimensions measurements were approximately 1% and about 0.1% for the weight measurement, this yields a uncertainty on the calculated density of approximately 3%. Densities determined by this method tended to be underestimated since the flat faces of the micrometer did not account for the depression of an hour glass shape or concavity of the ends yielding a larger volume than the corresponding to the sample weight and its true density. A typical underestimate would be of about 5 %th under the value obtained by image analysis (pore count, see next section). The density of SiC was taken as 3.21 gr/cm² in all cases.

7.2.4.2. Pore Count

SEM micrographs taken of polished surfaces were used to determine the fraction of the area intercepted by porosity. This fractional porosity was interpreted directly as fractional void volume, so the density of the sample was calculated to be 100% minus void-volume%.

Samples were polished down to a 1/4 of a micron finish with diamond paste. Pullouts or noticeable pore rounding was not observed in samples with densities greater than about 85 %th polished in this manner.

A Magiscan Image Analyzer was employed for pore area

measurement. Reproducibility of the area measurement was typically within approximately 2% of the resulting density out of the same micrograph. The main source of discrepancy between measurements of the same image lies in the segmentation procedure by means of which a threshold on the gray level is set permitting the analyzer to discriminate between pore area image and solid area image. Image analysis determination of pore area was not useful for samples with complex surface topography such as fracture surfaces and heavily etched samples.

7.2.4.3. Pycnometry

Pycnometric density determination proved to be a difficult and irreproducible way of measuring densities compared to the methods already discussed. Some of the encountered difficulties were: a) weight drift due to evaporation of residual solvent on the pycnometer joints, b) bubbles and c) irreproducibility (the error bar on the density value was never smaller than approximately 6% for the same sample in repeated measurements).

7.2.5. SEM and STEM

7.2.5.1. SEM: Sample preparation

Samples were observed as either fractured, polished, or

polished and etched surfaces. The instrument used was a Cambridge SEM model 1000A equipped with a Kevex dispersive x-ray elemental analyzer.

Fracture surfaces were obtained by merely breaking up the sample with a small ball head hammer immediately before observation. Polished sections had to be sliced off from the fired pellet with a Buehler low speed diamond saw. Typically the thickness of the slice would be approximately 0.030 in.. The slices were then ground and polished with 30, 6, 1 and 1/4 micron diamond paste with a Buehler automatic polisher. When etching was required a 1 part KOH, 1 part $K_3Fe(CN)_6$, two parts water solution, boiling, was employed for 6 min. This solution, reveals general microstructural features, polytypic boundaries, and stacking faults. Care must be exercised when etching samples which are known to contain a boundary phase, since overetching of this phase might easily occur.

All samples to be observed in the SEM were coated with approximately 50 to 100 Å of gold by evaporation to avoid charging effects.

7.2.5.2. STEM: Sample Preparation

STEM samples were sliced, ground, polished and ion-thinned. Slicing was done in the same way as for SEM samples but thinner slices were cut (approximately 0.010 in. thick). Grinding and polishing proceeded in the same way as for SEM samples.

7.2.5.3. X-Ray Elemental Analysis

Energy dispersive x-ray elemental analysis was performed on samples with both SEM and STEM. The two main issues to consider were elemental resolution of the analysis and detectability of light elements.

Elemental resolution is roughly estimated to be approximately from 0.1 to 1at% (the higher resolution for heavier elements) of the element to be detected. The SEM was not capable of detection of light elements (no element below atomic number 9) while the STEM was equipped with a windowless detector and so, is capable of detection of carbon and oxygen.

8. Results

8.1. System SiC-B-C

Tables 8 and 9 summarize the results obtained regarding density, weight loss and linear shrinkage in the system SiC-B-C.

8.1.1. Alpha vs. Beta SiC powders

There are two main differences in the observed sintering behaviour between alpha and beta SiC, these are: 1.-) upon sintering, the beta powders practically reach theoretical density [16], alpha SiC powders do not, but approach a limiting density lower than the theoretical, 2.-) beta powders exhibit a much lower weight loss than do the alpha powders. On the other hand, both powders showed expansion in the absence of boron additions, though the effect was slightly greater with the alpha powders. With B and C doping, the shrinkage is about in the same range for both powders. Alpha powders were usually easier to press than beta powders.

8.1.2. Effect of Boron and Carbon Additions

In general, at the higher temperatures, the greater the

carbon content the greater the final density, weight loss and shrinkage.

8.1.2.1. On final density

The absence of boron leads to no densification as expected. The alpha powders seem to have a limiting maximum final density, samples "K7" and "L7" were fired at 2200 °C for 6 hs reaching only 86.4 %th and 87.22 %th dense respectively. Sample K10 fired for 48 hs reached 85.5 %th (see table 8) while the beta powders reach almost full density [16]. On the alpha powder, for samples with boron, the larger the carbon content the denser the sample.

8.1.2.2. On linear shrinkage

The samples with excess carbon but without boron ("C" and "H") did not shrink and nearly all showed expansion. The addition of boron alone (no C) led to little shrinkage (<5%).

8.1.2.3. On weight loss

Weight loss is one of the least understood issues. 1.-) Weight losses were always greater than the total amount of volatiles and additives in the powder. 2.-) Weight loss seems to be quite independent of boron content, although there is

some indication that the absence of boron leads to a greater weight loss. 3.-) The average weight losses are greater as the firing temperature is increased. At higher temperature ($T > 2000$ °C) the weight loss follows a more definite trend: weight loss increases with carbon content for samples with boron.

8.1.2.4. Form of addition

For the alpha powders, the form of the boron additions (amorphous B powder or B_4C) did not cause a substantial difference in final densities between identical powders (same total B and C doping levels) fired under identical conditions. Depending on the particular batch, one form (of boron addition) seems to produce a higher final density than the other.

8.1.3. Effect of gas flow

Another observed feature is that for most runs with beta powders the up-stream sample showed greater weight loss and greater final density than the sample located at the downstream side of the crucible. For alpha SiC this effect was not observed.

A interesting result is observed in samples "J" fired at different gas flow rates; samples J1 and J2 were fired $3/4$ of the time at 2.0 scfh. of argon then lowered to the usual 0.1 scfh. for the rest of the run. J3 to J6 were fired under 0.1

scfh. and finally J7 and J8 were fired under 2.0 scfh. of argon. Samples fired at 1900 °C and high flow were considerably denser than identical samples fired at the same temperature and lower flow rate. Samples fired at 2000 °C did not show the same sintering enhancement with a high flow rate.

8.1.4. Effect of heating rate

The heating rate has some influence on the final density as well as on the weight loss and shrinkage. B3 and B4 were fired at a lower heating rate and became more dense than B5 and B6 that were fired at the standard (higher) heating rate.

8.2. System SiC-Al₂O₃-CaO

Table 10 summarizes the results (fired density, shrinkage and weight loss) obtained with different powder preparations within the system SiC-Al₂O₃-CaO. Table 10 also presents the relevant experimental parameters for all the samples in this system.

8.2.1. Final Density vs. CaO content

The final density of the fired samples was found to be a function of the amount of CaO added to the powder. The total amount of the additions was kept constant and only the ratio of

CaO to Al₂O₃ was varied. Increases in the fired density is brought about by very small additions of CaO, the fired density achieves a maximum and then drops gradually.

Fig.8 depicts the situation (fired density vs. CaO content) for samples containing increasing amounts of CaO and fired at 2110 ± 20 °C in a semi-open crucible for 5 hours and packed in its own powder. In this case the maximum density is achieved at about a weight ratio of CaO to Al₂O₃ of 0.02 for a total addition of 8 W% with respect to SiC.

Given the preceding observation, most of the experiments are focused on near optimal conditions and so, restricted to small amounts of CaO, typically a weight ratio of 0.04 CaO to Al₂O₃ was used.

8.2.2. Final Density vs. Packing Powder

For a given firing time and temperature, the final density of the samples depends on the immediate environment surrounding the sample. A typical environment would consist of a graphite crucible, which can be open, semi-open or closed, and a packing powder, usually the same composition as that out of which the sample is made.

The lowest density was obtained from samples in open crucibles and with no packing powder. The highest density is achieved by samples fired in closed crucibles and packed in

powders containing an excess of additives as compared with the sample itself. An intermediate case is a sample fired in a semi-open crucible packed in its own powder.

Higher densities were always achieved by samples which contained CaO in addition to Al_2O_3 , but otherwise identical. Fig.9 illustrates this dependence of final density on packing method.

Since proper packing favors the achievement of high densities, the focus of the investigation was on samples packed either on its own powder or in enriched powders and fired in semi closed or closed crucibles.

8.2.3. Final Density vs. time

The behavior with time at temperature for samples with and without CaO added differs considerably. The samples which contain CaO in addition to Al_2O_3 reach its highest density in time periods of less than an hour at temperatures of 1835 ± 20 °C and higher. There is no appreciable change in density for these samples when fired for longer times at temperature. On the other hand, samples which do not contain CaO but only Al_2O_3 reach densities lower than those containing CaO for the same period of time at temperature. This difference is narrowed for longer times and higher temperatures, as illustrated in table 6.

sample ID	time (hs)	temperature (± 20 °C)	density (%th)
h4	1	1960	97.3
T8	1	1960	91.2
h3	5	2110	98.5
T7	5	2110	97.4

Table 6
Fired density vs. temperature in
samples with and without CaO.

Samples without CaO improve in final density with longer firing times and higher temperatures but only to asymptotically approach those with CaO added as well.

8.2.4. Final Density vs. Temperature

The densification behavior of samples with and without CaO added to the powder and fired for 1 hr. in helium is illustrated in fig.10. The main distinguishing feature among both curves is the sharp increase in final density shown by samples which contained CaO at about 1835 ± 20 °C. The resulting densification is virtually complete, but localized flaws exist that are attributed to non-optimum preparation and fabrication of the powders. Samples made of SiC powders with no CaO added increase gradually in density as the temperature is increased, staying always lower than those which contained CaO. Fig.10 presents samples with a CaO to Al₂O₃ weight ratio of 0.04 identified as samples series "h" versus samples series "T"

containing Al_2O_3 only.

8.2.5. Linear Shrinkage and Weight Change

Linear shrinkage was measured as the percent change in a linear dimension of the sample (usually the diameter). Weight change can be either positive (weight gain) or negative (weight loss).

Alpha silicon carbide (LONZA UF-15, see table 4) powder compacts with a specific surface area of $15 \text{ m}^2/\text{gr}$ with no intentional additions fired in a open crucible with no packing powder at $2150 \pm 20 \text{ }^\circ\text{C}$ loose approximately 1.5 % of its green weight (sample "R2", see table 10).

Linear shrinkage was found to be proportional to the increase in density upon firing only if volatilization was allowed for the vapor species resulting during the firing process. Fig.11 illustrates this relationship. If volatilization is inhibited either by rich packing and/or firing in a closed crucible, shrinkage will be inhibited too. Figs.12a and 12b present the linear shrinkage and weight change of sample series "T" and "h" as a function of firing temperature. Series "T" samples contain Al_2O_3 only while series "h" samples contain Al_2O_3 plus CaO in a weight ratio of CaO to Al_2O_3 of 0.04. All samples in fig.12a and 12b were fired in a closed crucible and packed in enriched powders, with the exception of the data points at $1960 \pm 20 \text{ }^\circ\text{C}$ which were fired in a semi-open crucible

(see table 10). Shrinkage and weight loss seem to compensate for one-another as to keep a certain density constant (see fig.10). Figs. 12 and 10 are to be compared to observe the relationship between shrinkage, weight loss and fired density. A different level of activity in the vapor phase between samples "T" and "h" can be inferred by comparison of figs 12a and 12b. Fig 12b is a continuous curve with no sharp step at any temperature over the range studied. The variability in weight loss observed in figs.12 is due to different conditions of gas tightness of the different crucibles used. The crucible deteriorates considerably in just a few runs due to reaction of aluminum vapor species with the graphite out of which they are made, as evidenced by the difficulty to open them after some runs and the severe roughing up in the inside, thus affecting the gas tightness of the crucibles run after run. Table 7 compiles the weight changes along with the linear shrinkage of sample series "T" and "h".

ID	T (±20° C)	t (hs)	Packing powder	closed/ open	Linear shrinkage %	Weight change %
h1	2100	5	h	SO	21.15	-13.59
h2	2100	5	h	SO	20.32	-12.86
h3	2100	5	h	SO	21.15	-12.85
h4	1950	1	10-7-.7	SO	24.32	-11.90
h5	1800	1	10-7-.7	C	7.52	+ 6.58
h6	1850	1	10-7-.7	C	14.27	+17.03
h7	1900	1	10-7-.7	C	12.26	+27.66
h8	1750	1	10-7-.7	C	6.56	+10.02
h9	1925	1	10-7-.7	C	12.48	+24.80
h10	1875	1	10-7-.7	C	11.32	+29.90
h11	1825	1	10-7-.7	C	16.35	+ 5.34
h12	1775	1	10-7-.7	C	12.19	- 2.53

T1	1950	5	NO	O	8.16	-10.09
T3	2000	5	NO	O	9.31	-10.41
T4	2100	5	h	O	18.11	- 9.91
T6	2100	5	j	SO	20.13	- 9.27
T7	2100	5	T	SO	20.26	-10.27
T5	1950	5	10-7	SO	23.10	- 9.84
T8	1950	1	10-7	SO	18.11	- 2.60
T9	1800	1	10-7	C	9.06	+ 3.25
T10	1850	1	10-7	C	13.63	+ 0.68
T11	1900	1	10-7	C	17.12	- 1.10
T12	1750	1	10-7	C	3.20	- 4.36

Table 7
Shrinkage and weight change for sample series "h" and "T".
(Positive weight change=weight gain).

8.2.6. SEM: Microstructure

SEM was used to assess the amount and shape of the porosity present in the sintered specimens as well as the general microstructural features such as grain size and shape, fracture surfaces, voids, some grain boundary features and other structural defects.

8.2.6.1. Porosity

All porosity encountered in samples fired at 1835 ± 20 °C or beyond for one hour or more was closed and disconnected, regardless of its CaO content. All pores observed were at grain junctions, so no porosity was observed at the planar boundaries or within the grains. The porosity as quantified by image analysis scaled accurately with density determined by some other means (geometric or Archimides) in the same samples.

8.2.6.2. Grain Size

The addition of CaO to Al₂O₃ doped SiC samples tended to inhibit grain growth. For long times and high temperatures the samples containing CaO had smaller grain size than those lacking it. Fig.13 shows a pair of micrographs of identical samples (T7 and h3) being different only in the content of CaO. Sample T7 (fig 13a) contains no CaO while sample h3 (fig 13b) does in a CaO to Al₂O₃ weight ratio of 0.04. Both samples were fired at 2110 ± 20 °C for 5 hours in helium in a semi-open crucible and packed in its own powder. Fig.13a has a grain size larger than fig.13b by a factor of about two.

Grain shapes in samples containing CaO are more equiaxed and platelike grains were never observed. In contrast, aspect ratios of 4:1 were not uncommon in samples which did not con-

tain CaO, refer to fig.13.

8.2.6.3. Fracture surfaces

The fracture surfaces always exhibited both transgranular and intergranular fracture modes regardless of the CaO content, temperature, or time. Nevertheless, a shift towards preferential intergranular fracture was observed as the firing temperature decreased and packing powder was enriched. Fig.14 shows micrographs of fracture surfaces of samples fired under the different conditions mentioned above.

8.2.6.4. Voids

Void formation took place in all samples fired at 2110 ± 20 °C with or without CaO and irrespective of the amount of CaO added. The voids are in the form of connected cavities which resemble "wormholes". Fig.15a and fig.15b present micrographs of such samples fired at 2110 ± 20 °C in argon for five hours, the first contained Al₂O₃ but no CaO. The second has CaO in addition to Al₂O₃ in a weight ratio of 0.04. The interior of the cavities showed a different microstructure than the bulk of the sample, consisting mostly of faceted grains which, by EDAX was found to contain Si and C and a spectra indistinguishable from surrounding SiC material. So, it is presumed to be simply SiC. Fig.15c shows the interior of one such cavity taken from

a sample containing a CaO to Al₂O₃ weight ratio of 0.08 fired at 2110 ± 20 °C for five hours in argon.

8.2.6.5. Grain Boundaries

The apparent thickness of the boundary phase, as observed in the polished and etched samples, seemed to increase as the packing was enriched. This feature was encountered regardless of the CaO presence, although it was more pronounced when CaO existed in the packing powder. The etching procedures were the same for all samples. Figs.16a, 16b, 16c and 16d depict different etched samples fired at various temperatures and under different packing conditions. The samples in figs.16a and 16d were packed in its own powder, while samples in figs.16b and 16c were packed in enriched powders.

8.2.6.6. General Features

Anisotropic etching of stacking faults was observed within some of the SiC grains as well as preferential attack depending on the grain orientation. These features are all illustrated in fig.16a.

8.2.7. SEM: Energy Dispersive X-Ray Analysis

EDAX analysis on the samples was used to explore gross com-

positional features. It was observed that Ca persisted in the samples in every case, although its concentration was close to the limit of elemental resolution of the instrument. A Ca peak was observed for the samples which had CaO added to them. All samples analyzed, with and without CaO added, showed a distinct aluminum peak, though the Al peak was always somewhat higher in the samples which had CaO added to them. The peak height relationships are all taken in reference to the silicon peak and when a peak is said to be higher, it is meant that its ratio to the Si peak height is greater. Figs.17a and 17b illustrate EDAX spectra of samples with and without CaO added, fired under similar conditions. No information could be obtained regarding carbon and oxygen since its detection is beyond the capabilities of the instrument.

8.2.8. STEM: Microstructure

Fine microstructural detail and semiquantitative elemental analysis was possible to obtain with this instrument. Two representative samples, "h6" and "T11", were studied. Sample "T11" contained 6 W% Al₂O₃ while sample "h6" had CaO added in a weight ratio to Al₂O₃ of 0.04. They were fired in helium for one hour at 1860 and 1910 ± 20 °C, respectively. Both samples were packed in enriched powders and fired in closed crucibles. As can be observed in fig.10, both samples are located at the "knee" at the beginning of the high density plateau correspond-

ing to this particular firing time and conditions (enriched packing, He atmosphere, closed crucible, etc.).

8.2.8.1. Grain Size

Sample "h6" presented a larger grain size than "T11", which is in contrast with the observations in the SEM on samples "h3" and "T7" fired at 2110 ± 20 °C for five hours in argon, packed in its own powder into a semi-open crucible. Fig.18 presents two general area micrographs illustrating the different grain sizes. The equivalent spherical diameter of the starting powder is of about 0.1 microns.

8.2.8.2. Grain Shapes

Grains with no corners (mostly rounded) are characteristic of sample "h6", in contrast with the grains of sample "T11" which are of more polygonal shape. Refer to fig.18.

8.2.8.3. Grain Boundary Phase

The net amount of boundary phase was greater in the sample containing CaO than in the sample with only Al₂O₃ added.

In the CaO containing sample the intergranular phase had retracted to the grain junctions and formed clearly observable pockets. Nevertheless, a continuous grain boundary phase

remained between the grains as evidence of existence of a wetting phase during firing. Fig.19 shows a grain boundary (overfocused and underfocused) illustrating the presence of a boundary phase. From the micrographs, the thickness of the boundary phase can be estimated to be about 10 Å.

The sample with no CaO added did show a continuous grain boundary phase that appears to wet the boundaries, though the total amount is considerably less than in the sample with CaO. The formation of pockets at grain junctions was not as extensive as was the case with "h6". Again, the thickness of the boundary phase can be estimated to be approximately 10 Å, refer to fig.20. In some instances steps were observed on the boundaries, a feature not observed with CaO added, (refer to the section on elemental analysis).

8.2.9. STEM: Microdiffraction

The boundary phase observed in sample "h6" was found to have both crystalline and amorphous regions. Fig.21 shows a triple grain junction amorphous pocket imaged with the amorphous ring of its diffraction pattern so only the amorphous sections are highlighted. Due to the smaller amount of boundary phase in sample "T11" a microdiffraction pattern of the (planar) boundary phase could not be obtained, but amorphous regions were found at triple grain junctions.

Fig.22 presents an underfocused image of a grain boundary in

sample "T11" showing a boundary phase separating the two adjacent SiC grains. Fig.19 shows a boundary in sample "h6" with under and overfocus images to show contrast with the surrounding grains.

Lattice fringe images were obtained from SiC grains in both samples, in every instance, the fringes did not reach the adjacent grain but terminated in contact with an intermediate boundary phase, as illustrated in fig.22 for sample "T11". Identical observations were made in sample "h6".

8.2.10. STEM: X-Ray Elemental Analysis

Both "T11" and "h6" samples have a similar boundary phase composition. Aside from the strong silicon peak, the boundary phase always contained aluminum, oxygen, carbon and calcium. The calcium peak in sample "T11" was less than that from sample "h6" but nevertheless was present in all boundary phase spectra.

8.2.10.1. Sample "h6"

A triple grain junction for "h6" is shown in fig.23 and a crystalline pocket with a precipitate along with its spectra obtained from sample "h6". Fig.24 presents a pocket with some structural features; it was not possible to obtain compositional detail out of the different structures within the pocket

but only overall spectra. The pocket was found to be crystalline. Fig.25 presents some additional spectra obtained from other pockets, chosen at random within the sample.

Spectra from the SiC grains was very consistent and the variation in the ratio of the peak heights is due to preferential absorption of the softer x-ray signals from lighter elements, i.e. carbon, by thicker sections.

Some amorphous regions were observed and its spectra was usually rich in carbon, followed in intensity by silicon, oxygen and aluminum, fig.26 shows the pocket region along with the corresponding spectra.

8.2.10.2. Sample "T11"

The composition of the grain boundaries in sample "T11" was similar to that encountered in sample "h6". All boundaries contained silicon, carbon, oxygen, aluminum and calcium. The ratio of the carbon peak height to the silicon peak height was always greater in the boundary phase. Fig.27 shows a triple grain junction accompanied with the spectra corresponding to the boundary phase and the neighbor grains, note the light fringe in the underfocused boundary. Another grain boundary is depicted in fig.28 along with its spectra.

Some grains encountered happen not to be SiC at all, fig.29 shows a SiC grain neighboring a grain containing mostly aluminum and carbon, the oxygen signal is identical to that of

the neighbor grain acquired during the same time interval. The grain is presumed to be Al_4C_3 . This feature was not uncommon within sample "T11". Step structures in the boundaries were frequently observed.

ID	Powder	Temperature	Time (hrs)	Green Dens (%th)	Final dens (%th)	Shrink (lin %)	Mt loss (%)	Location	B W%	C W%

D1	Alfa-2B4CnC	1900	1.0	57.10	61.01	-0.99	-0.43	BOTTOM	0.640	0.170
D2	Alfa-2B4CnC	1900	1.0	57.09	60.97	-0.98	-0.32	TOP	0.640	0.170
D3	Alfa-2B4CnC	2000	1.0	57.09	64.51	-5.23	-2.93	BOTTOM	0.640	0.170
D4	Alfa-2B4CnC	2000	1.0	56.88	64.22	-5.01	-2.92	TOP	0.640	0.170

E1	Alfa-3B8B+C	1900	1.0	56.82	62.12	-4.59	-3.48	BOTTOM	0.600	0.800
E2	Alfa-3B8B+C	1900	1.0	56.87	62.25	-4.32	-3.28	TOP	0.600	0.800
E3	Alfa-3B8B+C	2000	1.0	57.39	74.33	-9.43	-3.25	BOTTOM	0.600	0.800
E4	Alfa-3B8B+C	2000	1.0	57.21	73.10	-8.93	-3.96	TOP	0.600	0.800
E5	Alfa-3B8B+C	2100	1.0	57.59	79.39	-11.19	-3.52	TOP-UN	0.600	0.800
E6	Alfa-3B8B+C	2100	6.0	57.51	81.38	-11.42	-3.72	BOTTOM	0.600	0.800

H1	Alfa-1+CnOB	1900	1.0	57.61	54.60	+0.95	-3.51	BOTTOM	0.000	0.800
H2	Alfa-1+CnOB	1900	1.0	57.38	54.47	+0.11	-4.17	TOP	0.000	0.800
H3	Alfa-1+CnOB	2000	1.0	57.89	54.65	+0.97	-3.83	BOTTOM	0.000	0.800
H4	Alfa-1+CnOB	2000	1.0	57.57	54.40	+0.89	-3.80	TOP	0.000	0.800

I1	Alfa-4B4C+C	1900	1.0	57.47	62.75	-4.30	-3.64	BOTTOM	0.640	0.800
I2	Alfa-4B4C+C	1900	1.0	57.44	62.68	-4.48	-3.80	TOP	0.640	0.800
I3	Alfa-4B4C+C	2000	1.0	57.72	70.12	-7.25	-3.76	BOTTOM	0.640	0.800
I4	Alfa-4B4C+C	2000	1.0	57.23	70.50	-8.27	-3.75	TOP	0.640	0.800
I5	Alfa-4B4C+C	2100	1.0	57.83	77.23	-9.40	-3.90	TOP-UN	0.640	0.800
I6	Alfa-4B4C+C	2100	6.0	57.76	80.70	-10.90	-4.16	TOP	0.640	0.800

J1 (2)	Alfa-5B8BnC	1900	1.0	57.49	60.71	-2.69	-1.98	BOTTOM	0.600	0.000
J2 (2)	Alfa-5B8BnC	1900	1.0	56.95	60.47	-3.04	-1.61	TOP	0.600	0.000
J3	Alfa-5B8BnC	2000	1.0	57.07	58.60	-1.54	-2.12	BOTTOM	0.600	0.000
J4	Alfa-5B8BnC	2000	1.0	57.28	58.69	-1.52	-2.30	TOP	0.600	0.000
J5	Alfa-5B8BnC	1900	1.0	57.08	57.88	-1.05	-2.02	TOP-UN	0.600	0.000
J6	Alfa-5B8BnC	2000	1.0	56.70	58.54	-1.10	-2.22	TOP-UN	0.600	0.000
J7 (1)	Alfa-5B8BnC	1900	1.0	56.80	53.85	-3.85	-2.03	TOP-UN	0.600	0.000
J8 (1)	Alfa-5B8BnC	2000	1.0	57.16	59.06	-1.68	-2.41	TOP-UN	0.600	0.000

K1	Alfa-6B8B+C	2200	1.0	57.73	84.11	-11.54	-1.52	BOTTOM	0.600	0.800
K2	Alfa-6B8B+C	1900	1.0	58.11	65.92	-4.63	-1.56	BOTTOM	0.600	0.800
K3	Alfa-6B8B+C	2200	1.0	57.97	85.41	-12.13	-2.07	TOP-UN	0.600	0.800
K4	Alfa-6B8B+C	2200	1.0	58.07	86.27	-12.47	-1.56	TOP	0.600	0.800
K5	Alfa-6B8B+C	2200	1.0	58.14	71.74	-7.05	-1.73	BOTTOM	0.600	0.800
K6	Alfa-6B8B+C	2000	6.0	57.98	86.39	-12.06	-1.61	BOTTOM	0.600	0.800
K7	Alfa-6B8B+C	2200	1.0	58.19	84.84	-12.06	-2.02	MED	0.600	0.800
K8	Alfa-6B8B+C	2200	48.0	57.72	85.52	-12.80	-1.86	TOP-UN	0.600	0.800
K9	Alfa-6B8B+C	2200	1.0	58.00	84.40	-11.36	-1.11	BOTTOM	0.600	0.800

L1	Alfa-7B4C+C	2200	1.0	58.00	84.96	-11.77	-1.71	TOP	0.600	0.800
L2	Alfa-7B4C+C	1900	1.0	58.23	66.27	-4.75	-1.60	TOP	0.600	0.800
L3	Alfa-7B4C+C	2200	1.0	58.39	86.64	-12.31	-1.56	BOTTOM	0.600	0.800
L4	Alfa-7B4C+C	2000	1.0	58.10	72.88	-7.57	-1.57	TOP	0.600	0.800
L5	Alfa-7B4C+C	2200	6.0	58.28	87.22	-12.94	-1.86	TOP	0.600	0.800

 slower heating rate
 (1)=high gas flow, (2)=low gas flow for first 3/4 of the time at temp

Table 8

Sintering results data for alpha-SiC powders in the system SiC-B-C.

ID	Powder	Temperature	Time (hrs)	Green Dens (%th)	Final dens (%th)	Shrink (lin %)	Wt loss (%)	Location	B WZ	C WZ
A1	GE#3	1900	1.0	56.94	63.41	-3.90	-0.47	BOTTOM	0.600	0.800
A2	GE#3	1900	1.0	57.36	64.27	-3.69	-0.54	TOP	0.600	0.800
A3	GE#3	1900	6.0	57.37	69.54	-6.74	-0.70	BOTTOM	0.600	0.800
A4	GE#3	1900	6.0	57.54	70.47	-6.38	-0.83	TOP	0.600	0.800
B1	GES+.688B4C	2000	1.0	59.71	87.53	-12.05	-0.89	BOTTOM	0.600	1.000
B2	GES+.688B4C	2000	1.0	59.81	88.68	-12.72	-1.02	TOP	0.600	1.000
B3 *	GES+.688B4C	1900	1.0	59.29	74.29	-7.47	-1.67	BOTTOM	0.600	1.000
B4 *	GES+.688B4C	1900	1.0	60.11	74.63	-6.76	-1.47	TOP	0.600	1.000
B5	GES+.688B4C	1900	1.0	59.93	66.20	-3.56	-0.84	BOTTOM	0.600	1.000
B6	GES+.688B4C	1900	1.0	60.37	66.18	-2.21	-0.89	TOP	0.600	1.000
C1	GES Plain	1900	1.0	58.32	57.34	+0.20	-1.49	BOTTOM	0.000	0.800
C2	GES Plain	1900	1.0	58.58	57.65	+0.00	-1.40	TOP	0.000	0.800
C3	GES Plain	2000	1.0	58.65	57.69	+0.19	-1.52	BOTTOM	0.000	0.800
C4	GES Plain	2000	1.0	58.48	57.37	+0.33	-1.45	TOP	0.000	0.800

*-lower heating rate
(1)-High gas flow, (2)-Low gas flow for first 3/4 of the time at temp

Table 9

Sintering results data for beta-SiC powders in the system SiC-B-C.

sample ID	fired along with	Temp. °C	time hr.	Packing	Vent ¹	Green dens. % th.	Fired dens. % th. geom.	Fired dens. % th. pore ct.	Al ₂ O ₃ -CaO wt%	% length change	% diameter change	% weight change
R2	A	2150	1.00	no	0	54	54		0 - 0	-0.80	0.00	-1.50
T1	A	1950	5.00	no	0	53	61		6 - 0	-7.35	-2.16	-10.09
T3	A	2000	5.00	no	0	50	60		6 - 0	-2.91	-9.31	-10.41
T4	h1	2100	5.00	h	0	50	86		6 - 0	-17.06	-18.11	-9.91
T5	A	1950	5.00	h	10-7	50	-	98	6 - 0	-	-23.10	-9.84
T6	j1	2100	5.00	h	10-7	50	-	98	6 - 0	-16.49	-20.13	-9.27
T7	A	2100	5.00	h	10-7	50	91	97	6 - 0	-17.21	-20.26	-10.27
T8	A	1950	5.00	h	10-7	50	91		6 - 0	-17.81	-18.71	-2.60
T9	A	1800	1.00	h	10-7	50	74		6 - 0	-10.35	-9.06	3.25
T10	A	1850	1.00	h	10-7	50	83		6 - 0	-16.15	-13.63	0.68
T11	A	1900	1.00	h	10-7	50	91	98	6 - 0	-16.18	-17.12	-1.11
T12	A	1750	1.00	h	10-7	50	58		6 - 0	-8.99	-8.20	-4.87
T13	A	1850	1.00	h	10-7-.7	50	96		6 - 0	-15.27	-15.87	-7.26
U1 ²	A	1950	5.00	no	0	51	57		6 - 0	-7.19	-8.48	-13.71
U2	v2	1900	5.00	no	0	51	58		6 - 0	-7.50	-9.28	-13.92
V1 ³	U1	1900	5.00	no	0	49	58		6 - 0	-9.64	-15.52	-23.47
V2	U2	1900	5.00	no	0	50	58		6 - 0	-10.43	-12.88	-23.13
Y1	X1	1950	5.00	no	0	53	73		6 - 2	-9.47	-15.52	-11.51
Y2	Y3	1950	5.00	Y	0	53	88	89	6 - 2	-17.03	-18.88	-12.23
Y2'	A	2150	1.00	Y	50	50	85		6 - 2	-17.09	-18.88	-12.60
Y3	Y2	1950	5.00	Y	0	53	85		6 - 2	-16.44	-18.50	-11.80
Y3'	Y4	1950	5.00	Y	0	53	85		6 - 2	-16.83	-18.50	-12.30
Y4	Y5	1950	5.00	Y	0	53	84		6 - 2	-16.28	-18.75	-15.43
Y6	Y5	1925	10.00	Y	0	53	90		6 - 2	-17.75	-20.13	-12.09
Y7	A	1800	5.00	Y	50	53	81		6 - 2	-13.57	-18.08	-11.64
Y8	b1	1900	1.00	b	50	53	80	38	6 - 2	-13.02	-16.80	-14.77
Y9	b2	1900	1.00	b	50	53	75		6 - 2	-13.38	-15.52	-14.44
Y10	g1	2100	1.00	Y	50	53	37		6 - 2	-16.51	-19.39	-10.88
Y11	g2	2100	5.00	Y	50	53	88	93	6 - 2	-	-19.39	-12.08
Y12	A	2100	0.05	Y	50	53	-		6 - 2	-	-	-
Y13	A	2100	0.10	Y	50	53	-		6 - 2	-	-	-
Y14	A	2100	0.10	Y	50	53	-		6 - 2	-	-	-
Y15	A	2100	1.00	Y	50	53	59		6 - 2	-5.78	-8.67	-13.28
b1	Y8	1925	1.00	b	50	54	82		6 - 3	-15.35	-17.79	-12.02
b2	Y9	1900	5.00	b	50	54	95		6 - 3	-13.61	-15.39	-13.71
c1	d1,e1	1930	5.00	c	50	54	87	89	9 - 3	-18.37	-20.13	-16.83
d1	c1,e1	1930	5.00	c	50	53	-	91	4.8-3.2	-	-	-
e1	c1,d1	1930	5.00	c	50	54	-	38	7.2-4.8	-	-	-
g1	Y10	2100	1.00	Y	50	53	88		7.38-0.6	-16.67	-20.51	-13.34
g2	Y11	2100	5.00	Y	50	53	89		7.38-0.6	-	-20.51	-12.37
h1	T4	2100	5.00	h	50	53	92	98	7.7-0.3	-19.17	-21.15	-13.59
h2	h3	2100	5.00	h	50	53	89		7.7-0.3	-17.60	-20.32	-12.86
h3	h2	2100	5.00	h	50	53	92	99	7.7-0.3	-19.08	-21.15	-12.85
h4	A	1950	1.00	h	50	53	99	99	7.7-0.3	-15.88	-24.32	-11.90
h5	A	1800	1.00	h	10-7-.7	50	72		7.7-0.3	-8.89	-7.52	6.38
h6	A	1800	1.00	h	10-7-.7	50	72		7.7-0.3	-8.47	-7.52	6.38
h7	A	1900	1.00	h	10-7-.7	50	95	100 ⁴	7.7-0.3	-11.53	-14.27	17.03
h8	A	1900	1.00	h	10-7-.7	50	72		7.7-0.3	-7.06	-12.26	27.65
h9	A	1750	1.00	h	10-7-.7	50	72		7.7-0.3	-7.34	-6.56	10.02
h10	A	1925	1.00	h	10-7-.7	50	94		7.7-0.3	-7.28	-12.68	24.31
h11	A	1875	1.00	h	10-7-.7	50	94		7.7-0.3	-7.13	-11.33	29.92
h12	A	1775	1.00	h	10-7-.7	50	76		7.7-0.3	-14.84	-16.35	-5.66
j1	T6	2100	5.00	j	50	53	92	97	7.84-0.1	-18.04	-21.66	-12.87

- 1.- "Vent.": under this heading are the crucible ventilation conditions. These can be:
0 = open, 50 = semi-open, and C = closed.
- 2.- LONZA UF-15 SiC powder, oxidized in air for 13 hs at 600 °C.
- 3.- LONZA UF-15 SiC powder, oxidized in air for 26 hs at 800 °C.
- 4.- With exception of local isolated flaws.

Table 10

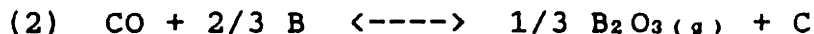
Sintering results data for the system SiC-Al₂O₃-CaO.

9. Discussion

9.1. System SiC-B-C

9.1.1. Gas transport

Samples without carbon (but with B added, series "J", see table 8) showed greater shrinkage (up to 5% at 1900 °C, 1 hr) when fired with a higher gas flow rate (2 scfh) than at the standard (0.1 scfh) flow rate. Samples without carbon fired at the standard flow rate at 1900 and 2000 °C for one hour, showed little shrinkage (<1.6%), refer to table 8. If the firing gas enters the carbon tube at one end carrying a certain amount of oxygen impurity⁵, (10 ppm maximum quoted for high purity argon), this oxygen will react with the existing carbon (i.e. tube wall) and form CO, which upon reaching the sample and accompanying packing powder, will be reduced by the boron and deposit a certain amount of carbon into the sample. If the carbon is considered not to be the limiting reactant (present in the tube, crucible etc.), then a reaction of the type:



5. The gases used later, on the system SiC-Al₂O₃-CaO, were ultrapurified and analyzed to contain <1ppm O₂.

could be taking place. Once the CO reaches the boron in the sample, reacts with it, and forms a volatile species, perhaps B_2O_3 ($T_{mp}=1860\text{ }^\circ C$), which goes into the gas stream and out of the sample. Thus the C is reduced and deposited in the sample. This would explain the enhanced densification at lower temperatures for samples with no carbon ("J") if the amount of carbon deposited at this temperature can reach more than a few tenths of a percent (0.8 W% is enough to significantly promote densification). Calculations show that for 10 ppm oxygen impurity in the firing gas flowing at 0.1 and 2.0 scfh during firing, the total amount of carbon which could be transported in one hour is approximately 8.3×10^{-4} gr for 0.1 scfh and 1.6×10^{-2} gr for 2.0 scfh. This will give 0.33 and 6.4 W% respectively, in a typical sample of about 0.25 gr. (But it is not expected that all carbon is deposited in the sample).

Thus, the slightly higher density of the pellets, made of beta SiC powder, located facing the gas stream could be accounted for by densification enhancement due to the carbon transport in the gas phase and into the sample.

9.1.2. Temperature effect

Shrinkage and weight loss seem to follow the same trend (higher carbon content leads to higher shrinkage and weight loss) at high temperature ($2000\text{ }^\circ C$). At lower temperature

(1900 °C) linear shrinkage and weight loss seem quite confusing. An explanation for this different behavior could be that the higher diffusivities of the additives at higher temperature promote a better distribution of additives so processing flaws (i.e. inhomogeneous dopant distribution) do not interfere with the net effect of the additive. Any trend seems to be easier to find and follow by experiments at higher temperatures.

9.1.3. Microstructure

Microstructural observations are consistent with the sintering results: in the absence of either boron or carbon no densification takes place. In the micrographs (fig.30) from low temperature samples (1900 °C) without carbon (in presence of boron), many fine particles are left in the sintered body (fired density 58% th), presumably from the starting powder. As the carbon content is increased the final density increases and the fine particles start to disappear, fig.31, (boron and carbon added, fired density 62% th). The disappearance of the fine particles takes place by coalescence with the existing larger particles. Carbon in the absence of boron does not cause/allow much coarsening at 2000 °C (fig.32). The addition of both B and C result in enhanced densification. Although no exaggerated grain growth was observed, elongated grains formed most of the structure at 2200 °C and were already present at 2100 °C, figs.33 and 34.

9.1.4. Form of addition

Boron additions were made in either one of two forms, B_4C or fine amorphous boron powder. The purpose of adding the boron in these two different forms was to determine whether it leads to differences in the sintered body or sintering rate.

In the B-SiC-C compatibility triangle there is no liquid below 2245 °C (which corresponds to a eutectic at approximately 30 mol% B_4C in the pseudobinary SiC- B_4C), while in the SiC-B-Si system the lowest eutectic temperature is at 1380 °C (approximately 19 mol% B) [124,131] and corresponds to a eutectic in the Si-B binary. By analyzing the phase relations in the Si-C-B phase diagram it can be seen that if a liquid is to be formed at temperatures less than 2100 °C it has to be in the boron-silicon side with a maximum of approximately 5 mol% carbon in it. No significant differences were observed as caused by the form of boron addition; this fact indicates that at least the direct melting of the boron is not an issue (boron $T_{mp}=2079$ °C) and that the presence of pure boron as opposed to B_4C is irrelevant as to the dominating sintering mechanism.

9.1.5. Powder Size Distribution

The existence of very fine particles in the starting powder was shown in the dispersion studies [130], where very fine par-

ticles were suspended for weeks after everything else had settled.

This could help explain the limiting final density of alpha powders (87% th). They may behave as a coarser powder than the BET specific surface area leads one to believe due to the large size distribution, or in other words to the existence of an appreciable amount of very large particles. If densification is controlled by boundary or lattice diffusion and coarsening by evaporation/condensation or densification controlled by boundary diffusion and coarsening by gas diffusion [40, 41], a significant portion of relatively large particles will lead to a limiting density due to the competitive character of the processes. So, it is predicted that if a narrow size distribution and finer average is obtained with alpha powders, a higher density can be achieved. Other factors such as impurity content of the powders are also important.

9.1.6. Weight loss

Weight losses were always greater than the total weight percent of volatile species added to the powders, see tables 8 and 9. Oleic acid was present at 0.5 W% in all but "J" samples (Alfa-5 powder). Despite this fact, all showed large weight losses, see table 8. For the alpha powders, the weight losses (0.3 to 5%) can not be accounted for by the volatiles added (ie. oleic acid). Weight loss varies with different alpha pow-

ders from different sources, or which have been processed in different ways (different milling time and/or media, solvent). Given the large weight losses by most of the alpha powders and comparison with those of the beta powders, losses of impurities such as oxides which form easily during the preparation (i.e. oxidation during mechanical grinding) and fabrication (i.e. carbothermic reduction of SiO_2) are suspected as being the principal source of weight loss among the alpha powders. Besides the impurities, decomposition of SiC and leaching out (i.e. oxidation and volatilization) of boron are presumed to contribute to the total weight loss.

Weight loss was always greater than the total amount of boron and carbon (and oleic acid, if used) added for all alpha powders.

9.2. System $\text{SiC-Al}_2\text{O}_3\text{-CaO}$

9.2.1. $\text{SiC-Al}_2\text{O}_3\text{-CaO}$

The fired density versus temperature results depicted in fig.10 for the system $\text{SiC-Al}_2\text{O}_3\text{-CaO}$ along with the micrographic evidence from the STEM analysis on the same system, show that a liquid is present during sintering above temperatures of approximately 1835 ± 20 °C.

Fig.10 shows a sharp increase in the fired density of sample series "h" at approximately 1835 ± 20 °C; the density increases

from about 73% of theoretical to greater than 95% th. Fig.10 has been plotted using geometrically determined densities. The equivalent densities of local patches examined, that were defect free, determined by image analysis of polished samples brings the above mentioned ranges to approximately 75% th and 100% th respectively. The sharp and substantial density increase at the mentioned temperature (1835 °C) is a typical sign of liquid phase sintering.

STEM micrographs further confirm this hypothesis. A boundary phase is found to extend into all grain boundaries observed; it appears as if the boundary was completely wetted during sintering. From the general morphology, and specially dihedral angles at grain junctions (~ 0) and rounding off of the SiC grains, the boundary phase is deduced to have been liquid at the sintering temperature.

The substantial rounding of the SiC grains suggests a high solubility of SiC in the liquid at the sintering temperature. Furthermore, considerable grain growth has taken place; the starting powder particle size was about 0.1 micron and sample "h6" fired at 1860 ± 20 °C already shows rounded SiC grains a few microns in size, fig.18a.

9.2.2. SiC-Al₂O₃

Samples in the system SiC-Al₂O₃ did not exhibit such a sharp step in the density temperature curve at any temperature in the

range studied, see fig.10. On the other hand, STEM analysis of sample "T11" ($\text{SiC} + 6 \text{ W\% Al}_2\text{O}_3$) shows evidence of a wetting boundary phase, see figs.20 and 22. Sample "T11" was fired for one hour at $1910 \pm 20 \text{ }^\circ\text{C}$ in a closed crucible. The amount of boundary phase present in sample "T11" was substantially less than the amount observed in sample "h6", fig.18b (compare with 18a) and fig.20 (compare with fig.21) with very few and small grain junction pockets. It is difficult to make an assessment of the dihedral angles at these junctions. The SiC grains in this sample are more polygonal in shape with mostly flat sides.

9.2.3. Composition of the boundary phase

A boundary phase exists in samples from both systems ($\text{SiC}-\text{Al}_2\text{O}_3$ and $\text{SiC}-\text{Al}_2\text{O}_3-\text{CaO}$). X-ray energy dispersive analysis was performed in the STEM on samples from each system and it was found that the composition of the boundary phase is strikingly similar, both contain silicon, carbon, oxygen and aluminum. The carbon to silicon ratio is greater in the boundary phase in both systems than in the SiC grains. By comparing the oxygen signal obtained from SiC grains and background with the oxygen peak from the boundary phase, it was concluded that most of the oxygen is present in the boundary phase (no oxygen in the SiC grains). There was no aluminum found, up to the detection limit of the instrument, in the SiC grains, so the aluminum signal is exclusively in the boundary phase. Silicon is

present in the boundary phase as found in the x-ray spectra, although at least part of the signal may be coming from the adjacent SiC grains, especially in the case of sample "T11" where the analysis was performed in areas of size close to the limit of the spatial resolution of the elemental analysis technique. Calcium was present in the boundary phase in both systems, in a lesser amount in sample series "T" than series "h", but always as a minor component.

9.2.4. Boundary Phase Stoichiometry

It has been found [90] that the main product of the reaction of SiC, Al₂O₃ and C at 1800 °C, under one atmosphere of inert gas is Al₄O₄C. Furthermore, in the Al₂O₃ rich side of the Al₂O₃-Al₄C₃ phase diagram [93] (fig.5) Al₂O₃ coexists with Al₄O₄C below 1840 °C. In addition, Al₄C₃ is the preferred reaction product from Al₂O₃ and C up to 2000 °C, [93,94]. If the amount of free carbon existing in the sample is insufficient to convert all of the Al₂O₃ to Al₄C₃ but only a minor amount, as is the case for the powders used in this investigation, then the system will be located at the Al₂O₃ rich side of the phase diagram and the equilibrium between Al₂O₃ and Al₄O₄C will be possible. This system forms liquid above 1840 °C, very close to the temperature at which the step in the density-temperature curve is observed. In a typical 15 m²/gr SiC powder (i.e. LONZA UF-15, see table 4) containing 6 W% Al₂O₃ there

will be approximately 0.4 W% free carbon, this amounts to 5.8 moles of Al_2O_3 per 3.3 moles of carbon. According to the reactions to be discussed later, only 2.2 moles of Al_2O_3 will be reacted to use up all the available free carbon; this will create 1.1 moles of $\text{Al}_4\text{O}_4\text{C}$. In the Al_2O_3 - $\text{Al}_4\text{O}_4\text{C}$ binary this corresponds to 23.3 mol% $\text{Al}_4\text{O}_4\text{C}$ out of a 100% Al_2O_3 - $\text{Al}_4\text{O}_4\text{C}$ solid solution.

The STEM x-ray elemental analysis data presents evidence for the existence of silicon, carbon, oxygen and aluminum at the boundary phase. The proportions of the x-ray signals from the former elements, with the exception of the silicon peak, support the notion of the existence of this phase as $\text{Al}_4\text{O}_4\text{C}$. The presence of the aluminum oxycarbides mostly as $\text{Al}_4\text{O}_4\text{C}$ as opposed to Al_2OC will be discussed later. STEM micrographs taken from sample "h6" show very pronounced rounding of the SiC grains along with some grain growth indicating considerable solubility of SiC into the boundary phase. This indicates that silicon ought to be present in the boundary phase. An issue worth bringing into consideration is the preferential absorption of the softer x-rays emitted by the lighter elements such as carbon and oxygen. Their concentrations in the sample can be much higher than the relative intensity of the signal indicates. Two sample regions of the same composition but of different thickness, in the sections examined, may have similar intensities for the high energy peaks but quite different peak heights in the soft x-ray side of the spectrum. It is because

of the former argument that semiquantitative assessments of elements concentration have to be approached with care. In general: 1.-) the concentration of the lighter elements will be higher than indicated by the strength of their corresponding X-ray energy peak. The lower the atomic number, the lower the elemental sensitivity will be, 2.-) At constant composition, the elemental sensitivity is inversely proportional to the specimen thickness, so comparison between different regions has to take this fact into account as well as preferential absorption of low energy X-rays. For a given thickness, the low energy peaks will be attenuated more than the higher energy ones. The energy corresponding to carbon and oxygen x-ray peaks are 0.16 and 0.42 eV., respectively, compared to 1.36 eV for aluminum, 1.64 eV for silicon and 3.58 for calcium. Given the above arguments, it is believed that the boundary phase is composed mainly of an Al_2O_3 - $\text{Al}_4\text{O}_4\text{C}$ mixture close to the eutectic composition, and the main difference between samples with and without CaO added is of quantity not of composition of the boundary phase.

9.2.5. Mechanism of Liquid formation

STEM micrographs show a wetting boundary phase present in samples from both systems and the composition is very similar in both cases, including the small amounts of calcium. So it is presumed that it is the same boundary phase that is present

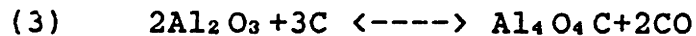
in either case, but formed at different rates and therefore different amounts during the relatively short sintering period for which samples "T11" and "h6" were fired. If the addition of CaO would promote the formation of an Al_2O_3 rich liquid, which forms in the Al_2O_3 rich side of the Al_2O_3 -CaO phase diagram at approximately 1860°C , fig.5b, the composition of the boundary phase would be different in the two samples. Also, it would form closer to 1860°C than to 1840°C , the liquid formation temperature in the Al_2O_3 - $\text{Al}_4\text{O}_4\text{C}$ system (see figs.5a and 5b). So, it is concluded that the addition of CaO to SiC- Al_2O_3 powder mixtures promotes the kinetics of formation of the aluminum oxycarbides and so enhances the densification of the powder compact. The formation of a CaO containing liquid in equilibrium with Al_2O_3 , as established in the Al_2O_3 rich side of the CaO- Al_2O_3 phase diagram, is rejected.

9.2.5.1. Al_2O_3 -C

Al_2O_3 in the presence of carbon and SiC forms $\text{Al}_4\text{O}_4\text{C}$ as a preferred reaction product although the reaction kinetics have been found to be quite sluggish [90]. After the oxycarbides have formed SiC promotes the formation of Al_4SiC_4 . It is assumed that Al_2O_3 will react with carbon preferentially rather than with SiC at the temperatures of interest. The issue then is to solve how the aluminum oxycarbide is formed from Al_2O_3 and C.

The SiC powders used in the present investigation have a free carbon content of 0.4 W% which compared to an Al₂O₃ addition of 6 W% are in a mol proportion of 1.14 mol of C for every 2 mol of Al₂O₃, this is the case for both series "T" and "h".

Al₂O₃ and carbon could react in the solid state, for which the particles would have to be in close contact, according to a reaction of the type:



or through a series of reactions with Al₄C₃ as an intermediate compound:

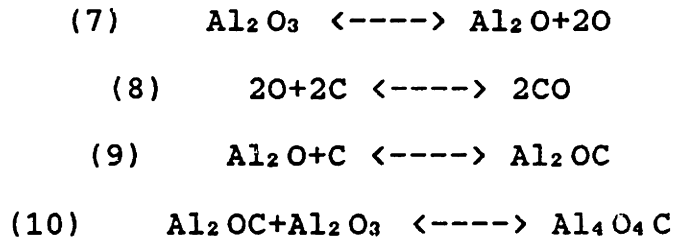


or normalized to 2 moles of Al₂O₃:



Another alternative is for Al₂O₃ and C to react through a gaseous component⁶. Al₂O₃ is known to decompose into aluminum suboxides under reducing conditions at the temperatures of interest, predominantly Al₂O [132, 46]. A possible reaction path is the following:

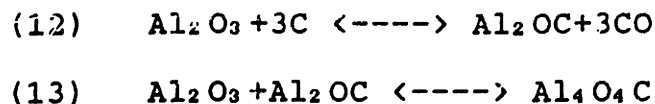
 6. No contribution to carbon transport is expected from the firing gas, since the gases used in this system were analyzed to contain <1ppm O₂. Refer to: "Experimental Procedures" and "Discussion, System SiC-B-C, Gas Transport".



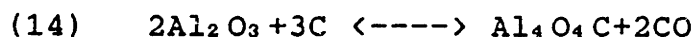
which adds up to:



Reactions 7 through 11 are an alternate path to the equivalent reaction 3, but allows for mass transport of the aluminum containing species (Al_2O), in the gas phase. Al_2OC , as indicated by the phase diagram in the Al_2O_3 rich side and by the experimental reports, exists in small amounts as compared to $\text{Al}_4\text{O}_4\text{C}$ (see fig.5a). Reactions 7 to 10 are consistent with this notion: as the carbon is consumed in an Al_2OC rich system Al_2OC is bound to disappear in favor of the aluminum rich oxycarbide. It has been reported [90] that Al_2OC forms first and disappears along with the creation of $\text{Al}_4\text{O}_4\text{C}$, so another equivalent reaction path includes the direct formation of the monoxycarbide with further reaction with Al_2O_3 to finally form the tetroxycarbide, according to reactions 12 through 14.



and normalized to two moles Al_2O_3 :



The preceding arguments are based on the existence of free carbon (in the SiC powder) for the formation of the aluminum oxycarbides (upon reaction with Al_2O_3) to then form a liquid that facilitates densification during sintering.

9.2.5.2. The Role of CaO

Samples in the systems SiC- Al_2O_3 and SiC- Al_2O_3 -CaO analyzed using the SEM EDAX capability which contained or were packed in CaO containing powders, always showed a higher aluminum content than samples which did not contain CaO and were not packed in CaO containing powder, see fig.17.

An ancillary experiment was performed in which undoped Al_2O_3 and CaO doped Al_2O_3 samples were fired under equivalent conditions as the SiC- Al_2O_3 -CaO system samples, with the result that the CaO containing samples lost much more weight than the pure Al_2O_3 counterpart: 7% against 0.9% respectively. Both samples were fired at 1830 ± 20 °C under helium for one hour; the CaO content in the doped sample was approximately 3.5 W%.

CaO added to SiO_2 during its carbothermic reduction is found to increase the volatilization of Si by approximately a factor of 10 [135], at temperatures between 1600 and 1800 °C. The Si is lost as SiO. Furthermore, Ca is an effective catalyst during

some gasification reactions of carbon [136]. Carbon forms CO_2 and 2CO when reacted with O_2 and CO_2 respectively. The oxidized form of Ca (CaO) is most likely the active catalyst species under these conditions. The carbon gasification rates are increased by two to three orders of magnitude by the presence of 1 at% Ca. Unfortunately, there is not enough information as to establish a mechanistic analog between the enhanced volatilization rates of Si, the accelerated gasification of carbon by the presence of CaO and the enhanced volatilization of Al_2O_3 (most probably as Al_2O) with additions of CaO . The gasification reactions of carbon involve oxidation of the carbon substrate, the volatilization of SiO_2 and Al_2O_3 involve partial reduction of the oxides⁷.

Al_2O_3 doped SiC compacts which were packed in CaO containing powder showed a weight increase of several percents, as illustrated in fig.12a. This last effect (weight gain) was observed irrespective of the CaO content of the sample. Samples which did not contain CaO but were packed in a CaO containing powder (i.e. 10-7-0.7) gained several percent weight. A sample of the series "T" containing no CaO but only 6 W% Al_2O_3 (sample "T13") was fired at 1860 ± 20 °C packed in enriched⁸ powder containing CaO (10-7-0.7). It experienced a weight gain of 7.2

7. For further detail on the catalytic effects of CaO refer to "Phase Relations, CaO as a Catalyst"

8. An enriched powder contains an excess of additives with respect to the sample. Two enriched powders were used: "10-7" and "10-7-0.7". See "Experimental Procedures, Packing Powders".

% and densified to approximately 96 %th compared to "T" pellets (i.e. sample "T10") fired under the same conditions but packed in enriched powder with no CaO (10-7) which gain less than 1% in weight. So it seems that in every case that CaO was present, transport in the vapor phase was more active. So the experimental evidence suggests that an aluminum containing vapor species (probably Al₂O) is transported at a considerably faster rate when CaO is added to the SiC-Al₂O₃ powder system.

9.2.6. Sintering Mechanism

There is enough evidence from the STEM analysis of the grain boundaries for both its microstructure and composition, general microstructural analysis by SEM, phase diagram relationships between the participant components, and temperature dependence of the final density, to conclude that densification takes place with the aid of a liquid phase in the systems SiC-Al₂O₃-CaO and SiC-Al₂O₃.

Having established the existence and identity of a liquid phase during sintering and the mechanism of its formation, a model for the sintering process is in order.

The general principles of liquid phase sintering apply to the present case [133, 50, 134], for which a liquid that wets the boundaries is formed in sufficient quantity and early enough during the process to effectively enhance the rate of sinter-

ing. In the present case the composition of the boundary phase is remarkably similar in the two systems of interest (SiC-Al₂O₃ and SiC-Al₂O₃-CaO), which leads to the conclusion that it is the same liquid present in either case but in different amounts due to widely different formation rates.

In the absence of CaO, the formation of the oxycarbide has to proceed, most probably, by a solid-solid reaction. It is apparent that when the melting temperature for the Al₂O₃-Al₄O₄C mix is reached there is still not enough liquid to considerably enhance the sintering rate. If evaporation is prevented and the sintering time extended to 5 hs, (sample "T5", fired at 1960 °C, see table 10), then the final density increases to over 98 %th. The same final density was achieved by any "h" series sample fired above 1830 ± 20 °C for one hour under the same conditions ("h" series contains CaO in addition to Al₂O₃).

When CaO is present, the transport of aluminum containing species through the vapor, very probably Al₂O^[46], is enhanced so as to promote the formation of the aluminum oxycarbide by a mechanism that does not require mechanical contact between the reactants. When the eutectic temperature for the Al₂O₃-Al₄O₄C mix is reached, the liquid forms and sintering proceeds at an accelerated pace, as evidenced by the density-temperature relationship depicted in fig.10. The contrasting difference in final density found in samples from series "T" fired for one hour versus five hours is attributed to the longer firing time

during which enough Al_4O_4C forms so the sintering rate is enhanced.

The role of the packing powder is deduced from the former arguments. If the packing powder is enriched in the components which are responsible for the formation of the aluminum rich vapor species (i.e. CaO and Al_2O_3), there will be a chemical gradient under which material will be transported to the depleted part of the system, (i.e. the sample) and so according to reactions 7 through 10 promoting the formation of the oxycarbides (i.e. by transport into the sample of Al_2O). So the presence of CaO in the packing powder is a desirable factor, since it seems to promote the formation of Al rich vapor species. Similar arguments lead to the conclusion that a closed firing environment is favorable for the achievement of high densities.

It is important to note the interplay between weight change and shrinkage, illustrated in figs.12a and 12b. Depending on the vapor pressure of the migrating gas species, which is fixed by the composition of the packing powder and the degree of gas tightness of the crucible, an equilibrium may be established between the sample and the surroundings. This determines the amount of shrinkage that the sample is to undergo while achieving full density. It must be noted that if evaporation is allowed for, the sample shrinks in a proportionally larger measure while becoming fully dense. By detailed analysis of

figs.12a and 10 it is observed that when a sample gains weight it shrinks less than a sample that gains less or loses weight. Furthermore, it must be noted that the weight gain does not account for the density increase. Samples which gain weight upon firing also shrink to a further extent. Samples "T10" and "T13" were fired under identical conditions with the exception of the packing powders, "T10" was packed in Al₂O₃ enriched SiC powder (with no CaO added, 10-7 packing powder) while "T13" was packed in the same enriched powder but with CaO added in an amount equivalent to 10% of the Al₂O₃ weight (10-7-0.7 packing powder). Sample "T13" reached about 96 %th density while "T10" reached only approximately 83 %th. If sample "T10" had had added to it the same weight percent as "T13" gained, (but keeping its same dimensions) it would only reach but about 88 %th density.

9.2.7. Boundary Phase Decomposition and Weight Loss

A sample will change its weight during firing if matter is transported into (weight gain, positive weight change), or out of (weight loss, negative weight change) the sample during the process.

Undoped alpha SiC powders (LONZA UF-15, see table 4) lost approximately 1.5% of their weight when fired (unpacked, open crucible) at 2150 ± 20 °C (sample "R2", table 10). Undoped, clean SiC powders will lose weight when fired in reducing at-

mospheres by the following mechanisms: 1.-) reaction of the SiO_2 impurity with SiC to form SiO and CO , 2.-) decomposition of the SiO_2 and 3.-) decomposition of the SiC into Si and graphite at high temperatures (i.e. 2000 °C and over). The manufacturer supplied chemical analysis quotes the SiC 15 m²/gr powder as containing 0.8 W% total oxygen. If the oxygen is present predominantly as SiO_2 then it will amount to about 1.5 W%.

In a doped powder the weight change mechanisms can be very complicated and usually mask the losses of the undoped SiC powder case. The powder used most extensively in this investigation contained approximately 0.4 W% free carbon, 0.8 W% O_2 (equivalent to 1.5 W% SiO_2) about 0.1 W% free Si and less than 0.05 W% Al . The additions were typically around 6 W% Al_2O_3 and, if added, CaO in a weight ratio to Al_2O_3 of 0.04.

Weight changes in Al_2O_3 - CaO doped SiC samples depended on a variety of factors, such as: 1.-) the total amount of additives, i.e. Al_2O_3 + CaO , 2.-) the amount of Al_2O_3 added, 3.-) the degree of gas tightness of the crucible and 4.-) the composition of the packing powder. The first two control the amount of reactants and volatiles available. The last two affect the ability of this reactants and volatiles to escape into the surrounding gas phase by setting up a chemical gradient favoring transport into (causing weight gain) or out of the sample (weight loss).

To study weight loss and the reactions leading to it, the

two last factors have to be arranged in such a way as to permit free transport out of the sample and into the gas stream of any volatile components that might result from any reaction occurring in the sample (i.e. open crucible and non-enriched packing powder). The weight loss characteristics of undoped SiC powder are known, so any differences will be attributed to the effect of the additives.

Weight losses in samples where the escape of volatiles was permitted (open or semi-open crucibles and non-enriched packing powders) were always greater than the sum of all the added compounds, table 7 summarizes weight changes and firing conditions for sample series "T" and "h" (table 10 summarizes results for all samples in the SiC-Al₂O₃-CaO system). This leads one to believe that the additions are reacting with the SiC powder, the free carbon and SiO₂, thus, some of it (SiC) reacts and subsequently volatilizes. There are a few different reaction paths and combinations thereof that could account for the observed weight losses.

Once Al₄O₄C is formed by any of the equivalent reactions such as 3,6 or 11 it will form a solution with Al₂O₃ in the Al₂O₃ rich side of the Al₂O₃-Al₄O₄C system and dissolve an amount of SiC into it, as evidenced by the x-ray STEM spectra. After the temperature reaches 1840 °C, liquid forms and sintering proceeds at an accelerated rate. Any further reaction at this stage would depend on the relative values of the instant partial pressures of the evolving gas species in the sample and

in the immediate vicinity as well as on the ability of the sample to channel or diffuse them out. For example, reaction 15 would lead to the evolution of 1 mole of SiO_2 plus 0.33 mole CO while reaction 19 would evolve 0.82 mole of SiO and 0.27 mole of CO per mole of SiC . The kinetics may be more favorable for reaction 15 than for 19⁹; SiC is known to form Al_4SiC_4 only after the formation of $\text{Al}_4\text{O}_4\text{C}$ when reacted with Al_2O_3 and C, and the $\text{SiC-Al}_2\text{O}_3$ reaction proceeds at a slower rate by comparison. If the temperature is high enough, the pressure of the gaseous species could rise to a level such as to form cavities in the sintered compact. An alternative cause for cavity formation is an excess of liquid being squeezed during densification into the channels, leaving a cavity after subsequent volatilization. Cavity formation has been observed to happen when any sample containing Al_2O_3 was fired at 2110 ± 20 °C (see figs.15a and 15b). Nevertheless, when evaporation is allowed, (i.e. open crucible and not enriched packing powder), volatilization takes place at a significant rate. Table 11 summarizes weight losses for some samples in the series "Y".

9. See "Literature Review, Phase Relations" for literature data on Al_2O_3 - SiC reaction kinetics.

ID	Temp. (°C)	time (hs)	weight loss (%)	fired dens. (%th)
Y8	1935	1	11.7	80.2
Y3	1960	5	11.8	84.6
Y4	1960	10	12.4	84.3
Y3'	1960	15	12.3	84.9

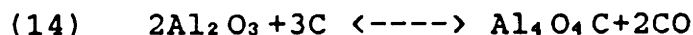
Table 11
Selected samples weight loss in series "Y".
(6W% Al₂O₃+2W%CaO). All temperatures are
± 20 °C. All samples were fired in open
or semi open crucibles.

It is to be noted that most of the weight loss has already taken place at one hour. This uninhibited evaporation prevents densification by allowing the aluminum oxycarbides to decompose before enough densification has taken place. The processes by which the oxycarbides decompose is the subject of the remaining of this section.

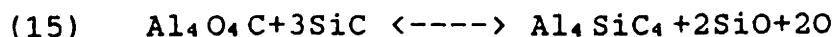
Two cases are going to be illustrated with the purpose of modeling the weight loss mechanisms and calculation of the expected weight loss by each one of them. To calculate the expected weight losses from a given set of reactions, the set is added up and all the gas species resulting from the set are assumed lost. This mass loss is then expressed as a percent of Al₂O₃ weight. CaO is assumed to be lost into the gas phase in all cases (unless indicated otherwise), since it was never found in considerable amounts in any of the samples regardless of the initially added quantity. Both cases of weight loss

share a common starting point: the initial amount of Al_4O_4C is fixed by the limiting reactant in either one of the equivalent reactions 3, 6, or 11 for Al_4O_4C formation. Since the amount of carbon (0.4 W%) is fixed for the SiC powder used, and the Al_2O_3 was always added in greater amounts than carbon, there was always Al_2O_3 left unreacted. The Al_4O_4C will react with SiC to form Al_4SiC_4 and subsequently decompose and partly volatilize according to reaction 17. The two models differ in what is assumed to happen to the Al_2O_3 initially unreacted. One model assumes that the unreacted Al_2O_3 will react with SiC, according to reaction 19. The second model assumes that the carbon regenerated during the decomposition of Al_4SiC_4 (reaction 17) is available to react with Al_2O_3 and form Al_4O_4C , with no participation of SiC.

The first step is the formation of the aluminum oxycarbide which forms by a reaction of the type¹⁰:



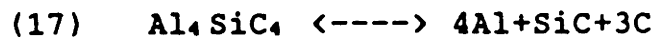
The aluminum oxycarbide can react with SiC according to the following reactions:



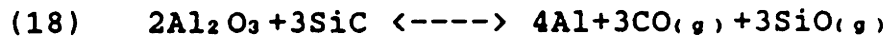
10. See section: "Boundary Phase Stoichiometry".



to form Al_4SiC_4 and evolve SiO and CO . $\text{Al}_4\text{O}_4\text{C}$ is known to react with SiC and form Al_4SiC_4 under similar circumstances [90]11. Furthermore Al_4SiC_4 has been found to decompose according to the following reaction [110]:



so after completion the above series of reactions, (14 to 17) add up to:



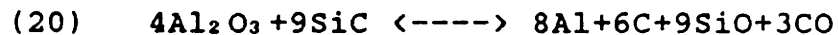
reaction 18 would take along with it all the added Al_2O_3 and an additional 3 moles of silicon and 3 moles of carbon per every two moles of Al_2O_3 (or an additional 58.9% of the alumina weight). But as already was discussed (see page 95) there is not enough free carbon in the sample (there are 1.14 moles of carbon for each 2 moles of Al_2O_3 and reaction 14 requires 3 moles of C for 2 moles of Al_2O_3) to react with all the Al_2O_3 added according to reaction 14 but with only 37.8% of all the Al_2O_3 available. The remaining Al_2O_3 (62.2 mol%) will remain as Al_2O_3 in solution with the formed $\text{Al}_4\text{O}_4\text{C}$. Upon decomposi-

11. See section: "Phase Relations".

tion of the Al_4SiC_4 (resulting from reaction 15) there are a few conceivable reactions that could take place between Al_2O_3 and SiC or some of the other reaction by-products, either sequentially or in parallel with the decomposition. One path leads to the following reactions:



which upon decomposition of Al_4SiC_4 (by adding reactions 17 and 19) results in:



so, the Al_2O_3 reacting along this path takes along with it approximately 71% of its own weight ($9Si+3C$). Using the mol fraction of Al_2O_3 (0.37 and 0.62 respectively) that goes through each set of reactions (15 to 18 and 19 to 20) as weighing factors for each set's expected weight loss contribution (58.9 and 71%), the expected weight loss is approximately 66.34% of the Al_2O_3 weight. It must be noted that the weight loss mechanism proposed above assumes Al_2O_3 will go through two sequential steps: 1.-) it will react with all the available carbon and, 2.-) the remaining will proceed to react with the SiC. To estimate the total weight loss according to the simple reaction scheme proposed above, it has to be added to the total weight of the additions 66.3% of the Al_2O_3 weight, i.e. for

series "Y" which contains 6W% Al₂O₃ and 2W% CaO:

Total Al₂O₃ weight: 6%

Total CaO weight 2%

Total additions weight .. 8%

so, the estimated weight loss would be:

$$(\text{total weight of additions}) + (0.663 \times \text{Al}_2\text{O}_3 \text{ weight}) = 12.0\%$$

or:

$$(8\%) + (0.663 \times 6\%) = 12.0\%$$

The following table further illustrates the point:

	powder series					
	Y	b	c	g	h	T
Al ₂ O ₃ (%)	6	6	9	7.4	7.7	6
CaO (%)	2	3	3	0.6	0.3	0

loss as percent of Al ₂ O ₃ wt.	loss as % of sample weight calculated according to the respective model, see text.					
66.3	12.0	13.0	18.0	12.9	13.1	10.0
41.0	12.4	13.4	17.6	12.9	13.1	10.4
41.0*	12.1	12.9	17.1	12.8	13.0	10.4
actual loss ----->	12.1	12.9	16.8	13.1	13.1	10.1

Table 12
Expected versus actual weight losses in differently doped SiC powders. (for * see text).

A different way to approach the weight loss estimation is to assume that, since carbon is (to a first approximation) regenerated during the Al₄SiC₄ decomposition (reaction 17), Al₂O₃ which was not initially reacted with carbon will be reacted in the next cycle after all the Al₄SiC₄ originally formed out of the liquid is decomposed. In this fashion Al₂O₃ would carry along only 41% (just 3 moles of Si, see reactions 14 to 17) of its own weight in addition, in every cycle until all the Al₂O₃ and other reactants (i.e. carbon and SiO₂) are gone. In this approximation it is assumed that Al₂O₃ reacts almost exclusively with carbon; Al₂O₃ will react with carbon to form aluminum oxycarbides, these in turn will react with SiC to form aluminum-silicon carbide which will decompose regenerating

the carbon, which will then react with the alumina and so on. Furthermore, the total loss of carbon and SiO₂ is assumed to occur by the end of the process. So the expected weight loss is calculated by adding the total amount of the additions to 41% of the Al₂O₃ weight plus 1.9 W% accounting for the free C and SiO₂¹², i.e. for series "h" which contain 7.7W% Al₂O₃ plus 0.3W% CaO.

Total Al ₂ O ₃ weight	7.7%
Total CaO weight	0.3%
Total additions weight ..	8.0

so, the estimated weight loss would be:

$$(\text{total weight of additions}) + (0.41 \times \text{Al}_2\text{O}_3 \text{ weight}) + (1.9\%) = 13.1\%$$

or:

$$(8\%) + (0.41 \times 7.7\%) + (1.9\%) = 13.1\%$$

The results of these calculations for various powder compositions in the system SiC-Al₂O₃-CaO are presented in table 12.

CaO was never found in large amounts in any of the samples

12. See section: "System SiC-Al₂O₃-CaO, SiC Powders"

analyzed so it is assumed most of it volatilized into the gas stream and out of the system. The "*" in the last 41% calculation is to indicate an additional correction factor which would account for a non-total loss of CaO, in this case only 85% was assumed to volatilize, for calculation purposes.

The presented (simplified) analysis of the weight loss mechanisms still account quite well for the observed losses. The fact that the boundary phase actually decomposes and volatilizes is supported by the SEM microstructural analysis of samples fired as to permit volatilization (versus others fired under conditions not allowing for it). The SEM observations showed a widening of the etched boundary phase on those samples in which evaporation was inhibited plus a tendency to intergranular fracture, see Figs.14 and 16.

9.2.8. Summary

One of the first questions arising out of the prospect of liquid phase sintering of Al_2O_3 doped SiC regards the nature of the liquid phase. In the present work an $\text{Al}_4\text{O}_4\text{C}$ rich boundary phase in the system Al_2O_3 - $\text{Al}_4\text{O}_4\text{C}$ was found to be present after cooling following sintering and is assumed to have been liquid at sintering temperature, and is responsible for densification. Transport in the gas phase was found to play an important role during the whole sintering process. Prevention of the volatilization of the aluminum oxycarbides and possible reac-

tion products with SiC is imperative in order to achieve high final densities. The role of CaO additions was found to be the enhancement of the transport of aluminum rich vapor species as opposed to the formation of a CaO rich liquid in the CaO-Al₂O₃ system. The possibility of exerting control to some extent on the composition and amount of the boundary phase is posed by the results regarding weight change and density as a function of local atmosphere (i.e. packing powder, closed versus open crucible), this in turn can influence the fracture mechanism in the sintered bodies.

Liquid phase sintering of SiC has been unexplored, the present work presents a new perspective in the sense that some influence can be exerted on the amount, composition and kinetics of formation of the liquid phase. It is conceivable that similar work could be done in other systems and improvements on the present one are a definite possibility.

10. Conclusions

The present work leads to the following conclusions on sintering of SiC powders with additions of boron and carbon.

- 1.-Both alpha and beta SiC powders densified in the presence of combined boron and carbon additions. The amounts normally used were 0.6 W% B and 0.8 W% C.
- 2.-Sintered beta SiC powders were always denser than alpha powders for the same time-at-temperature. Sintered alpha powders seem to reach a final limiting density which is less than the theoretical. This is attributed mainly to the fact that starting alpha powders have wider size distribution and a larger average crystallite size than beta SiC powders, alpha powders are dirtier than beta powders also.
- 3.-No shrinkage occurred in the absence of boron for sintered SiC powders. Most samples even showed a small dimensional expansion.

- 4.-Without carbon additions, only a very small amount of shrinkage and densification occurred for sintered SiC powders. The extent of densification depends on the gas flow rate, this may be because carbon is being transported from the furnace to the sample.
- 5.-The densification behavior of the alpha powders is essentially the same for boron added as boron carbide or as elemental boron. The effect of the different form of boron addition is not large either at temperatures higher or lower than the boron melting point (2079 °C). So, if a liquid is present during sintering it has to be in the B-Si side of the diagram.
- 6.-Even though the samples were buried in powder of comparable composition to inhibit evaporation, all samples lost from 0.3 to 5% weight during sintering. Weight loss in sintered SiC powders was smaller for beta SiC than for alpha SiC powders.
- 7.-Despite the possibility of boron enhancing transport of a limiting species through a densifying path; the presence of boron seems to inhibit early coarsening, perhaps by surface transport.

For pressureless sintering of silicon carbide with additions

of Al_2O_3 and CaO , the following conclusions have been reached:

- 1.-Silicon carbide compacts with additions of Al_2O_3 and CaO proceeds via liquid phase sintering.
- 2.-Silicon carbide compacts with Al_2O_3 added also sinter with the aid of a liquid phase. In this latter system the liquid forms at a slower rate than in the presence of CaO , hence, the sintering rate is also slower.
- 3.-The liquid formed in both cases originates in the Al_2O_3 - $\text{Al}_4\text{O}_4\text{C}$ binary. The presence of free carbon is required as to form the oxycarbides. Proof that the liquid was present was shown by TEM and STEM analysis: amorphous pockets at three grain junctions and by films of amorphous phase at grain:grain facets.
- 4.-The role of CaO additions is to promote the formation of aluminum rich vapor species, and thereby enhance the creation of the initial oxycarbides.
- 5.-Preventing the loss of the gas species is a necessary condition to achieve high fired densities.
- 6.-One hundred percent dense silicon carbide bodies can be obtained when fired for less than one hour at temperatures greater than 1835 ± 20 °C

in the system SiC-Al₂O₃-CaO. In the absence of CaO it required five hours at temperatures equal or higher to 1960 ± 20 °C to achieve densities greater than 98 %th in the system SiC-Al₂O₃.

11. Suggestions for Future Work

There is a lack of thermochemical data, in particular, vapor pressure versus temperature data in systems such as $\text{Al}_2\text{O}_3\text{-CaO}$ and $\text{SiC-Al}_2\text{O}_3\text{-CaO}$. Therefore, it will be very useful to do Knudsen cell mass spectrometry on compositions in these systems as well as in the Al-O-C system. This will identify the existing vapor species and its activity dependence on temperature and composition (i.e. Al_2O_3 vs. $\text{Al}_2\text{O}_3\text{+CaO}$).

Optimization of the effect of additives, such as CaO , on the sintering behavior of Al_2O_3 doped SiC will be an interesting project to pursue. Variables such as the amount of addition as well as the optimum sintering time and temperature have to be more finely adjusted.

12. Figures

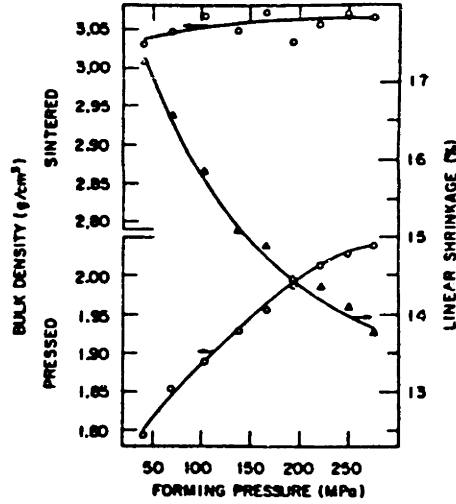


Fig.1. Bulk density of green and fired (2300 °C, Ar-He) alpha-SiC (0.6 W% B and 2.8 W%C doped), as function of forming pressure. From reference 43.

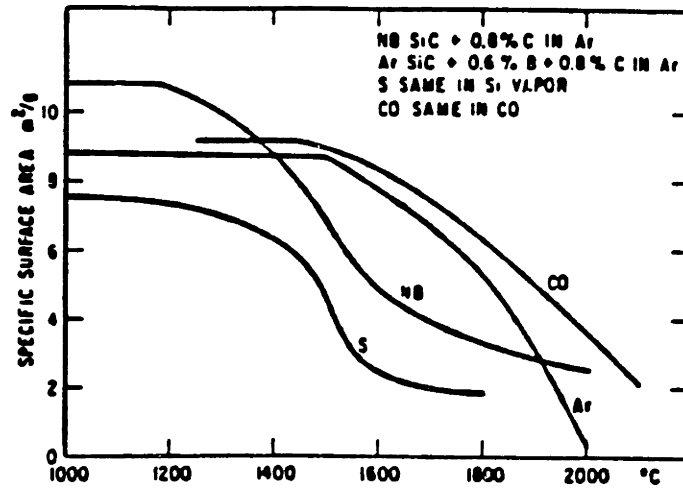


Fig.2. Specific surface area of SiC compacts fired at several temperatures under various sintering atmospheres. From reference 15.

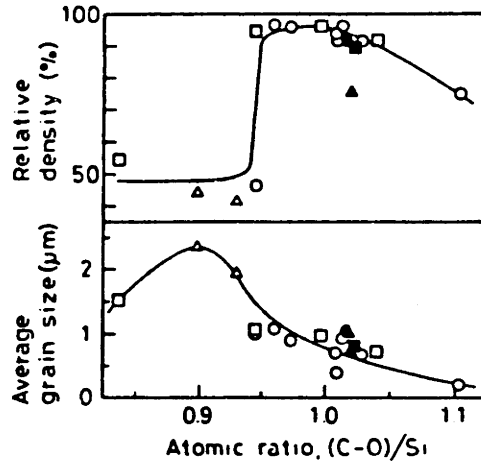


Fig.3. Variations in relative density and average grain size for beta-SiC sintered at 2050 °C (0.4 atm Ar) for 30 min, with 1W% B vs. the atomic ratio (C-O)/Si of the original powders (heating rate approximately 20 °C/min). From reference 7.

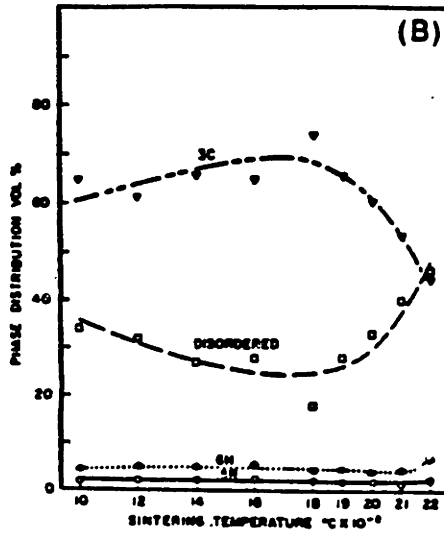
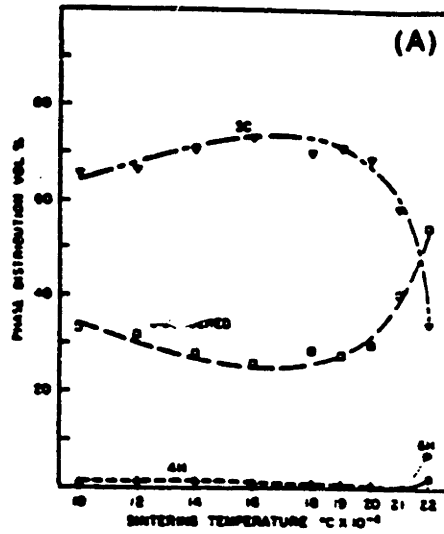


Fig.4. Polytype distribution of (A) SiC powder with no dopants, (B) boron- and carbon-doped SiC. From reference 83

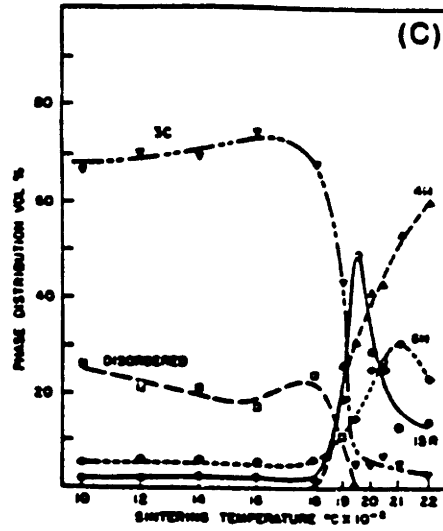


Fig.4.(cont.) Polytype distribution of (C) boron-, carbon- and aluminum-doped SiC. From reference 83.

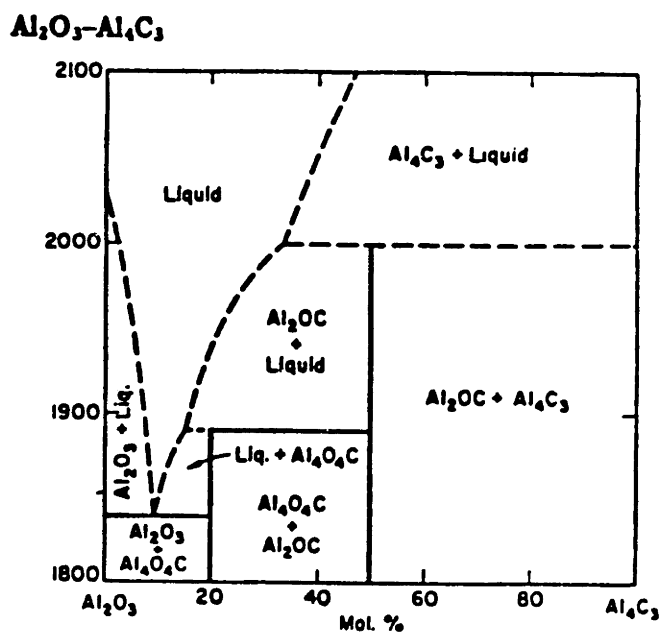


Fig.5a. Phase diagram of the system $\text{Al}_2\text{O}_3\text{-Al}_4\text{C}_3$. From reference 93.

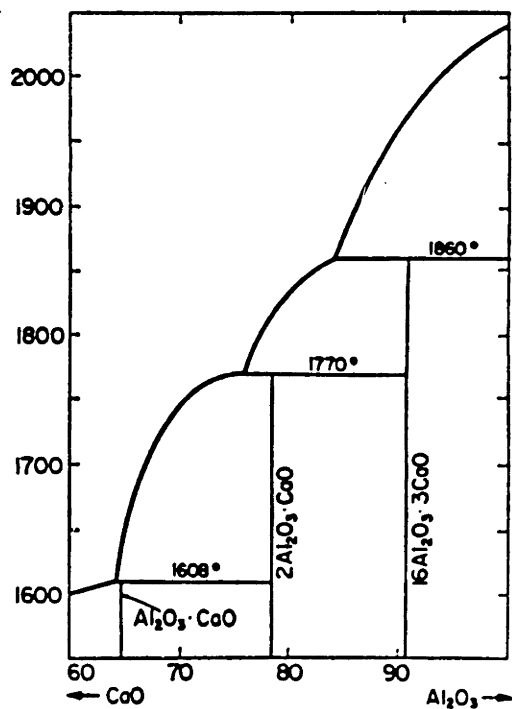


Fig.5b. Phase diagram of the system $\text{CaO-Al}_2\text{O}_3$. From reference 114.

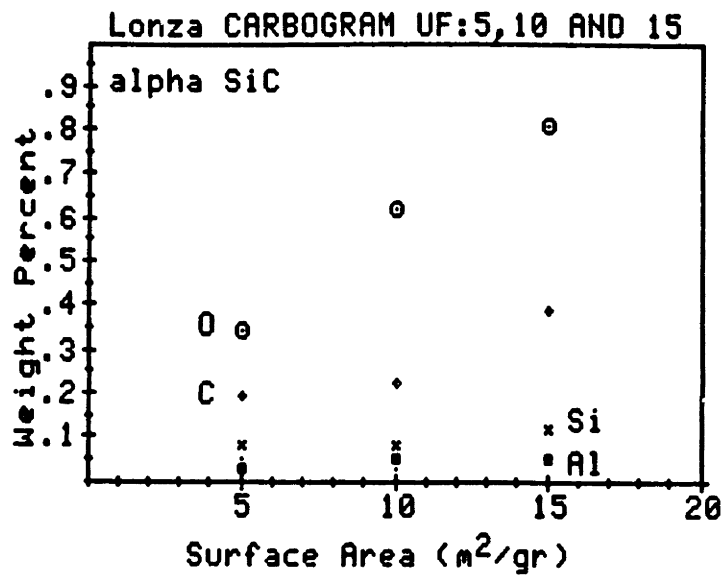


Fig.6. Impurity content as function of specific surface area for Lonza CARBOGRAM alpha-SiC powders. From data provided by the manufacturer.

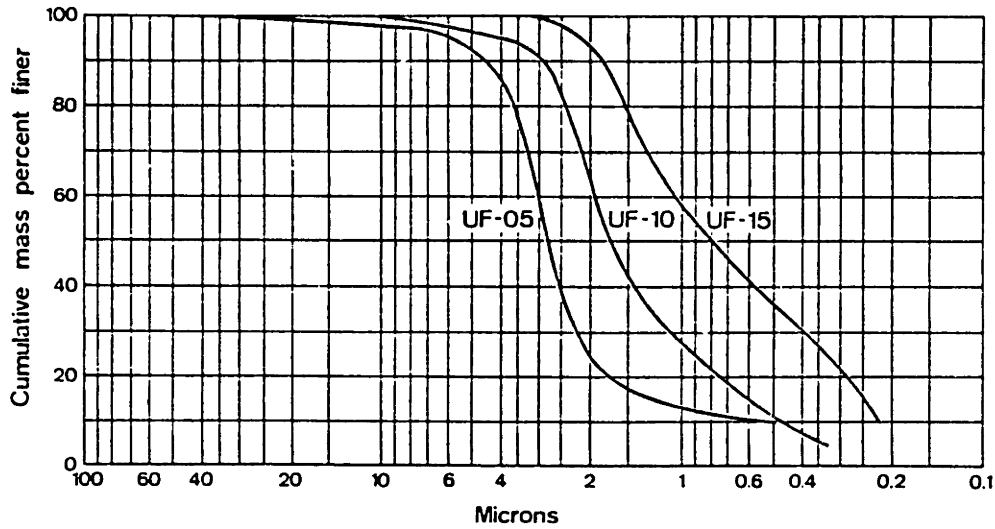


Fig.7. Particle size distribution for Lonza CARBOGRAN alpha-SiC powders. From product literature.

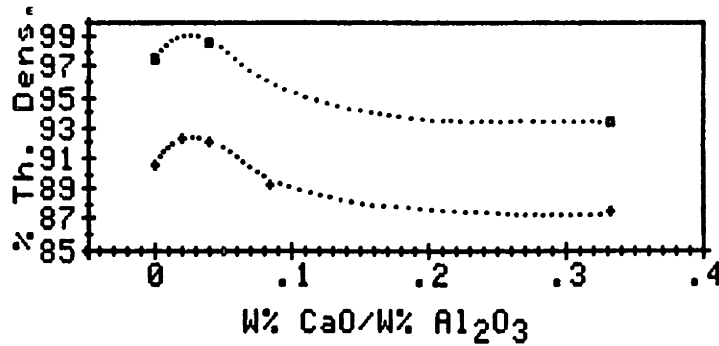


Fig.8. Fired density vs. CaO content (as W%CaO/W%Al₂O₃) for alpha SiC powders fired at 2100 °C, 5 hs under Ar. Upper curve shows density determined by image analysis, lower curve by geometrical means.

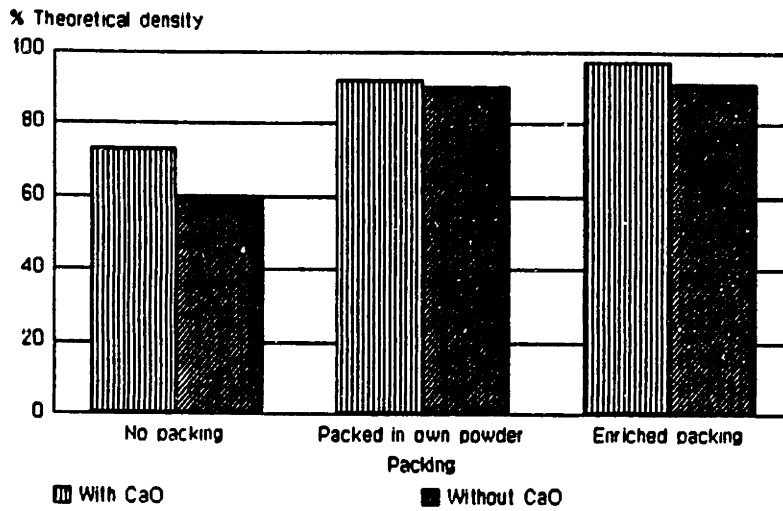


Fig.9. Fired density of SiC powders with and without CaO vs. packing. Enriched powders were 10-7-.7 for "h" series and 10-7 for "T" series.

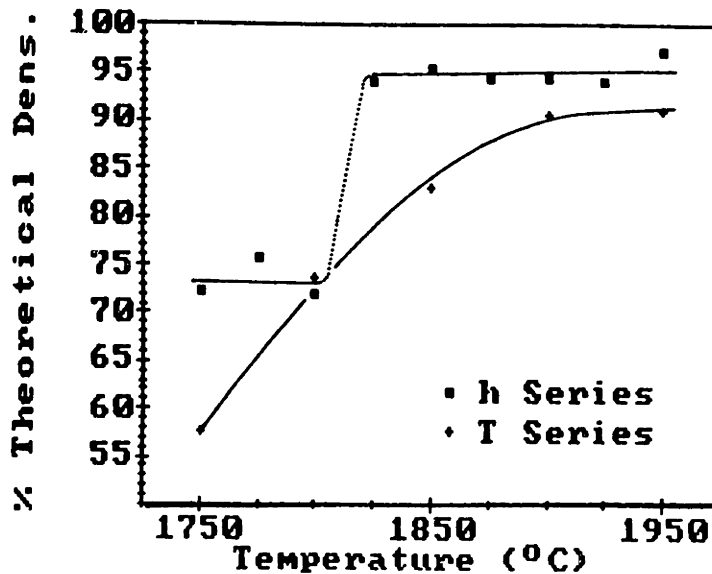


Fig.10. Fired density vs. temperature for sample series "h" (squares) and "T" (crosses), fired at different temperatures. Temperature shown is uncorrected for window losses (+10 °C offset). ("h" series: 7.7W% Al₂O₃+0.3W% CaO) ("T" series: 6W% Al₂O₃)

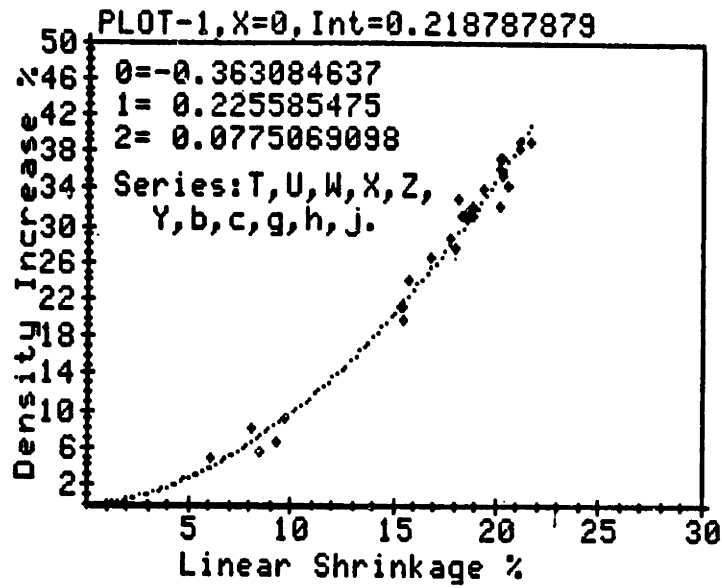


Fig.11. Percent density increase vs. shrinkage for samples in the SiC-Al₂O₃-CaO system fired in open or semi-open crucibles.

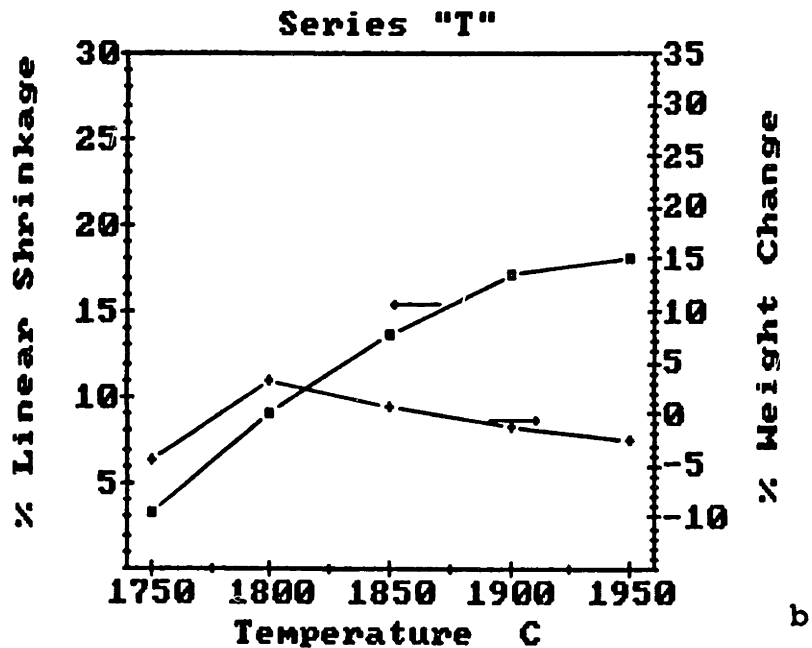
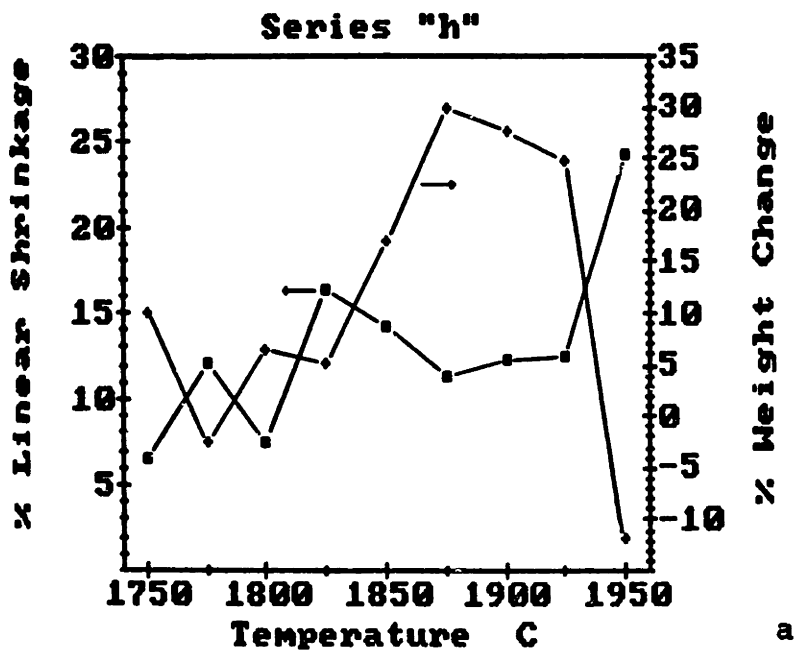


Fig.12. Shrinkage and weight loss vs. firing temperature for sample series "h" (a) and "T" (b). Sample series "h" packed in enriched 10-7-0.7 powder. Series "T" packed in enriched powder 10-7. All samples fired in closed crucibles, except points at 1950 °C.
 ("h" series: 7.7W% Al₂O₃+0.3W% CaO)
 ("T" series: 6W% Al₂O₃)

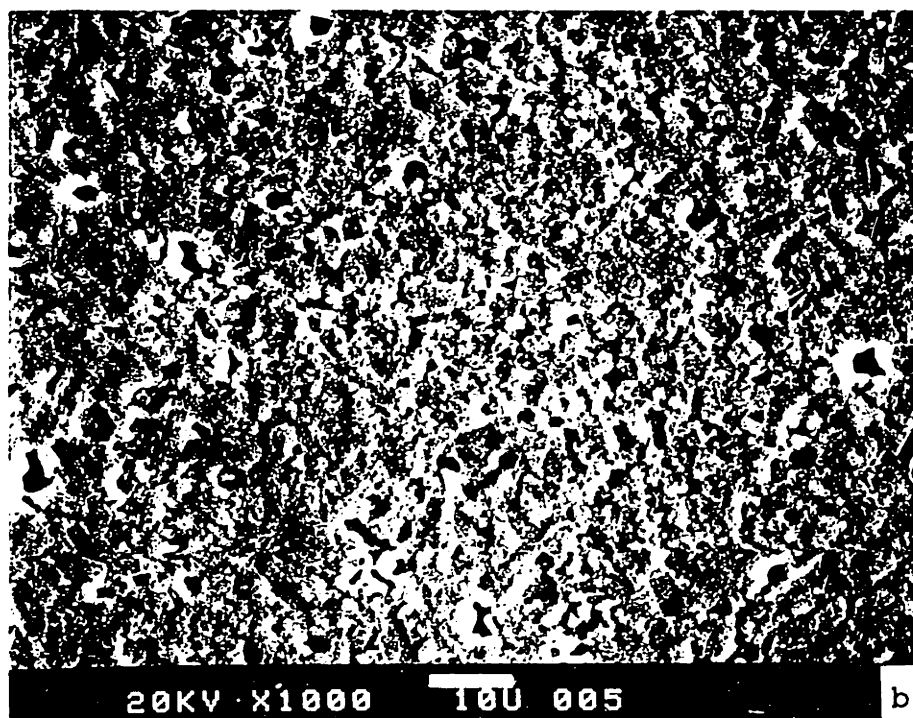
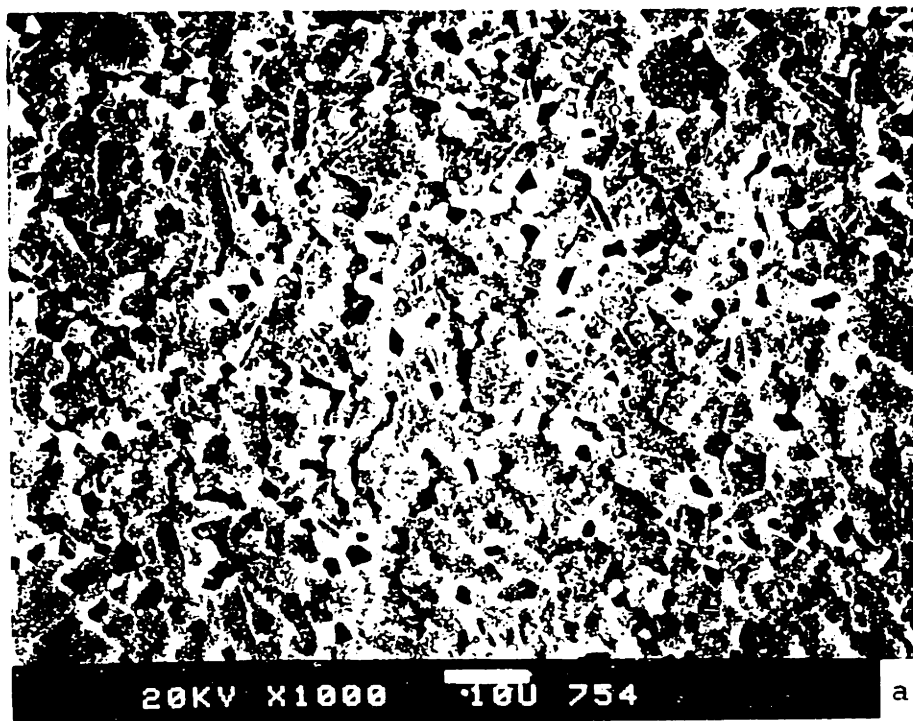


Fig.13. Polished and etched sections of samples "T7" (a) and sample "h3" (b).
("T7": 6W% Al_2O_3 , 2100 °C, 5h, packed in "T", semi-open)
("h3": 7.7W% Al_2O_3 +0.3W% CaO, 2100 °C, 5h, packed in "h", semi-open)

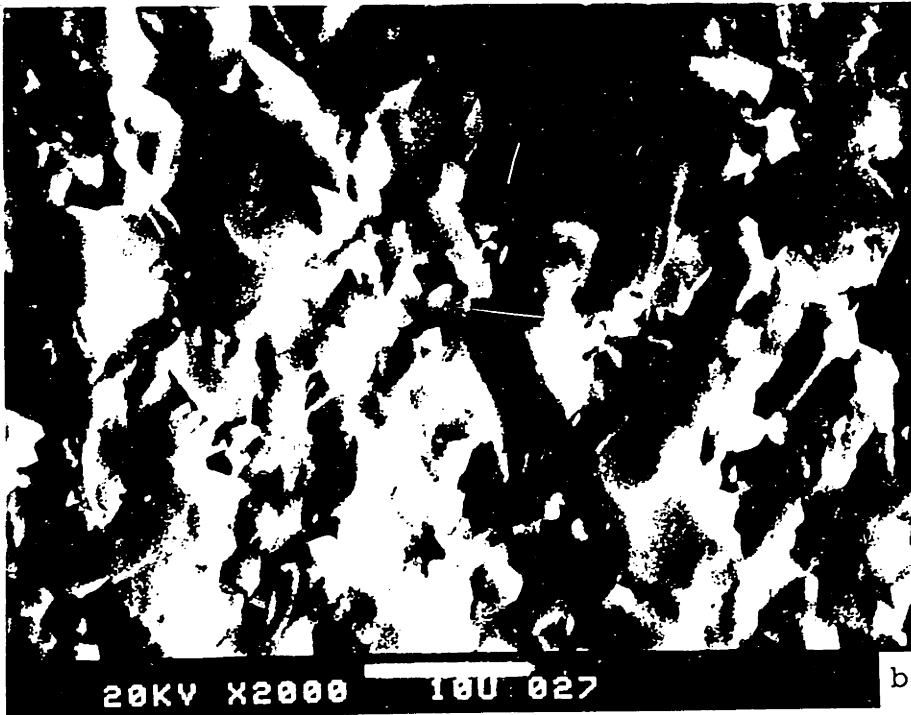
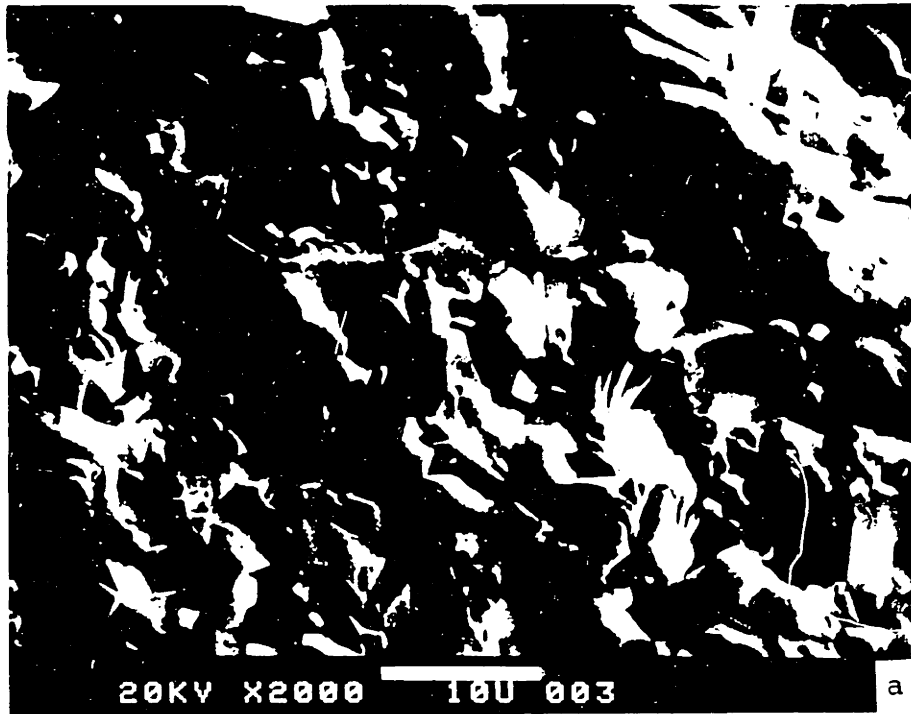


Fig.14. Fracture surfaces of samples "T7" (a), and "h1" (b).
("T7": 6W% Al₂O₃, 2100 °C, 5h, packed in "T", semi-open)
("h1": 7.7W% Al₂O₃+0.3W% CaO, 2100 °C, 5h, packed in "h", semi-open)

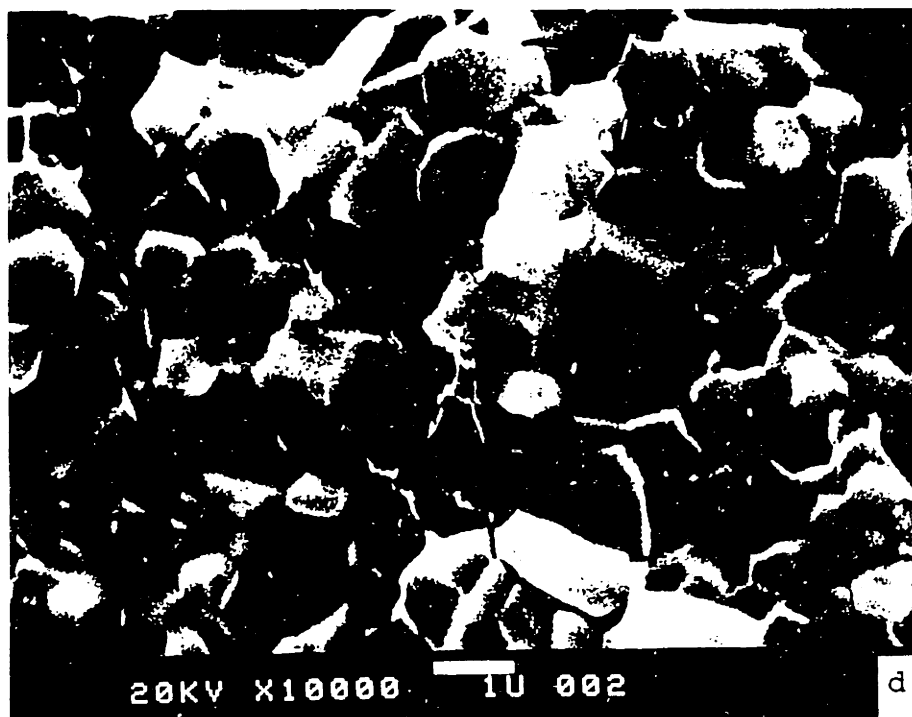
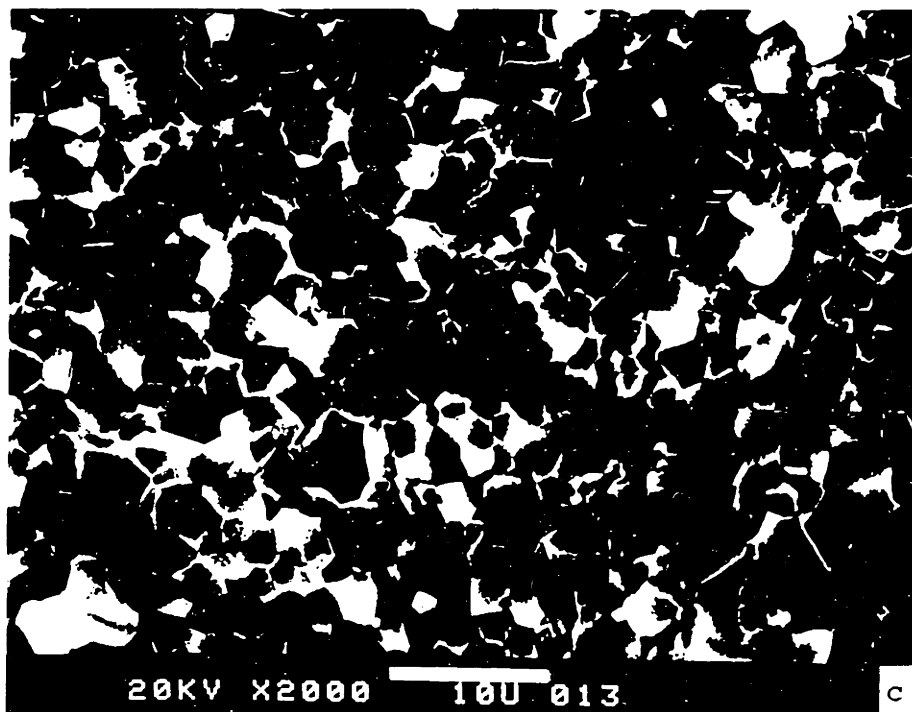


Fig.14.(cont.) Fracture surfaces of samples "T5" (c), and "h4" (d).
 ("T5": 6W% Al_2O_3 , 1950 °C, 5h, packed in 10-7, semi-open)
 ("h4": 7.7W% Al_2O_3 +0.3W% CaO, 1950 °C, 1h, packed in 10-7-0.7, semi-open)

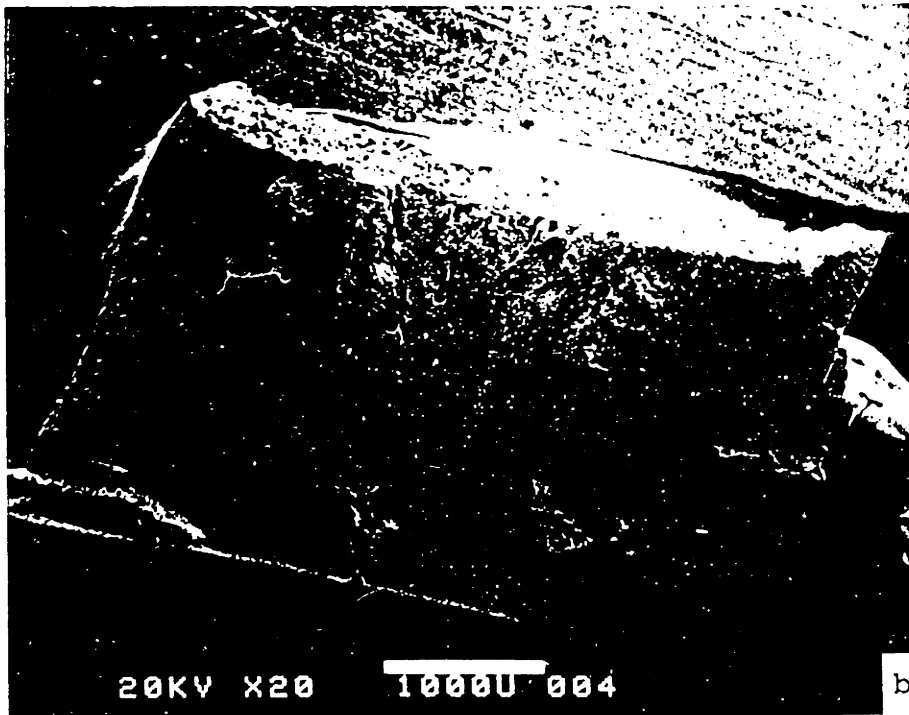


Fig.15. Sample fracture cross sections showing "channels". Sample "T7" (a), sample "h1" (b).
("T7": 6W% Al₂O₃, 2100 °C, 5h, packed in "T", semi-open)
("h1": 7.7W% Al₂O₃+0.3W% CaO, 2100 °C, 5h, packed in "h", semi-open)

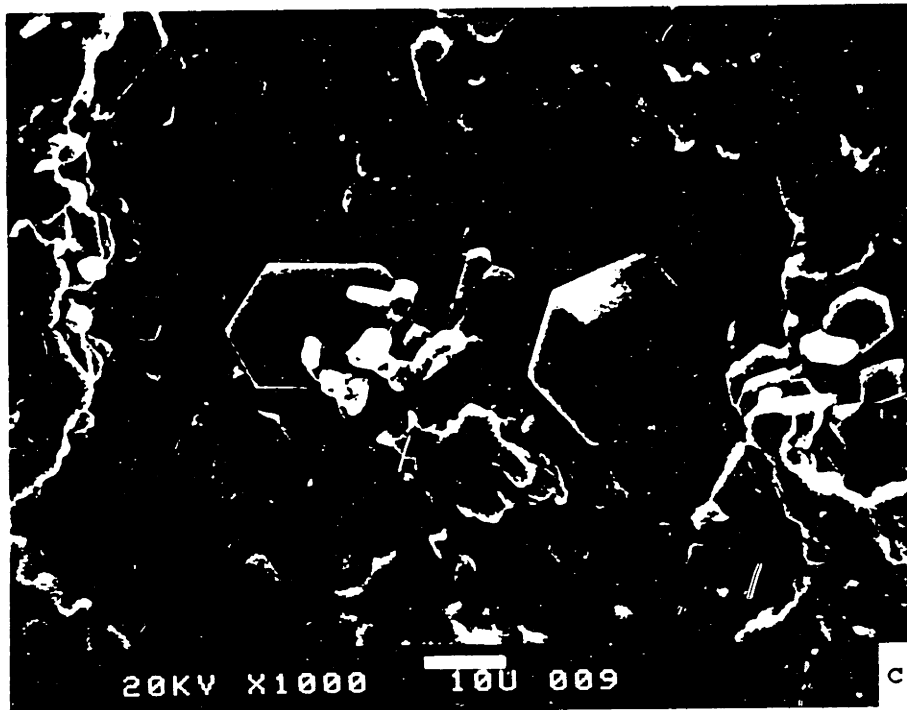


Fig.15.(cont.) In (c) the interior of a "channel" in sample "g2" is shown.
("g2": 7.4W% Al_2O_3 +0.6W% CaO, 2100 °C, 5h, packed in "Y", semi-open)
("Y" powder: 6W% Al_2O_3 +2W% CaO)

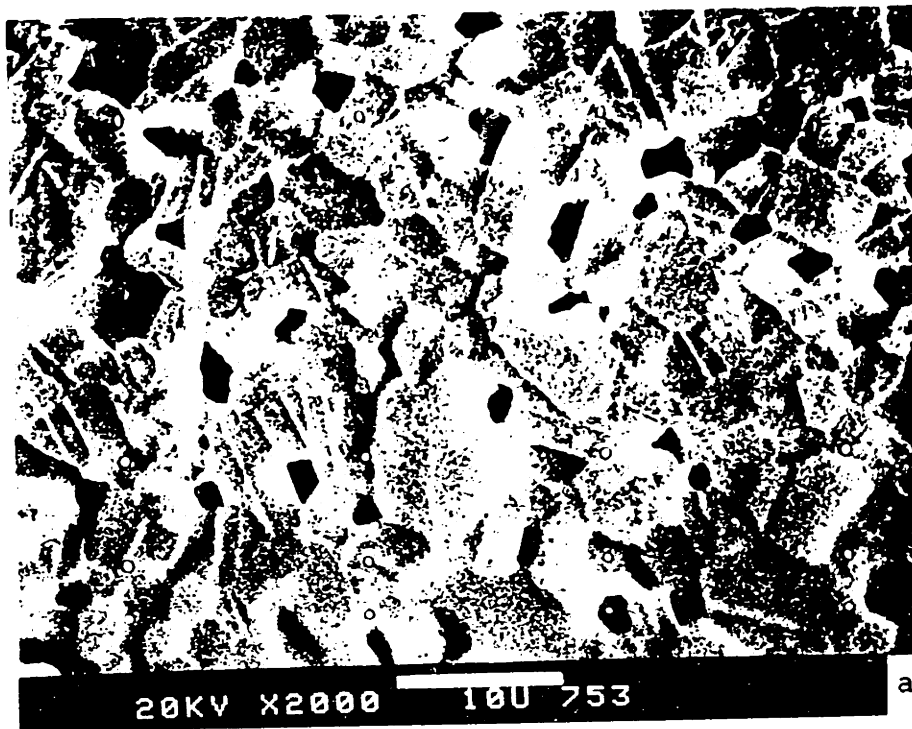


Fig.16. Polished and etched sections of samples "T7" (a), "T5" (b).
("T7": 6W% Al₂O₃, 2100 °C, 5h, packed in "T", semi-open)
("T5": 6W% Al₂O₃, 1950 °C, 5h, packed in 10-7, semi-open)

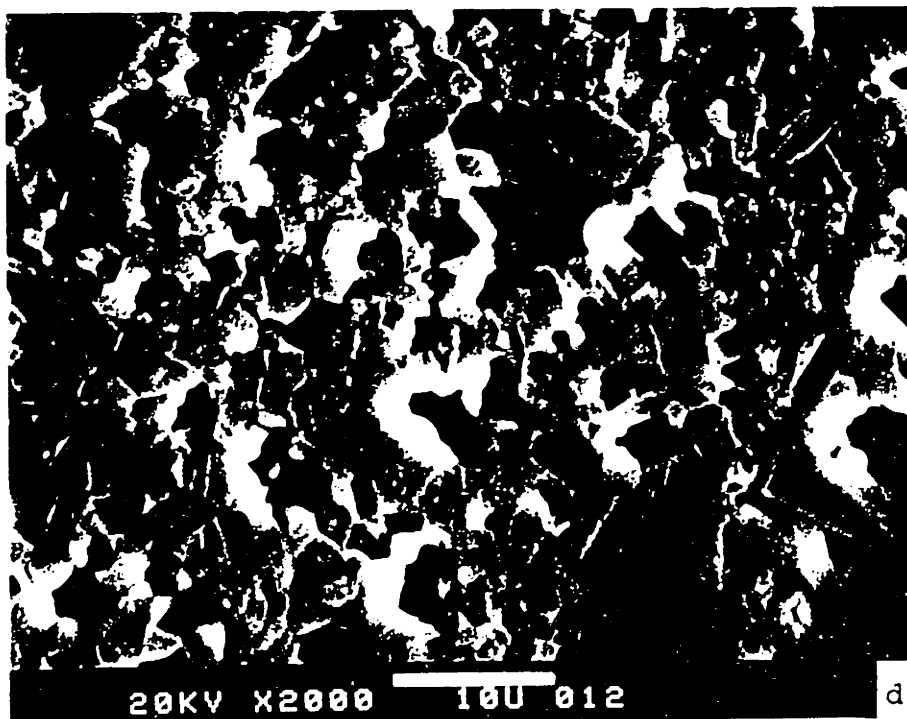
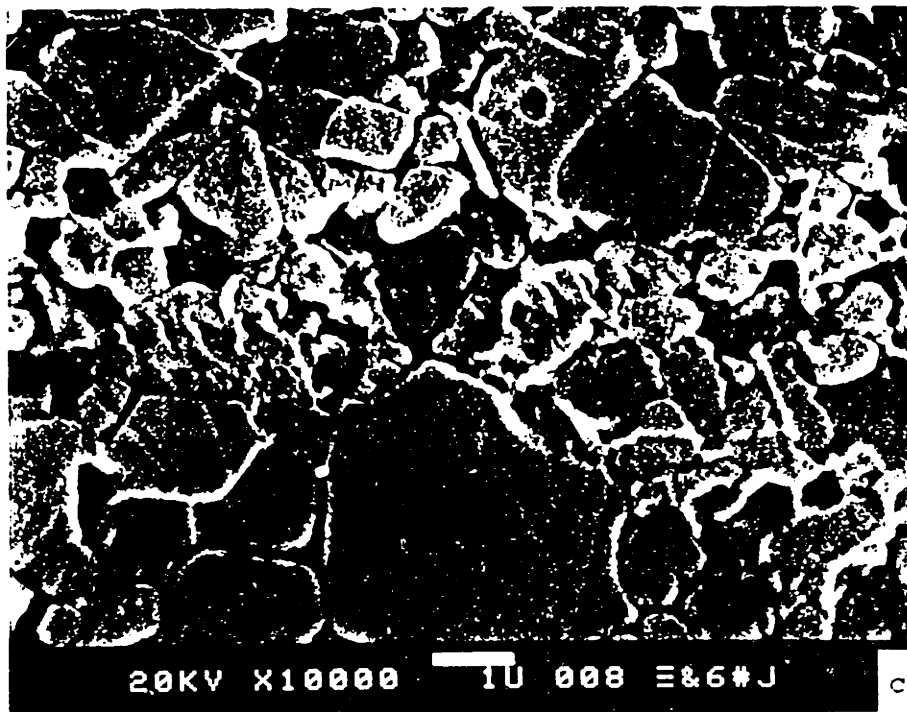


Fig.16.(cont.) Polished and etched sections of samples "h4" (c), "Y2" (d).
 ("h4": 7.7W% Al_2O_3 +0.3W% CaO, 1950 °C, 1h, packed in 10-7-0.7, semi-open)
 ("Y2": 6W% Al_2O_3 +2W% CaO, 1950 °C, 5h, packed in "Y", open)

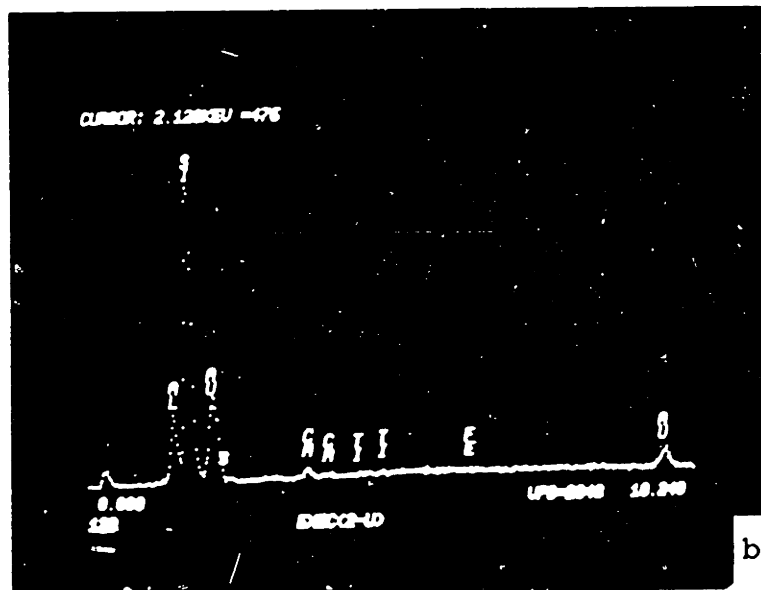
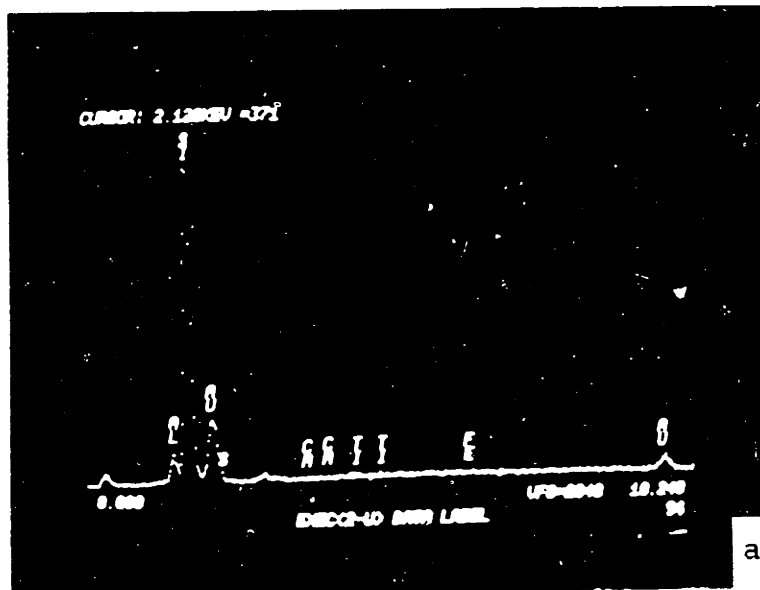


Fig.17. EDAX spectra of samples "T11" (a) and "h6" (b).
 ("T11": 6W% Al₂O₃, 1900 °C, 1h, packed in 10-7, closed)
 ("h6": 7.7W% Al₂O₃+0.3W% CaO, 1850 °C, 1h, packed in 10-7-0.7,
 closed)



Fig.18. STEM micrograph of samples "h6" ((a), 5,000 X) and "T11" ((b), 10,000 X).
("h6": 7.7W% Al_2O_3 +0.3W% CaO, 1850 °C, 1h, packed in 10-7-0.7, closed)
("T11": 6W% Al_2O_3 , 1900 °C, 1h, packed in 10-7, closed)

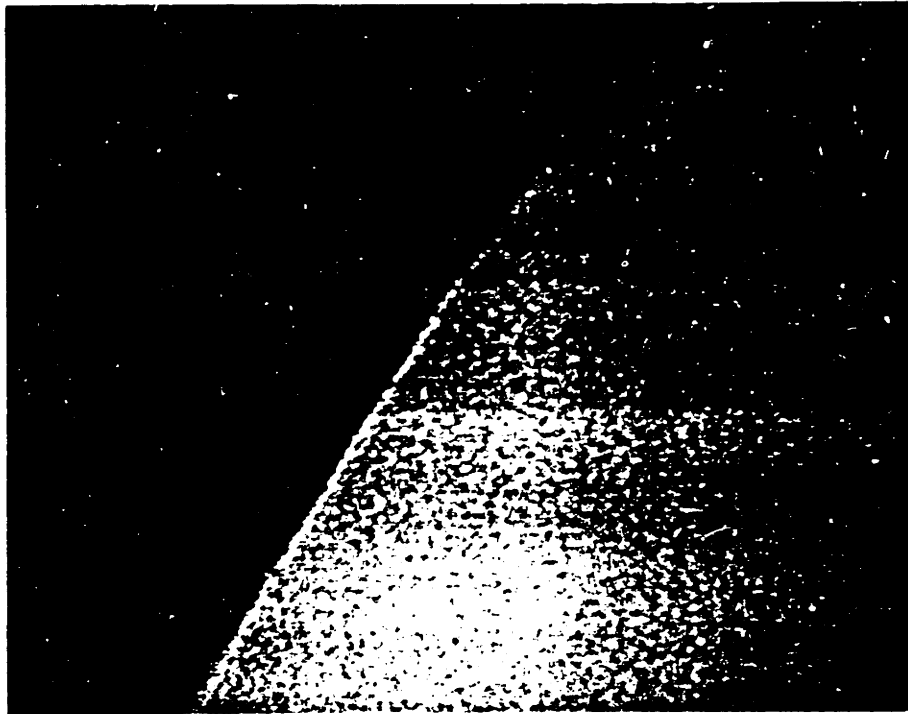


Fig.19. STEM micrograph of over- and under-focused grain boundary in sample "h6", showing a boundary phase about 10 Å wide (1,000,000 X). ("h6": 7.7W% Al₂O₃+0.3W% CaO, 1850 °C, 1h, packed in 10-7-0.7, closed)

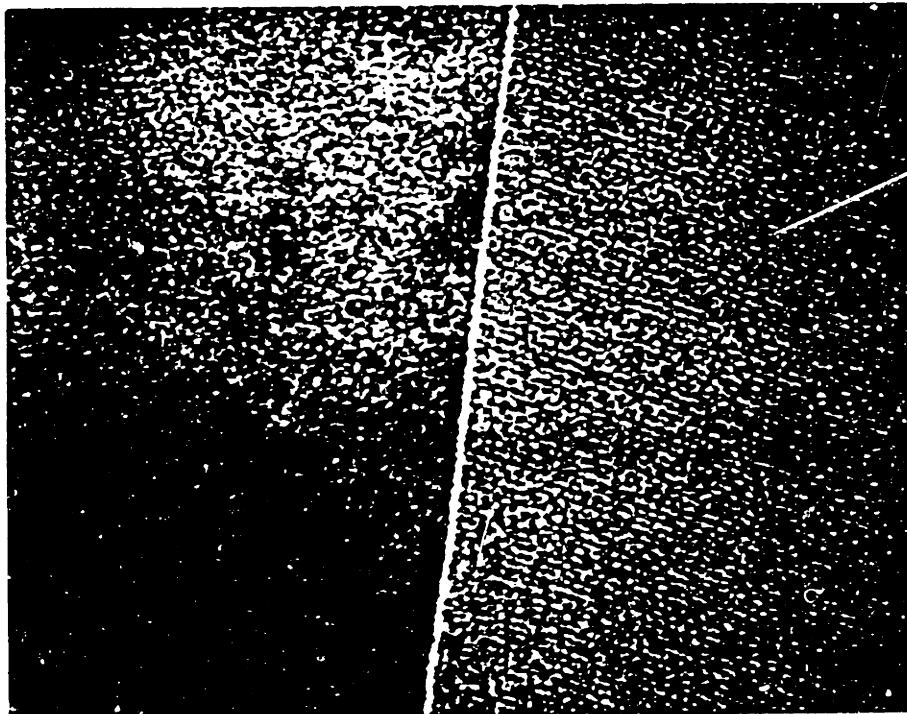
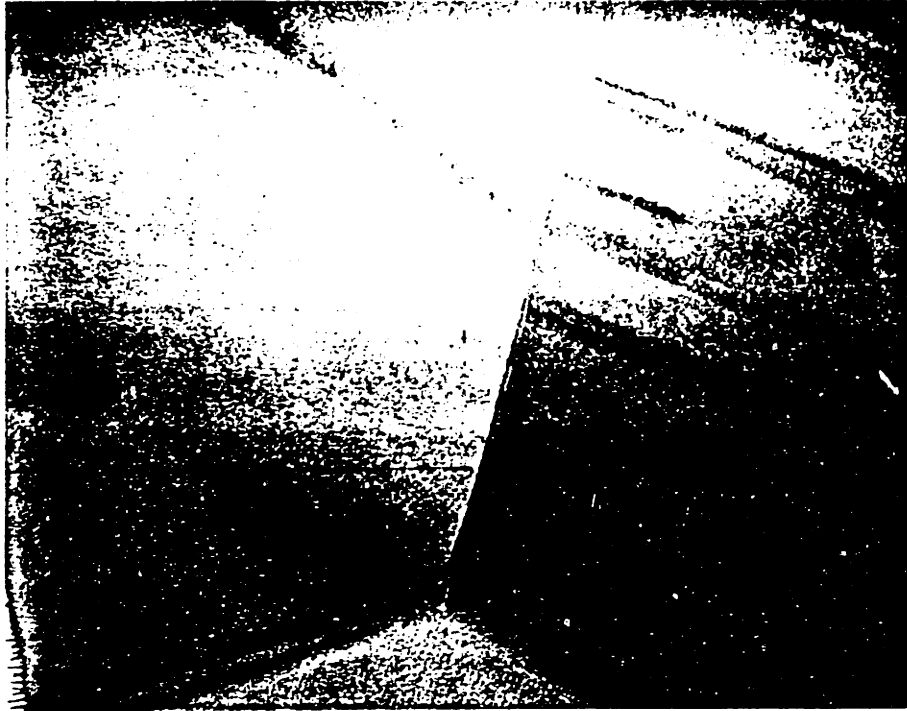


Fig.20. STEM micrograph of a triple grain junction ((top), over-focused, 500,000 X) and a grain boundary ((bottom), under-focused, 1,000,000 X) in sample "T11".
("T11": 6W% Al₂O₃, 1900 °C, 1h, packed in 10-7, closed)

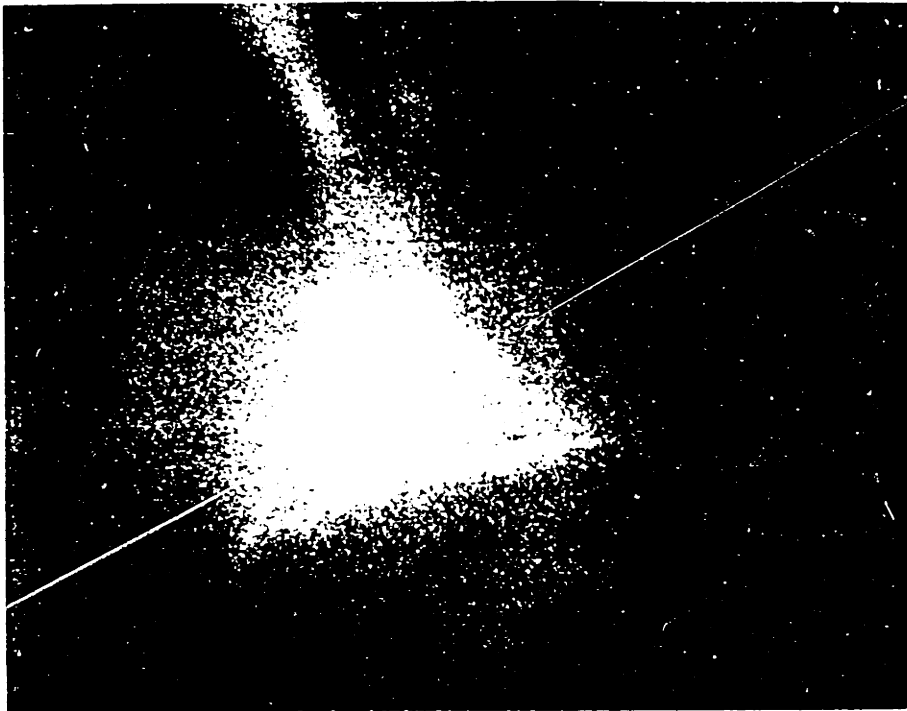


Fig.21. STEM micrograph of an amorphous triple grain junction phase in sample "h6" (500,000 X).
("h6": 7.7W% Al_2O_3 +0.3W% CaO, 1850 °C, 1h, packed in 10-7-0.7, closed)

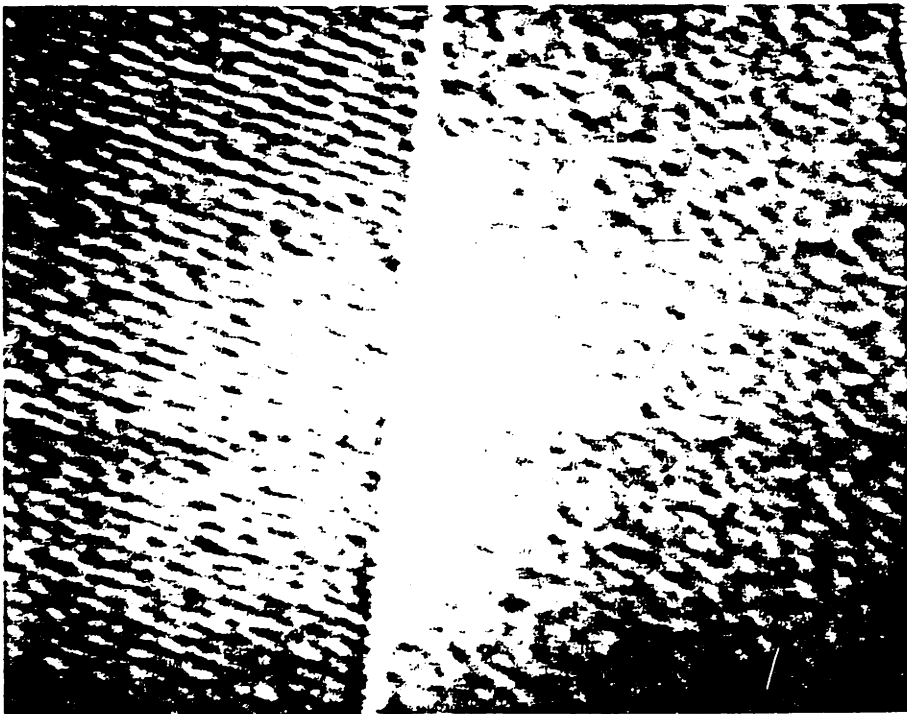


Fig.22. STEM micrograph of sample "T11" showing lattice fringes terminating in contact with boundary phase (2,000,000 X).
("T11": 6W% Al_2O_3 , 1900 °C, 1h, packed in 10-7, closed)

Fig.23. STEM EDAX spectra from different regions in a triple grain junction in sample "h6". A amorphous region, a precipitate and a SiC grain compositions are shown (1,000,000 X). ("h6": 7.7W% Al₂O₃+0.3W% CaO, 1850 °C, 1h, packed in 10-7-0.7, closed)

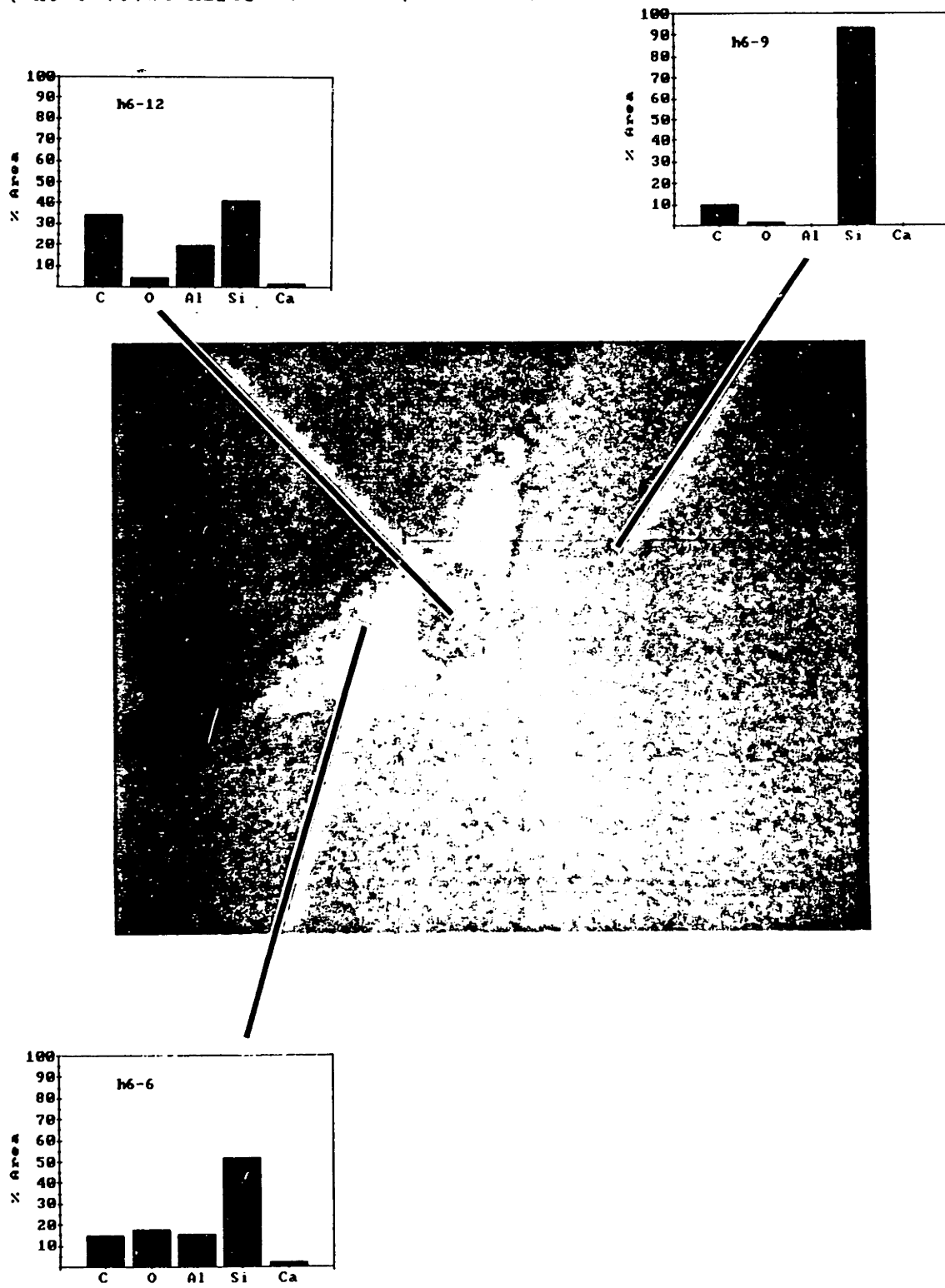
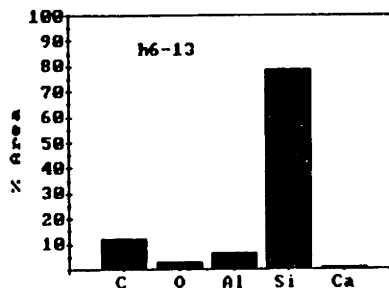
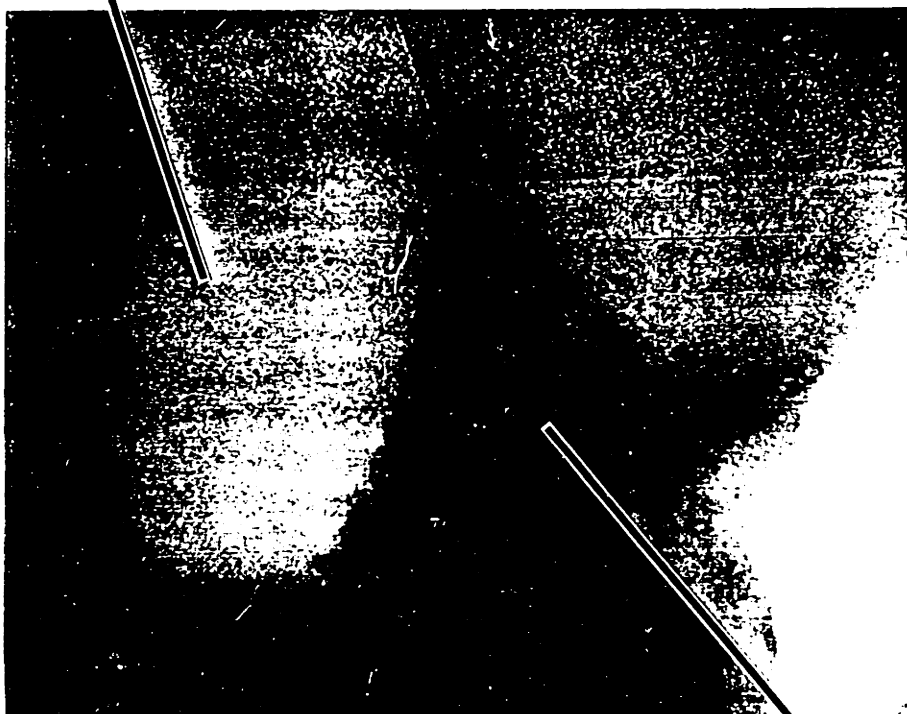
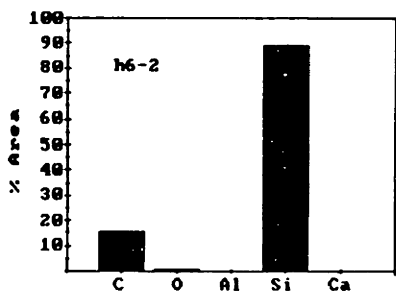


Fig.24. STEM EDAX spectra of a crystalline pocket with some structural features and surrounding SiC grain from sample "h6" (500,000X). ("h6": 7.7W% Al₂O₃+0.3W% CaO, 1850 °C, 1h, packed in 10-7-0.7, closed)



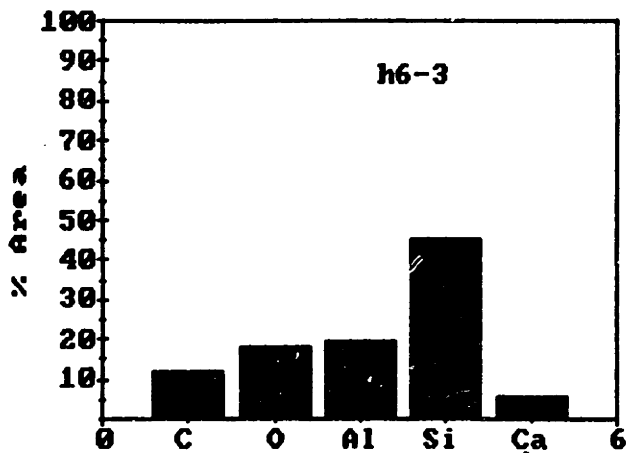
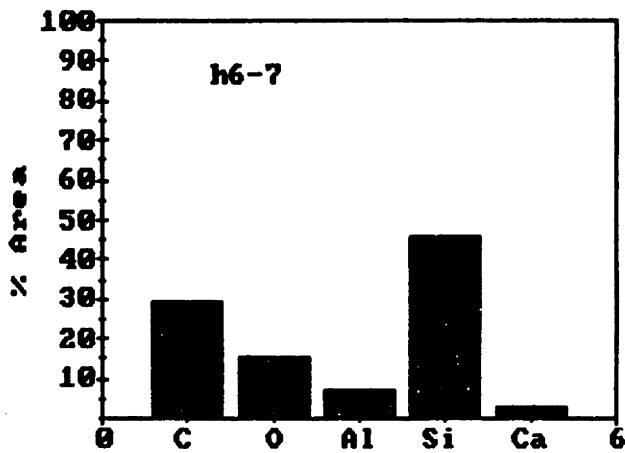
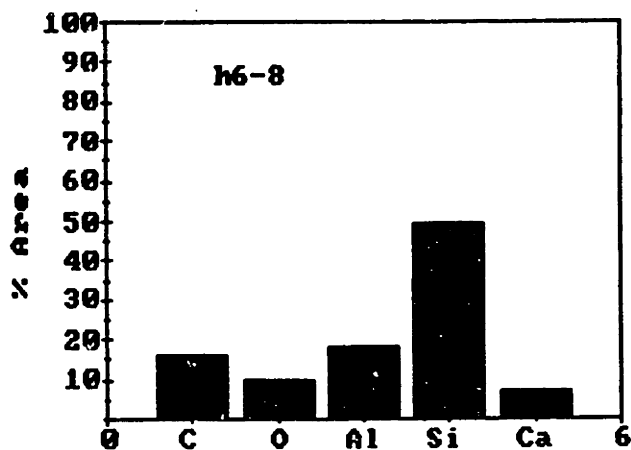


Fig.25. Additional STEM EDAX spectra from randomly chosen pockets and grain boundaries in sample "h6". ("h6": 7.7W% Al₂O₃+0.3W% CaO, 1850 °C, 1h, packed in 10-7-0.7, closed)

Fig.26. STEM micrograph of triple grain junction and surrounding grain along with EDAX spectra in sample "h6" (500,000 X).
 ("h6": 7.7W% Al₂O₃+0.3W% CaO, 1850 °C, 1h, packed in 10-7-0.7, closed)

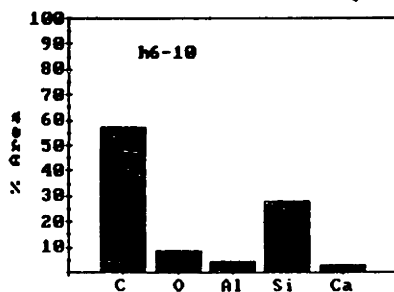
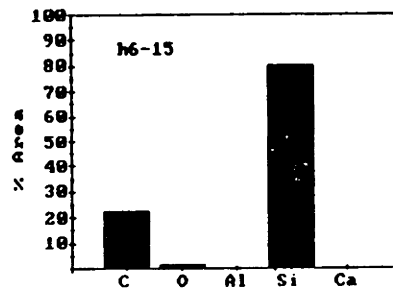


Fig.27. STEM micrograph of grain boundary and neighboring SiC grain along with EDAX spectra from sample "T11" (500,000 X). ("T11": 6W% Al₂O₃, 1900 °C, 1h, packed in 10-7, closed)

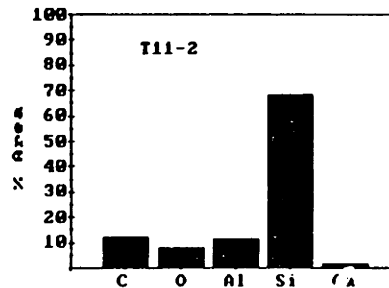
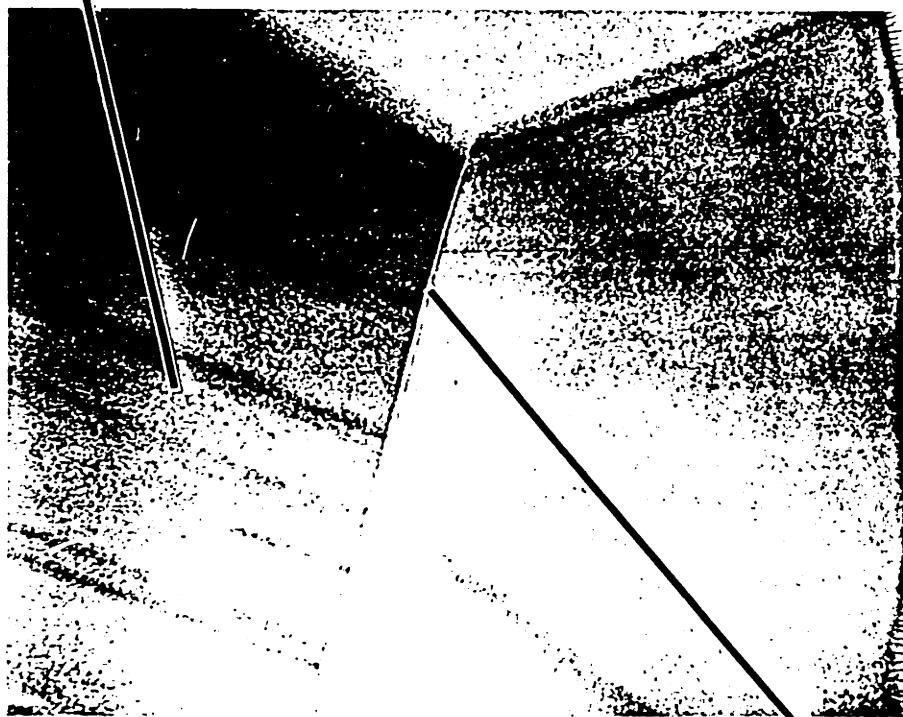
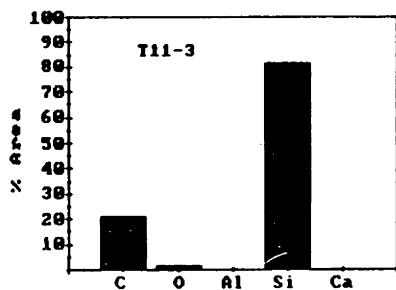


Fig.28. STEM image and EDAX spectra of grain boundary in sample "T11" (1,000,000 X).
("T11": 6W% Al₂O₃, 1900 °C, 1h, packed in 10-7, closed)

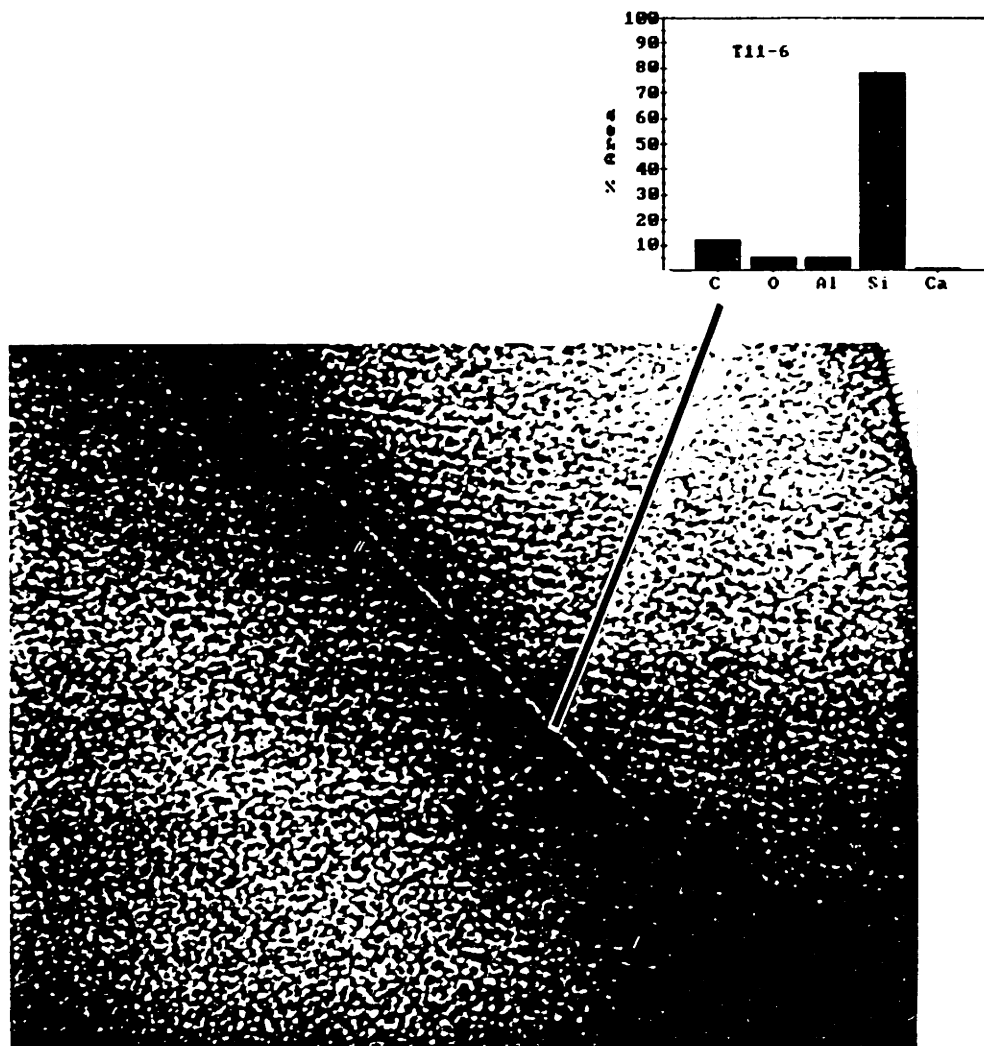


Fig.29. STEM micrograph of SiC and Al₄C₃ grains with overlapping (tilted) boundary showing their EDAX spectra, sample "T11" (1,000,000 X). ("T11": 6W% Al₂O₃, 1900 °C, 1h, packed in 10-7, closed)

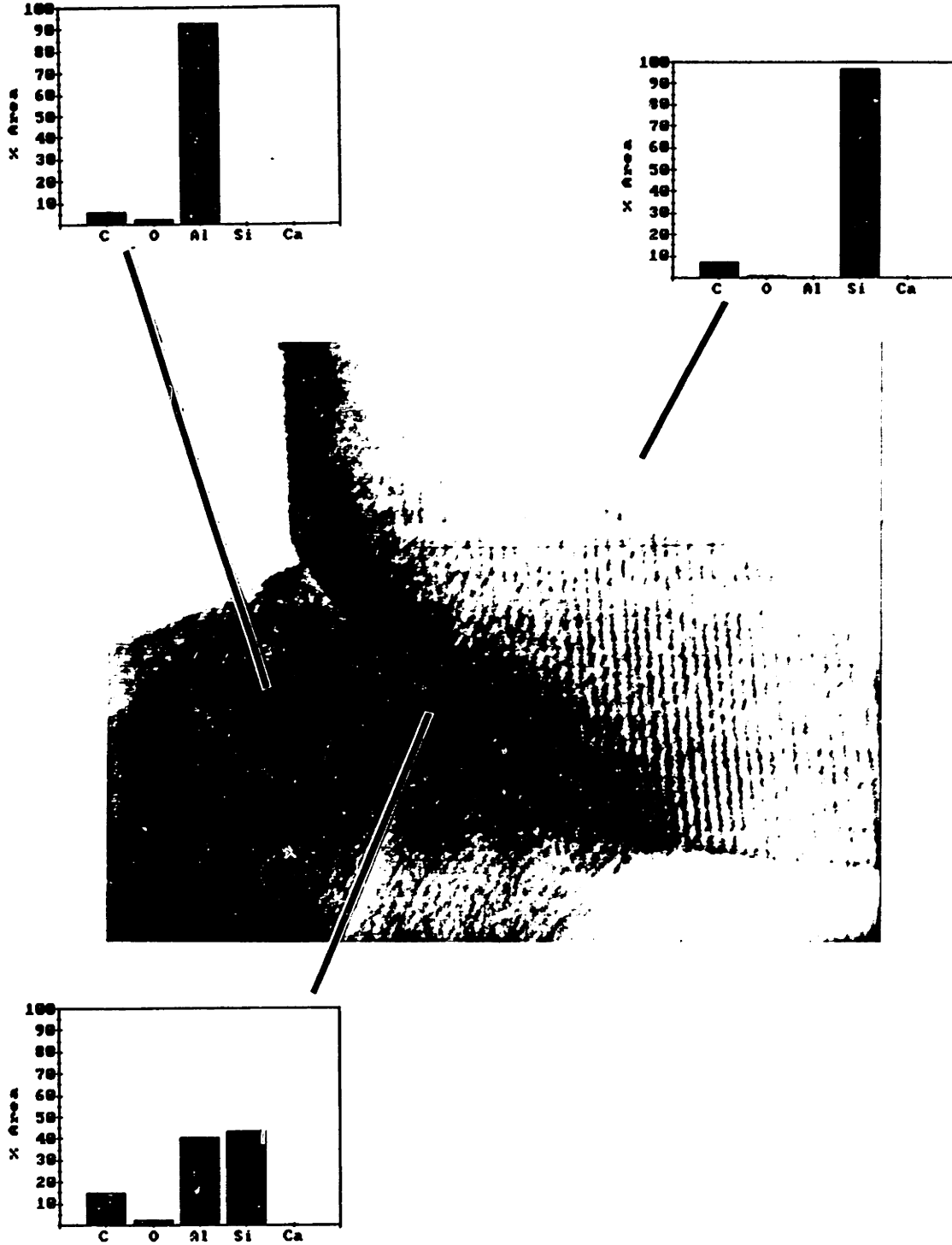




Fig.30. SEM fracture image of sample "J5" (boron and no carbon, (10,000 X)).
("J5": 0.6W% boron as amorphous powder, NO carbon, 1900 °C, 1h)



Fig.31. SEM micrograph of fracture surface in sample "E1" (boron and carbon, (10,000 X)).
("E1": 0.6W% boron as amorphous powder, 0.8W% carbon, 1900 °C, 1h)

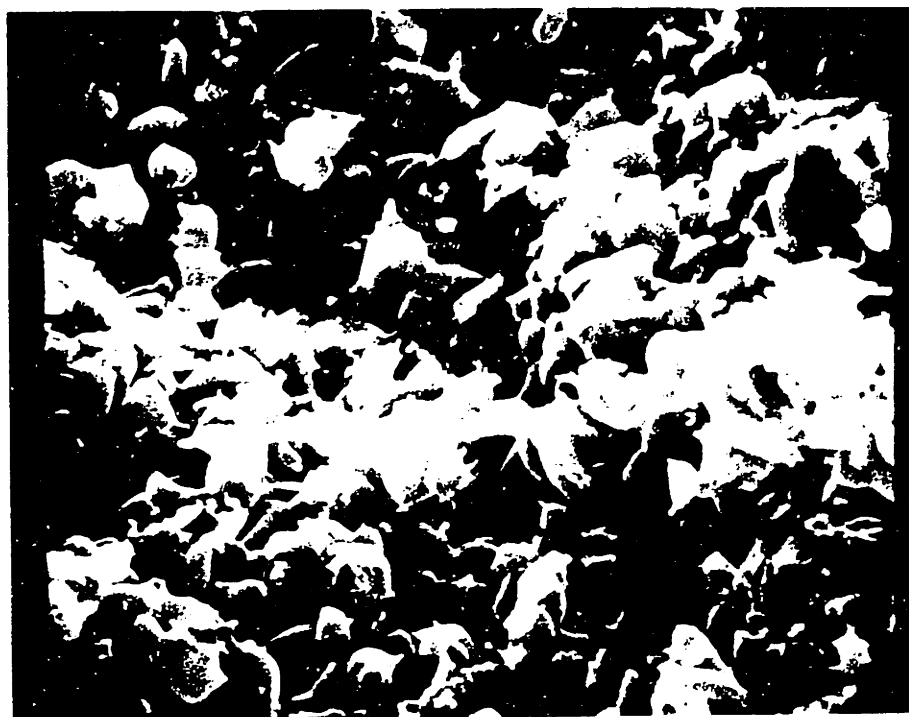


Fig.32. SEM fracture image of sample "H3" (carbon with no boron, (5,000 X)).
("H3": NO boron, 0.8W% carbon, 2000 °C, 1h)



Fig.33. SEM micrograph of fracture surface in sample "E6" (boron and carbon, (5,000 X)).
("E6": 0.6W% boron as amorphous powder, 0.8W% carbon, 2100 °C, 6h)

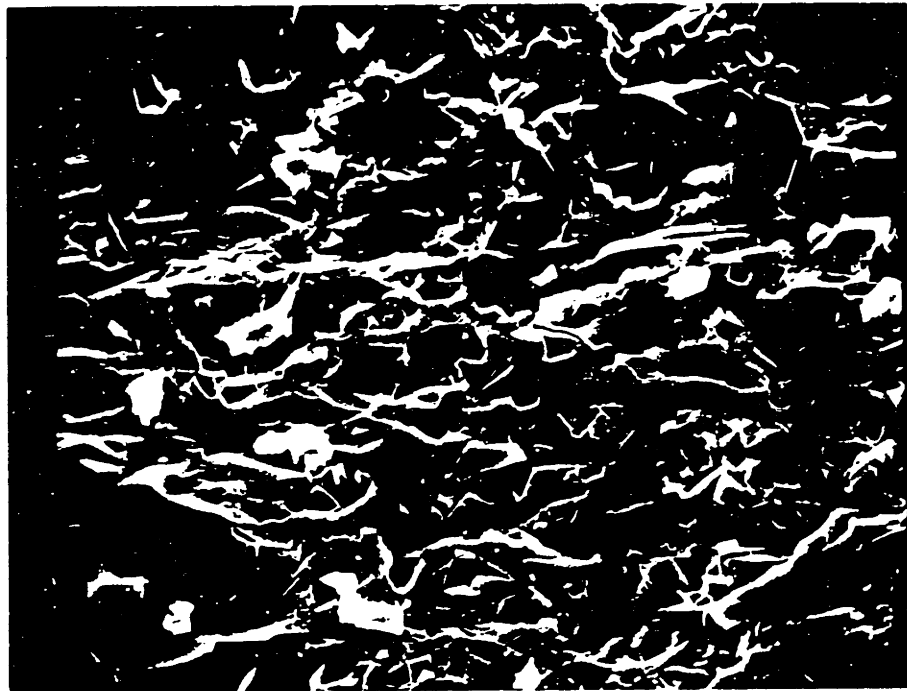


Fig.34. SEM fracture surface image of sample "K7" (boron and carbon, (1,000 X)).
("K7": 0.6W% boron as amorphous powder, 0.8W% carbon, 2200 °C, 6h)

13. References

- 1.- C. Greskovich and J. H. Rosolowski, J. Am. Ceram. Soc., 59 [7-8] 336-343 (1976).
- 2.- S.R. Billington, J. Chown and A.E.S. White, Special Ceramics 1964 pp.19-34.
- 3.- W. Bocker and H. Hausner, Powder Metallurgy International, 10 [2] 87-89 (1978).
- 4.- Shinozaki, R. Williams, B. Juterbock, W. Donlon, J. Hangan, C. Peters, Ceram. Bull., 64 [10] 1389-1393 (1985).
- 5.- Hidehiko Tanaka, Yoshizo Inomata, Kazuhisa Hara, and Haruhisa Hasegawa, J. Mater. Sci., 4 pp. 315-317 (1985).
- 6.- S. Prochazka, Special Ceramics 6, Pub. by The British Ceram. Res. Assc., pp 171-81, June 1975.
- 7.- Junichi Hojo, Kenji Miyachi, Yasuzu Okabe and Akio Kato, Comm. Am. Ceram. Soc., 66 [7] C-114-115 (1983).
- 8.- Hiroshige Suzuki and Teizo Hase, Proc.Int.Symp. of Factors in Densification and Sintering of Oxide and Non-oxide Ceram. (1978) 345-65.
- 9.- Keiichiro Suzuki and Mikio Sasaki, Japan-U.S. Seminar on Fundamental Structural Ceramics, Univ. Washington, Aug. 13-14, 1984.
- 10.- Mamoru Omori and Humihiko Takei, Comm. Am. Ceram. Soc., 65 [6] C-92 (1982).
- 11.- W. Bocker, H. Landfermann and H. Hausner, Powder Metallurgy International, 11 [2] 83-85 (1979).
- 12.- Sunil Dutta, J. Mater. Sci., 19 pp 1307-1313 (1984).
- 13.- Doris H. Stutz, Svante Prochazka and Josef Lorenz, J. Am. Ceram. Soc., 68 [9] 479-482 (1985).
- 14.- R.L. Coble, J. Applied Physics, 32 [5] 787-792 (1961).
- 15.- S. Prochazka, C.A. Johnson, and R.A. Giddings, General Electric, Technical Information Series, 78CRD192 pp.1-24 (Oct. 1978).
- 16.- S. Prochazka, C.A. Johnson and R.A. Giddings, General Electric Company, SRD-75-126 pp. 5-21 (1975).

- 17.- R.L. Coble, J. Am. Ceram. Soc. 41 [2] 55-62 (1958).
- 18.- W.D. Kingery and M. Berg, J. Appl. Phys., 26, 1205 (1955).
- 19.- R.L. Coble, Kinetics of High Temperature Processes, Ed. by W.D. Kingery (Technology Press, Cambridge, MA, and John Wiley and Sons, Inc., New York, 1959).
- 20.- C.S. Smith, Trans. AIME, 175, 15 (1948).
- 21.- R.L. Coble and R.M. Cannon, Current Paradigms in Powder Processing, Department of Materials Science and Engineering, MIT, Internal Communication (1979).
- 22.- W.S. Coblenz, J.M. Dynys, R.M. Cannon and R.L. Coble, Sintering Processes, Ed. G.C. Kuczynski, Plenum (1980).
- 23.- R.M. German and Z.A. Munir, Mat.Sci.Res., V.10, "Sintering and Catalysis", 1975, ed. G.C. Kuczynski.
- 24.- R.M. German and Z.A. Munir, Mat.Sci.Res., V.10, "Sintering and Catalysis", 1975, ed. G.C. Kuczynski.
- 25.- Conyers Herring, J. Appl. Phys., 21 pp. 437-445 (1950).
- 26.- D. Lynn Johnson, Mat.Sci. Monog., 14, "Sintering-Theory and Practice", 1982, ed. Kolar, Pejovnik and Ristic.
- 27.- F.A. Nichols and W.W. Mullins, J. Appl. Phys., 36 [6] 1826-35 (1965).
- 28.- K.E. Easterling and A.R. Tholen, Metal Sci. J., 4, 130, (1970).
- 29.- R.M. German and J.F. Lathrop, J. Mater. Sci., 13, 921 (1978).
- 30.- P. Bross and H.E. Exner, Acta Met., 27, 1013-20 (1979).
- 31.- D.L. Johnson, J. Appl. Phys., 40, 192-200 (1969).
- 32.- D.L. Johnson, Ultrafine-grain Ceramics, Ed. J.J. Burke, N.L. Reed and V. Weiss, Syracuse Univ. Press, 1970, pp.173-183.
- 33.- D.L. Johnson, Powder Metallurgy for High Performance Applications, Ed. J.J. Burke and V. Weiss, Syracuse Univ. Press, 1972, pp.139-149.
- 34.- S. Brennom and D.L. Johnson, Materials Science Research Vol.6, Plenum Press, 1973, p.269. Ed. G.C. Kuczynski.
- 35.- M.F. Ashby, Acta Met., 22, 275-289 (1974).
- 36.- M. Harmer, E.W. Roberts and R.J. Brook, Trans. J. Br. Ceram.

Soc., 78, 22-25 (1979).

- 37.- K-S. Hwang and R.M. German, Mat.Sci.Res., V.16, "Sintering and Heterogeneous Catalysis", 1983, ed. Kuczynski, Miller, Sargent.
- 38.- G.C. Kuczynski, Mat.Sci. Monog.,14, "Sintering-Theory and Practice", 1982, ed. Kolar, Pejovnik and Ristic.
- 39.- G. C. Kuczynski, Mat.Sci.Res., V.10, "Sintering and Catalysis", 1975, ed. G.C. Kuczynski.
- 40.- D. Cranmer, K. Osamura, W. Coblenz and R. Cannon, Coarsening and Densification in SiC, Department of Materials Science and Engineering, MIT, Internal Communication, 1980.
- 41.- D.C. Cranmer, W.S. Coblenz and R.M. Cannon, Coarsening and Densification in SiC, Department of Materials Science and Engineering, MIT, Internal Communication, (1980).
- 42.- Sunil Dutta, Comm. Am. Ceram. Soc., 68 [10] C-269-270 (1985).
- 43.- R. M. Williams, B.N. Juterbock, C. R. Peters and T. J. Whalen, Comm. Am. Ceram. Soc., 67 [4] C-62-64 (1984).
- 44.- W. Bocker, H. Landfermann and H. Hausner, Powder Metallurgy Intl., 13 [1] 37-39 (1981).
- 45.- C. Greskovich and K.W. Lay, J. Am. Ceram. Soc, 55 [3] 142-46 (1972).
- 46.- Richard F. Porter, Paul Schissel and Mark G. Inghram, J. Chem. Phys., 23 [2] 339-342 (1955).
- 47.- F. V. Lenel, Trans. Am. Inst. Mining Met. Engrs., 175, 878-905 (1948).
- 48.- Joseph Gurland and J.T. Norton, Trans. Am. Inst. Mining Met. Engrs., 194, 1051-56 (1952).
- 49.- H.S. Cannon and F.V. Lenel, Some Observations on Mechanism of Liquid Phase Sintering, Plansee Proc., pp.106-22 (1952). Ed. F. Benesovsky, Metalwerk Plansee, Reutte-Tyrol, 1953.
- 50.- W.D. Kingery, J. Appl. Phys., 30 [3] 301-306 (1959).
- 51.- W.D. Kingery, E. Niki and M.D. Narasimhan, J. Am. Ceram. Soc. 44 [1] 29-35 (1961).
- 52.- W.J. Huppmann, Mat.Sci.Res., V.10, "Sintering and Catalysis", 1975, ed. G.C. Kuczyn.
- 53.- G. Petzow, W.A. Kaysser and M. Amtenbrink, Mat.Sci. Monog.,V.14,

- "Sintering-Theory and Practice", 1982, ed. Kolar, Pejovnik and Ristic.
- 54.- R. Bagley and H. K. Bowen, Bull. Am. Ceram. Soc., 56, 732 (1977).
- 55.- S. Prochazka and R.M. Scanlan, J. Am. Ceram. Soc., 58 [1-2] 72 1975.
- 56.- William Samuel Coblenz, P.H.D. Thesis, Department of Materials Science and Engineering, MIT, Jun. 1981.
- 57.- Sunil Dutta, Comm. Am. Ceram. Soc., 65 [1] C-2-3 (1982).
- 58.- J. A. Costello and R.E. Tressler, J. Am. Ceram. Soc., 64 [6] 332-335 (1981).
- 59.- S. Prochazka, Ceramics for High-Performance Applications, Proc. of the 2nd. Army Matls. Conf., Nov., 1973 pp 239-52.
- 60.- Jorulf Brynestad, Carlos E. Bamberger, Dale E. Heatherly & J. Fred Land, Comm. Am. Ceram. Soc., 67 [9] C-184-185 (1984).
- 61.- Svante Prochazka, U.S. Patent No. 4,004,934, Jan. 25, 1977.
- 62.- John A. Coppola and Larry A. Lewler, U.S. Patent No. 4,123,286, Oct. 31, 1978.
- 63.- R. Hamminger, G. Grathwohl and F. Thummler, J. Mater. Sci., 18 pp. 3154-3160 (1983).
- 64.- Robert Sherman, Comm. Am. Ceram. Soc. 68 [1] C-7-10 (1985).
- 65.- R. Hamminger, G. Grathwohl and F. Thummler, J. Mater. Sci. 18 pp. 353-364 (1983).
- 66.- G.A. Lomakina, Silicon Carbide 1973, pp. 520-526.
- 67.- Peter T.B. Shaffer, Res. Bull., 4 pp. 213-220 (1969).
- 68.- Yu A. Vodakov and E.N. Mokhov, Silicon Carbide 1973, pp. 508-519.
- 69.- Yorihiro Murata and R.H. Smoak, Proc. Int. Symp. of Factors in Densification & Sintering of Oxide and Non-Oxide Ceramics, 1978 382-399.
- 70.- D.R. Secrist, J. Am. Ceram. Soc., 47 [3] 127-130 (1964).
- 71.- Hiroshige Suzuki and Teizo Hase, J. Am. Ceram. Soc., 63 [5-6] 349-350 (1980).
- 72.- Yo Tajima and D. W. Kingery, Comm. Am. Ceram. Soc., 65 [2] C-27-29 (1982).

- 73.- Yo Tajima, P.H.D. Thesis, Department of Materials Science and Engineering, MIT, Feb. 1982.
- 74.- H.H. Woodbury and G.W. Ludwig, Physical Review, 124 [4] 1083-1089 (1961).
- 75.- H.D. Batha and L.H. Hardy, Silicon Carbide 1973, pp. 435-42.
- 76.- R. Fuentes, Atom Transport in SiC, MIT, Department of Materials Science, unpublished work (1984).
- 77.- Howard Reiss, J. Chem. Phys., 21 [7] 1209-1217 (1953).
- 78.- R.N. Ghoshtagore and R.L. Coble, Physical Review 143 [2] 623-626 (1966).
- 79.- J.D. Hong, R.F. Davis and D.E. Newbury, Submitted to the J. Am. Ceram. Soc., (1979).
- 80.- M.H. Hon, R.F. Davis and D.E. Newbury, Submitted to J. Mater. Sci., May. 1, 1979.
- 81.- J.D. Hong and R.F. Davis, J. Am. Ceram. Soc., 63 [9-10] 546-552 (1980).
- 82.- M.H. Hon and R.F. Davis, J. Mater. Sci. 14 pp. 2411-2421 (1979).
- 83.- R.M. Williams, B.N. Juterbock, S.S. Shinozaki, C. Peters, T.J. Whalen, Am. Ceram. Soc. Bull., 64 [10] 1385-1389 (1985).
- 84.- Yoshizo Inomata, H. Tanaka, Z. Inowe and H. Kawabata, Yogyo-Kyokai-Shi, 88 [6] 353-355 (1980).
- 85.- K.T. Faber and Anthony G. Evans, Comm. Am. Ceram. Soc., 66 [6] C-94-96 (1983).
- 86.- R.A. Alliegro, L.B. Coffin and J.R. Tinklepaugh, J. Am. Ceram. Soc., 39 [10] 386-389 (1956).
- 87.- F.F. Lange, J. Mater. Sci. 10 pp. 314-320 1975.
- 88.- F.F. Lange, Comm. Am. Ceram. Soc., 65 [2] C-23 (1982).
- 89.- Vitomir Smolej, Comm. Am. Ceram. Soc., 66 [2] C-33-34 (1983).
- 90.- Harumi Yokokawa, Masao Fujishige, M. Dokiya, T. Kameyama, S. Ujiie, K. Fukuda, Trans. Japan Inst. of Metals, 23 [3], 134-45, (1982).
- 91.- C.H. Prescott, Jr., and W.B. Hincke, J. Am. Chem. Soc., 49, 2753-59 (1927).

- 92.- E.J. Kohlmeier and S. Lundquist, Z. anorg. Chem., 260, 208-30 (1949).
- 93.- L.M. Foster, G. Long and M.S. Hunter, J. Am. Ceram. Soc., 39 [1] 1-11 (1956).
- 94.- G. Scheneider, L.J. Gauckler and G. Petzow, Ceramurgia International, 5 [3], 101-4, (1979).
- 95.- B.L. Kidwell, L.L. Oden and R.A. McCune, J. Appl. Cryst., 17, 481-2, (1984).
- 96.- Jean-Claude Viala, Patrice Fortier, Claude Bernard et Jean Bouix, C.R. Acad. Sc. Paris, t.299, Serie II, No. 12, 777-9, (1984).
- 97.- Zenzaburo Inoue, Yoshizo Inomata, Hidehiko Tanaka and Haruo Kawabata, J. Mater. Sci., 15, 575-80, (1980).
- 98.- H. Moissan, Compt. rend., 119, 16-20 (1894).
- 99.- R. Brunner, Z. Elektrochem., 38, 55-68 (1932); Ceram. Abstr., 12 [9] 342 (1933).
- 100.- W.D. Treadwell and A. Gyger, Helv. Chim. Acta, 16, 1214-25 (1933).
- 101.- Emil Baur and Roland Brunner, Z. Elektrochem., 40, 154-58 (1934).
- 102.- J. Schoennahl, B. Willer and M. Daire, Materials Science Monographs, 4, (Sintering-New Developments), 338-45, (1977).
- 103.- R. Dolloff, WADD Technical Report 60-143, July 1960, 22 pp., Union Carbide Corp., Parma Res. Lab., Ohio (1960).
- 104.- H. Ginsberg and V. Sparwald, Aluminum, 41, 181-219 (1965).
- 105.- R. Scace and G. Slack, J. Chem. Phys., 30, 1551 (1959).
- 106.- P. Stroup, Trans. Metall. Soc. AIME, 230, 356 (1964).
- 107.- M. Bruno, Final Report for the period 9/77-2/83. Contract DEAC01-77CS40079, Feb., 1983, pp.326-349. Alcoa Labs., Alcoa Ctr., PA..
- 108.- V.J. Barczak, J. Am. Ceram Soc., 44 [6] 299 (1961).
- 109.- P. Dorner, Doctorate Thesis, Stuttgart, June 22nd 1982.
- 110.- Robert G. Behrens and Gary H. Rinehart, J. Am. Ceram. Soc., 67 [8] 575-578 (1984).
- 111.- T. Kikuchi, T. Kurosawa and T. Yagihashi, J. Japan Inst. Metals, 32, 866 (1968).

- 112.- Fig.231, Phase Diagrams for Ceramists, Am. Ceram. Soc..
- 113.- Fig.233, Phase Diagrams for Ceramists, Am. Ceram. Soc..
- 114.- Fig.232, Phase Diagrams for Ceramists, Am. Ceram. Soc..
- 115.- H. Nowotny, E. Parthe, R. Kieffer and F. Bensorsky, Monatsh Chemie, 85, 255 (1954).
- 116.- A. R. Kieffer, Mat. Res. Bull., 153 (1969).
- 117.- R.R. Ridgway, Trans. Electrochem. Soc., 66, 117 (1934).
- 118.- G.V. Samsonov, Fiz. Metal. i Metalloved. Akad. Nauk USSR Ural. Filial., 3, 309 (1956).
- 119.- R.P. Elliot, Final Report on contract ARF-2200-12, 45 (1961).
- 120.- F. J. Tone, Ind. Eng. Chem., 30, 232 (1938).
- 121.- R. T. Dolloff, Wright Air Development Division Technical Report No.60-143, 22pp. July 1960.
- 122.- K.I. Portnoi, G.V. Samsonov and L.A. Salonnikova, Zhur. neorg. Khim., 5, 2632 (1960).
- 123.- G.V. Samsonov, Izd. An Uzhr USSR, Kiev, (1960).
- 124.- Kozo Osamura and Rowland M. Cannon, Jr., A comment on the Ternary Phase Diagram of SiC-C-B System, Department of Materials Science and Engineering, MIT, Internal Communication, (1979) pp. 1-8.
- 125.- J.V. Milewski, F.D. Gac, J.J. Petrovic, Los Alamos National Lab., LA-9650-MS (1983).
- 126.- J.J. Petrovic, J.V. Milewski, D.L. Rohr, F.D. Gac, J. Mater. Sci., 20 pp. 1167-1177 (1985).
- 127.- A.J.G. Op Het Veld and J.D.B. Veldkamp, Fibre Sci. Technol., 2, 269 (1970).
- 128.- Yoko Suyama, Robert M. Marra, John S. Haggerty and H. Kent Bowen, Am. Ceram. Soc. Bull., 64 [10] 1356-1359 (1985).
- 129.- Kevin W. Bowie, 3.082 Lab. Project, Department of Materials Science and Engineering, MIT, May. 1980.
- 130.- R. Fuentes, MIT, Dept. of Matl. Sci., M.S. Thesis, (1983).
- 131.- Von R. Kieffer, E. Gugel, G. Leimer und P. Ettmayer, Deutschen Keramischen Gesellschaft., 49 [41-72] 41-46 (1972).

- 132.- L. Brewer and A.W. Searcy, J. Am. Chem. Soc., 73, 5308 (1951).
- 133.- R.L. Coble, Mat.Sci. Monog.,14, "Sintering-Theory and Practice", 1982, ed. Kolar, Pejovnik and Ristic.
- 134.- W.D. Kingery and M.D. Narsimhan, J. Appl. Phys., 30 [3] 307-310 (1959).
- 135.- V.G. Mizin, I.V. Ryabchikov and N.V. Tolstoguzov, Izv. Vyssh. Ucheb. Zaved., Chern. Met. 10 [12], 51-4 (1967).
- 136.- Joachim K. Floess, MIT, Ph.D. Thesis, Department of Chemical Engineering, Dec., 1985.

14. Appendix 1: Carburization and VLS Growth

In this appendix, work on silicon fiber conversion to polycrystalline SiC and vapor-liquid-solid (VLS) SiC whisker growth is briefly documented. This work was carried out during the course of the investigation on sintering of SiC as brief incursions and was not further developed.

Si Fiber Conversion

Single crystal and polycrystalline silicon fibers of approximate square section and about 0.5 mm per side were exposed to a 99% hydrogen-1% CH₄ atmosphere for various periods of time (20 min to 4 hs) at 1400 °C.

Pure silicon fibers resulted in hollow SiC tubes in which the inner cross section was identical to the starting fiber outer cross section, indicating that the silicon diffusivity under the chemical gradient was dominant and the rate of transport of carbon through the (polycrystalline) scale was negligible. Boron doped silicon fibers resulted in a rather different geometry: the inner cross section was smaller than the fiber's original outer cross section. Thus, the presence of

boron accelerated the transport of carbon through the SiC scale.

Given the relatively low temperatures at which the experiment was carried out, the diffusion of both, Si and C, is believed to proceed via the grain boundaries.

Attempts to "seed" the silicon fiber surface (by dipping the fiber into submicron SiC powder dispersions, amorphous carbon dispersions, and by plasma sputtering SiC onto one face of the Si fiber) before carburization failed to produce a different grain size than the "unseeded" fiber. Some runs gave indications of different growth rates but were irreproducible. Furthermore, regular polishing and etching procedures proved to be inappropriate for the very fragile SiC tubes in either full or partly converted form. No information regarding grain size or microstructure was obtained, with the sole exception of the fact that the tube wall appeared in fractured specimens under the SEM to be completely dense.

VLS SiC Whisker Growth

Beta SiC whiskers were grown in a 99.6% hydrogen-0.4% CH₄ atmosphere at 1400 °C. SEM studies shown evidence of VLS growth, such as a metallic "cap" at every end of the

whiskers. The metallic seeds proved to be iron scrapings from a steel knife, used to clean the alumina sample holder. Two different types of whiskers were observed to grow: 1) thinner, smaller and imperfect ones, seemed to be nucleated onto imperfections on the substrate, and 2) larger, more perfect ones were grown by a VLS mechanism. The work was no longer pursued.

15. Biographical Note

Ricardo I. Fuentes; born in Mexico City, Mexico, the 25th of January, 1958.

During my childhood I lived in a wide variety of places, ranging from the tropical climates in the Istmo de Tehuantepec to the candent semi-desertic Hermosillo, Son., in Mexico. I finished high school there, first of my class.

I attended college in Monterrey, N.L., Mexico, and majored in Physics. Graduated with honors in 1979, first of my class. During this period I was elected president of the Association of Physics Students. In addition I served for a year as the representative of the Science Division before the Students Federation. I was an assistant professor in the physics department during the last three years in college.

After graduation from college, I worked for a year as a consultant to the Federal Electricity Commission and as a full time researcher at the Institute for Electrical Research, both in Mexico.

I came to M.I.T. in the summer of 1980 and entered the Ceramics panel of the Department of Materials Science and Engineering. I received my Master Degree in 1983, having worked under Professor R. M. Cannon on dispersion of SiC powders. At this point I got married and my wife, Irma, joined me at M.I.T.. Later, in the summer of 1986 received my Ph.D. Degree. I worked under the supervision of Professor R.L. Coble on Sintering of SiC. My minor program was on the area of robotics and artificial intelligence.

In the meantime I was elected president of the Association of Mexican Students at M.I.T. for a year and worked for a summer in I.B.M.'s Thomas J. Watson Research Center in Yorktown Heights, N.Y.. Out of the later job a paper on the "Determination of the Electron Temperature and Density Using a Langmuir Probe in a SF₆-O₂ Downstream Microwave Plasma Etcher" has been submitted for publication. During my graduate student years I founded along with my wife and my friend Chris Wee a computer consulting and sales and electronic security systems firm.

I enjoy doing sculpture, computers, electronics, music, camping, skiing and cactus collecting.